

# Angular Correlation in Inelastic Nucleon Scattering

ERIC SHELDON\*

Laboratorium für Kernphysik,  
Eidgenössische Technische Hochschule,  
Zürich, Switzerland

## CONTENTS

1. Introduction . . . . .	795
2. Scattering theory with spin-orbit interaction . . . . .	797
3. Theoretical cross sections for CN mechanism . . . . .	799
A. Angular correlation theory for CN mechanism (with spin-orbit interaction) . . . . .	799
B. Angular distribution for CN mechanism (with spin-orbit interaction) . . . . .	804
C. Total inelastic scattering cross section for CN mechanism (with spin-orbit interaction) . . . . .	805
4. Angular correlation theory for DI mechanism . . . . .	805
5. Evaluation of the correlation function . . . . .	810
A. Choice of optical model . . . . .	810
B. Transmission coefficients . . . . .	812
C. CN correlation functions . . . . .	812
6. Angular correlation surfaces . . . . .	813
7. Angular correlation analysis for inelastic nucleon scattering . . . . .	818
A. Mg <sup>24</sup> , $Q = -1.368$ MeV . . . . .	819
B. Si <sup>28</sup> , $Q = -1.78$ MeV . . . . .	822
C. S <sup>32</sup> , $Q = -2.25$ MeV . . . . .	826
D. Ti <sup>48</sup> , $Q = -0.987$ MeV . . . . .	828
E. Cr <sup>52</sup> , $Q = -1.433$ MeV . . . . .	829
F. Fe <sup>56</sup> , $Q = -0.845$ MeV . . . . .	832
G. Ni <sup>58,60</sup> . . . . .	838
H. Zn <sup>64,66,68</sup> . . . . .	843
8. Concluding remarks . . . . .	845
9. Appendix: Legendre Hyperpolynomials . . . . .	849

## 1. INTRODUCTION

IN the field of angular correlation of radiations following inelastic scattering, there have recently been both theoretical and experimental developments which the present paper sets out to review. It thereby supplements the various other published surveys<sup>1-3</sup> and deals, in particular, with calculations of absolute double-differential cross sections for arbitrarily high orbital angular momenta of incident and outgoing radiation, incorporating consideration of the effects of spin-orbit coupling interaction. Since its scope would otherwise become unmanageably

extensive, the survey has been limited to neutron and proton inelastic scattering from medium-heavy nuclei. It thereby aims in the first place to shed light on nuclear reaction mechanism studies and concentrates in the main upon low incident energies for which the compound-nucleus (CN) mechanism may be considered to predominate. Some rather preliminary analysis on the basis of distorted-wave direct-interaction (DWDI) theory for scattering at higher energies is also presented. In the underlying choice of optical-model parameters for scattering analysis, the recent developments due to Perey and Buck<sup>4</sup> have been incorporated in the present work. In particular, the neutron nonlocal potential of Perey and Buck has the merit of containing no explicit energy dependence and is inherently more satisfactory than any of the various local potentials<sup>5-7</sup> hitherto employed, or the nonlocal potential of Wyatt, Wills, and Green<sup>8</sup> since the latter, involving as it does the effective mass approximation, is formally valid only for rather low energies. For analysis of proton scattering, the local potential of Perey<sup>9</sup> was used unless otherwise stated. The strong-coupling approach of Buck<sup>10</sup> for deformed nuclei has also been tried for correlation analysis: The results proved to be practically identical with those obtained from conventional DWDI theory. An outline of the above potentials is presented in Sec. 5A. In Sec. 2 formulation of scattering theory generalized to take account of spin-orbit interaction is described. This

<sup>4</sup> F. Perey and B. Buck, Nucl. Phys. **32**, 353 (1962).

<sup>5</sup> J. R. Beyster, R. B. Schrandt, M. Walt, and E. W. Salmi, Los Alamos Report LA-2099, 1957 (unpublished).

<sup>6</sup> W. S. Emmerich, Westinghouse Research Report 6-94511-R 19, 1958 (unpublished); P. A. Moldauer, Argonne Report ANL-6323, 1961 (unpublished).

<sup>7</sup> F. Bjorklund and S. Fernbach, Phys. Rev. **109**, 1295 (1958).

<sup>8</sup> P. J. Wyatt, J. G. Wills, and A. E. S. Green, Phys. Rev. **119**, 1031 (1960).

<sup>9</sup> F. Perey, in Proceedings of the International Symposium on Direct Interactions and Nuclear Reaction Mechanisms, Padua, 1962 (to be published).

<sup>10</sup> B. Buck, Phys. Rev. **130**, 712 (1963).

\*On leave of absence at the Oak Ridge National Laboratory until October 1962.

<sup>1</sup> L. C. Biedenharn and M. E. Rose, Rev. Mod. Phys. **25**, 729 (1953).

<sup>2</sup> S. Devons and L. J. B. Goldfarb, in *Handbuch der Physik*, edited by S. Flügge (Springer-Verlag, Berlin, 1957), Vol. 42, p. 362.

<sup>3</sup> L. C. Biedenharn, in *Nuclear Spectroscopy*, edited by F. Ajzenberg-Selove (Academic Press Inc., New York, 1960), Part B, p. 732.

is utilized in Secs. 3 and 4 for generating the absolute magnitudes of the double-differential cross sections  $d^2\sigma/d\Omega_1 d\Omega_2$  for CN and DWDI mechanisms with spin-orbit interaction. The only remaining adjustable parameter in the DWDI calculations is the relative magnitude of the spin-flip contribution, which is, at present, unknown.

It is understandable that the complexity of CN correlation theory has throughout previous formulations<sup>11-13</sup> led to the perpetration of both basic and calculational errors.<sup>14</sup> The present analysis has aimed to detect and correct these; such emendations are described in detail in the text. In Sec. 3A, the influence upon the correlation function of higher momenta than  $l = 2$  for even-even nuclei having  $0+$  ground states and  $2+$  first excited states is studied for the first time, as is also the azimuthal dependence of the CN correlation function. Plans are now under way to extend the computer codes to consideration of arbitrary target spins and  $\gamma$  multipoles, as well as to calculate the actual tensor parameters for direct comparison with the corresponding quantities furnished by the DWDI code of Bassel, Drisko, and Satchler.<sup>15</sup> These latter were used in the present work to determine the absolute magnitudes (for a given spin-flip intensity) of the quantities  $P$ ,  $Q$ ,  $R$ ,  $\theta'$  and  $\theta''$  which enter into the DWDI correlation expression

$$W(\theta_1, \theta_2, \varphi = \pi) = P + Q \sin^2 2(\theta_2 - \theta') + R \sin^2 (\theta_2 - \theta''), \quad (1)$$

where  $\theta_1$  and  $\theta_2$ , respectively, represent the c.m. angles of emission of scattered nucleons and  $\gamma$  radiation referred to the incident direction and  $\varphi$  is the azimuthal angle of the latter (illustrated for proton scattering in Fig. 1). In the present work, the following coordinate convention is used: The  $z$  axis of a right-handed system is taken to lie along the incident direction and the  $y$  axis along the normal to the scattering plane (the  $x$  axis, hence, in the scattering plane). Such computed magnitudes represent a theoretical advance over those which had in the past been selected rather arbitrarily to fit experimental results. The fact that the present DWDI code does not take spin-orbit interaction into account may possibly be responsible for the markedly poor agreement between the theoretical results so obtained and

the experimental correlation results at intermediate energies. A more fundamental source of discrepancy is, however, suggested by the fact that results of strong-coupling theory agree very closely with the DWDI theoretical values, even though the former take spin-orbit interaction into account. Use of absolutely computed DWDI correlation parameters in place of the semiempirical approach employed hitherto has, in certain instances, indicated that the

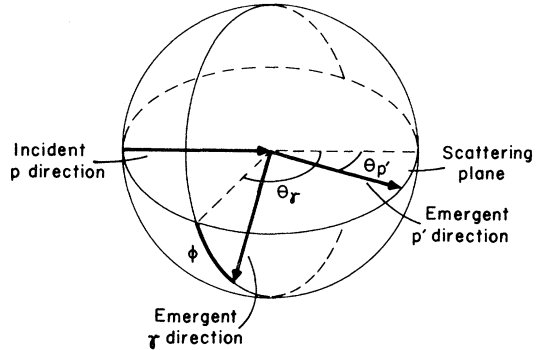


FIG. 1. Angular convention for the correlated radiations, illustrated for inelastic proton scattering.

interpretation of the predominant reaction mechanism has been erroneous. It was found that results could be fitted reasonably well with computed CN correlation curves, whereas the absolute DWDI fit was poor. The present analysis, thus, to some extent complements that of Gove<sup>16</sup> in examination of experimental evidence for DI processes.

To improve further the sensitiveness of angular correlation as an aid to investigation of reaction mechanism, it would be desirable to have access to measurements of the absolute double-differential cross section in order to obviate the present arbitrary normalization of experimental results. Some preliminary work in this direction is analyzed in Sec. 7. Also therein are theoretical predictions of the azimuthal dependence of the CN correlation function for given pairs of values of  $\theta_1$  and  $\theta_2$ . The angular variation was found to be rather weak. As a diagnostic criterion of reaction mechanism, correlation measurements are particularly valuable when combined with measurements of the angular distribution of the emitted radiations and when undertaken over a wide range of angles with particular emphasis upon the inherent symmetry relations<sup>13,17</sup> predicted theoretically.

<sup>11</sup> G. R. Satchler, Phys. Rev. **94**, 1304 (1954).

<sup>12</sup> G. R. Satchler, Phys. Rev. **104**, 1198 (1956).

<sup>13</sup> E. Sheldon, Helv. Phys. Acta **34**, 803 (1961).

<sup>14</sup> G. R. Satchler and E. Sheldon, in Proceedings of the International Symposium on Direct Interactions and Nuclear Reaction Mechanisms, Padua, 1962 (to be published).

<sup>15</sup> R. H. Bassel, R. Drisko, and G. R. Satchler, Oak Ridge Report ORNL-3240, 1962 (unpublished).

<sup>16</sup> H. E. Gove, in *Proceedings of the Rutherford Jubilee International Conference*, edited by J. E. Birks (Heywood and Company Ltd., Manchester, England, 1962), p. 437.

<sup>17</sup> E. Sheldon, Phys. Letters **2**, 178 (1962).

Throughout the text which follows, distinction is made between angular *distribution*, which displays the angular dependence of the differential cross section, and the angular *correlation*, which displays the angular dependence of the *double*-differential cross section. Since the latter is concerned with the directional correlation of three radiations (incident and emergent nucleons and de-excitation  $\gamma$  radiation), it has often been termed a "triple correlation," a designation which could be misleading (especially as it led to angular distributions being labeled as "double correlation" or, more loosely, simply "correlation") since *angular* correlation essentially involves the study of *two angles* of emission at a given azimuth. The present nomenclature is clear and self-consistent.

As a preliminary before proceeding to outline correlation theory, it is necessary to examine the influence of spin-orbit coupling upon scattering matrix elements and nuclear cross sections, since thereby a definition is introduced of generalized transmission coefficients which play a role in CN correlation theory incorporating spin-orbit interaction.

For brevity and convenience, throughout this paper we shall employ the notation

$$\hbar \equiv (2h + 1)^{\frac{1}{2}}; \quad \hbar^2 \equiv 2h + 1. \quad (2)$$

Vector addition (Clebsch-Gordan) coefficients will be written in the form  $\langle jm | j_1 j_2 m_1 m_2 \rangle$  when momenta  $j_1$  and  $j_2$  having projections  $m_1$  and  $m_2$  are vectorially coupled to yield a resultant total momentum  $j$  having projection  $m$ .

Thus,

$$\langle jm | j_1 j_2 m_1 m_2 \rangle \equiv C_{m_1 m_2 m}^{j_1 j_2 j} = (-)^{j_1 - j_2 + m} \hat{j} \begin{pmatrix} j_1 & j_2 & j \\ m_1 & m_2 & -m \end{pmatrix}. \quad (3)$$

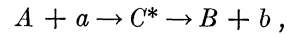
## 2. SCATTERING THEORY WITH SPIN-ORBIT INTERACTION

In the Hauser-Feshbach treatment<sup>18</sup> of inelastic nucleon scattering proceeding by way of CN formation, no explicit incorporation of spin-orbit interaction was undertaken, with the result that transmission coefficients were considered to be determined only by the energy and orbital angular momentum of the incident or emergent particles, but not by their *total* angular momentum  $\mathbf{j} = \mathbf{l} + \mathbf{s}$ . In the presence of spin-orbit interaction, the theory has to be generalized to yield scattering amplitudes that are dependent both on  $l$  and  $j$ , since from these ampli-

tudes the respective transmission coefficients and, hence, cross sections are elucidated.

The treatment which follows in generalizing the Hauser-Feshbach approach bears some resemblance to the calculations of Yoshida<sup>19</sup> as applied to neutron scattering by deformed nuclei in the paper of Chase, Wilets, and Edmonds,<sup>20</sup> though the latter authors, in their calculations, reverted to the use of ordinary transmission coefficients excluding spin-orbit interaction. In fact, the treatment below is based upon unpublished theoretical work by Satchler generalizing the statistical model of nuclear reactions, which the author was kindly permitted to use in the analysis which follows.

We consider the process



wherein a particle  $a$  of total angular momentum  $\mathbf{j}_1 = \mathbf{l}_1 + \mathbf{s}_1$  impinges with relative momentum  $k$  (in the center-of-mass system) upon a target nucleus  $A$  of spin  $J_0$  to excite a level having spin  $J_1$  in the compound nucleus  $C$ . For the present, we leave the direction of the quantization axis arbitrary and, respectively, write the magnetic quantum numbers corresponding to the momenta  $j_1, l_1, s_1, J_0, J_1$  as  $m_1, \mu_1, s_1, M_0, M_1$ . It should be mentioned at this stage that special nomenclature has been introduced for this section alone; in subsequent portions of this paper a modified and simpler system of nomenclature is employed.

We start with the channel spin representation, analogously to Hauser and Feshbach, whereby the spins of the incident particle and the target nucleus are coupled to yield an incident channel spin

$$\mathfrak{S} = \mathbf{s}_1 + \mathbf{J}_0, \quad (4)$$

which has projection  $\mathfrak{M}$  along the  $z$  axis. The total angular momentum transfer is then the vector sum of the channel spin and the orbital momentum of the incident particle, viz.,

$$\mathbf{J}_1 = \mathfrak{S} + \mathbf{l}_1. \quad (5)$$

In the absence of scattering, the wave function for the initial system  $A + a$  can, for incident plane waves, be written as

$$\Psi_{J_0, M_0, i\sigma_1, s_1, i\mathbf{k}} = \psi_{J_0, M_0} \psi_{\sigma_1, s_1} e^{i\mathbf{k} \cdot \mathbf{r}}, \quad (6)$$

where  $\mathbf{r}$  is the c.m.s. coordinate of the incident particle. Carrying out the vector coupling in channel-

<sup>19</sup> S. Yoshida, Proc. Phys. Soc. (London) **A69**, 668 (1956).

<sup>20</sup> D. M. Chase, L. Wilets, and A. R. Edmonds, Phys. Rev. **110**, 1080 (1958).

<sup>18</sup> W. Hauser and H. Feshbach, Phys. Rev. **87**, 366 (1952).

spin representation, we can write this wave function in the form

$$\Psi_{J_0 M_0 \sigma_1 s_1; \mathbf{k}} = \sum_{\mathcal{S}\mathcal{N}\mathcal{L}} \langle \mathcal{S}\mathcal{N}\mathcal{L} | J_0 \sigma_1 M_0 s_1 \rangle \psi_{J_0 \sigma_1; \mathcal{S}\mathcal{N}\mathcal{L}} e^{i\mathbf{k} \cdot \mathbf{r}} \quad (7)$$

with

$$e^{i\mathbf{k} \cdot \mathbf{r}} = 4\pi \sum_{l_i \mu_i} i^{l_i} Y_{l_i}^{\mu_i*}(\mathbf{k}) Y_{l_i}^{\mu_i}(\mathbf{r}) j_{l_i}(kr) \quad (8)$$

as the usual expansion of a plane wave in terms of spherical harmonics having as argument the directions of the incident momentum  $\mathbf{k}$  and particle coordinate  $\mathbf{r}$ , together with a spherical Bessel function  $j_{l_i}(kr)$  of order  $l_i$ .

We next proceed to relate the description of the process in channel-spin representation to that in spin-orbit representation, noting that in the former Eq. (7) can equivalently be written as

$$\Psi_{J_0 M_0 \sigma_1 s_1; \mathbf{k}} = \sum_{\mathcal{S}\mathcal{N}\mathcal{L}} \sum_{J_1 M_1 \mu_1} \langle \mathcal{S}\mathcal{N}\mathcal{L} | J_0 \sigma_1 M_0 s_1 \rangle \langle J_1 M_1 | \mathcal{S} l_1 \mathcal{N} \mu_1 \rangle \times 4\pi Y_{l_1}^{\mu_1*}(\mathbf{k}) j_{l_1}(kr) \Phi_{\mathcal{S} l_1; J_1 M_1} \quad (9)$$

on vectorially coupling channel spin  $\mathcal{S}$  to orbital momentum  $l_1$  in formation of the compound nucleus of spin  $J_1$ , wherein

$$\Phi_{\mathcal{S} l_1; J_1 M_1} \equiv \sum_{\mu_1} \langle J_1 M_1 | \mathcal{S} l_1, M_1 - \mu_1, \mu_1 \rangle \times \psi_{J_0 \sigma_1; \mathcal{S}\mathcal{N}\mathcal{L}} i^{l_1} Y_{l_1}^{\mu_1}(\mathbf{r}) \quad (10)$$

$$= \sum_{\mu_1 M_0 s_1} \langle J_1 M_1 | \mathcal{S} l_1, M_1 - \mu_1, \mu_1 \rangle \times \langle \mathcal{S}\mathcal{N}\mathcal{L} | J_0 \sigma_1 M_0 s_1 \rangle \psi_{J_0 M_0} \psi_{\sigma_1 s_1} i^{l_1} Y_{l_1}^{\mu_1}(\mathbf{r}). \quad (11)$$

The corresponding expression in spin-orbit representation can be derived on coupling the momenta as

$$\mathbf{j}_1 = \mathbf{l}_1 + \mathbf{s}_1 \quad \text{and} \quad \mathbf{J}_1 = \mathbf{J}_0 + \mathbf{j}_1, \quad (12)$$

whence

$$m_1 = \mu_1 + s_1 \quad \text{and} \quad M_1 = M_0 + m_1, \quad (13)$$

so that

$$\Psi_{J_0 M_0 \sigma_1 s_1; \mathbf{k}} = \sum_{J_1 j_1 \mu_1} \langle j_1 m_1 | l_1 \sigma_1 \mu_1 s_1 \rangle \langle J_1 M_1 | J_0 j_1 M_0 m_1 \rangle \times 4\pi Y_{l_1}^{\mu_1*}(\mathbf{k}) j_{l_1}(kr) \Phi_{j_1 l_1; J_1 M_1}, \quad (14)$$

with

$$\Phi_{j_1 l_1; J_1 M_1} \equiv \sum_{M_0 s_1 \mu_1} \langle J_1 M_1 | J_0 j_1 M_0 m_1 \rangle \langle j_1 m_1 | l_1 \sigma_1 \mu_1 s_1 \rangle \times \psi_{J_0 M_0} \psi_{\sigma_1 s_1} i^{l_1} Y_{l_1}^{\mu_1}(\mathbf{r}). \quad (15)$$

Comparing Eqs. (11) and (15) one finds

$$\Phi_{j_1 l_1; J_1 M_1} = \sum_{\mathcal{S}} u(\mathcal{S} j_1) \Phi_{\mathcal{S} l_1; J_1 M_1}, \quad (16)$$

where

$$u(\mathcal{S} j_1) \equiv (-)^{j_1 - l_1 - \sigma_1} \hat{\mathcal{S}} j_1 W(\sigma_1 J_0 J_1 l_1; \mathcal{S} j_1) \quad (17)$$

is the Lane-Thomas  $S$ -matrix element<sup>21</sup> written in

<sup>21</sup> A. M. Lane and R. G. Thomas, Rev. Mod. Phys. **30**, 257 (1958); E. Vogt, *ibid.* **34**, 723 (1962).

the more convenient form

$$\mathfrak{u}_{21} = S_{21} \exp(2i\omega_2), \quad (18)$$

wherein  $\omega_2$  denotes the Coulomb phase and the  $\mathfrak{u}$ 's have the property

$$\sum_{\mathcal{S}} |\mathfrak{u}(\mathcal{S} j_1)|^2 = \sum_{j_1} |\mathfrak{u}(\mathcal{S} j_1)|^2 = 1. \quad (19)$$

We now progress to consideration of scattering by a central field of force and introduce generalized matrix elements in place of the  $S$ - (or the  $\mathfrak{u}$ -) matrix elements which take account of the spin-orbit interaction and which are defined as the average of "generalized"  $S$ -matrix elements for elastic scattering. Symbolically,

$$\mathfrak{u}_{\alpha\beta} \rightarrow \eta_{\alpha\beta} \exp(2i\omega_{\alpha}), \quad (20)$$

where the scattering amplitude  $\eta_{\alpha\beta}$  need not be unitary. This latter condition corresponds to a description of the field of force by a complex (optical) potential and leads to nonconservation of flux in the scattering process. Physically, one interprets the flux reduction as associated with formation of a compound nucleus, so that one can equate the flux loss with the cross section for formation of a compound nucleus whose decay is independent (except for the operation of selection rules) of its formation.

For scattering, we replace the spherical Bessel function  $j_{l_1}(kr)$  by a term representing incoming [ $\mathcal{G}_{l_1} \leftrightarrow r^{-1} \exp(-i\mathbf{k} \cdot \mathbf{r})$ ] and outgoing [ $\Theta_{l_1} \leftrightarrow r^{-1} \exp(+i\mathbf{k} \cdot \mathbf{r})$ ] radial waves,

$$j_{l_1}(kr) \rightarrow (i/2k) (\mathcal{G}_{l_1} - \eta_{l_1 j_1} \Theta_{l_1}). \quad (21)$$

Thus, explicitly, in terms of the scattering amplitude generalized to take account of spin-orbit interaction, the scattering function becomes

$$\Psi_{J_0 M_0 \sigma_1 s_1; \mathbf{k}} = (2\pi i/k) \sum \langle j_1 m_1 | l_1 \sigma_1 \mu_1 s_1 \rangle \times \langle J_1 M_1 | J_0 j_1 M_0 m_1 \rangle Y_{l_1}^{\mu_1*}(\mathbf{k}) \times [\mathcal{G}_{l_1} - \eta_{l_1 j_1} \Theta_{l_1}] \Phi_{l_1 j_1; J_1 M_1}, \quad (22)$$

with the summation extended over  $l_1, j_1, J_1, \mu_1, M_1$ . The cross section for CN formation can now be determined by calculating the total flux loss (due to absorption of incident particles  $a$ ) over a sphere of large radius  $\mathbf{r}_b \rightarrow \infty$ . For definite target and projectile spin orientation given by  $J_0, M_0; j_1, m_1$ , this cross section for an entrance channel  $\alpha$  and exit channel  $\beta$  assumes the form

$$\sigma_C(\alpha; J_0 M_0 \sigma_1 s_1; \mathbf{k}) = (2\pi/k)^2 \sum \langle \mathcal{S} \mathcal{N} \mathcal{L} | J_0 \sigma_1 M_0 s_1 \rangle \times \langle \mathcal{S}' \mathcal{N}' \mathcal{L}' | J_0 \sigma_1 M_0 s_1 \rangle \langle J_1 M_1 | \mathcal{S} l_1 \mathcal{N} \mu_1 \rangle \langle J_1 M_1 | \mathcal{S}' l_1' \mathcal{N}' \mu_1' \rangle \times Y_{l_1}^{\mu_1*}(\mathbf{k}) Y_{l_1'}^{\mu_1'}(\mathbf{k}) [\delta_{l_1 l_2} \delta_{l_1 l_1'} \delta_{\mathcal{S} \mathcal{S}'} \delta_{\mathcal{S} \mathcal{S}'} \delta_{\mathcal{S} \mathcal{S}'} \delta_{\alpha\beta} - \eta_{\beta \mathcal{S}_2 l_2; \alpha \mathcal{S}_1 l_1} \eta_{\beta \mathcal{S}_2 l_2; \alpha \mathcal{S}_1 l_1}^*], \quad (23)$$

with the summation over  $l_i, l'_i, \mu_i, J_i, \beta$ , the incident channel spins  $S_i, S'_i$  (written with a suffix "1" for clarity), outgoing channel spin  $S_2$ , and outgoing orbital momentum  $l_2$ .

Following Hauser and Feshbach, this can equivalently be written as

$$\sigma_C(\alpha; J_0 M_0, \sigma_1 S_1; \mathbf{k}) = \sum_{J_1 M_1} \sigma_{C, J_1 M_1}(\alpha; J_0 M_0, \sigma_1 S_1; \mathbf{k}), \quad (24)$$

where the partial cross section  $\sigma_{C, J_1 M_1}$  is

$$\begin{aligned} \sigma_{C, J_1 M_1}(\alpha; J_0 M_0, \sigma_1 S_1; \mathbf{k}) &= (2\pi/k)^2 \sum \langle S_1 \mathfrak{N}_1 | J_0 \sigma_1 M_0 S_1 \rangle \\ &\times \langle S'_1 \mathfrak{N}'_1 | J_0 \sigma_1 M_0 S_1 \rangle \langle J_1 M_1 | S_1 l_1 \mathfrak{N}_1 \mu_1 \rangle \langle J_1 M_1 | S'_1 l'_1 \mathfrak{N}'_1 \mu_1 \rangle \\ &\times Y_{l'_i}^{\mu'_i}(\mathbf{k}) Y_{l_i}^{\mu_i}(\mathbf{k}) [\delta_{l_i l'_i} \delta_{S_i S'_i} \\ &- \sum_{\beta l_2 S_2} \eta_{\beta S_2 l_2, \alpha S_1 l_1} \eta_{\beta S_2 l_2, \alpha S_1 l'_1}^*], \end{aligned} \quad (25)$$

with the initial sum over  $l_i, l'_i, S_i, S'_i$ . The final square bracket above represents a generalized transmission coefficient

$$T_{l_i j_i} \equiv (1 - |\eta_{l_i j_i}|^2). \quad (26)$$

On invoking the principle of reciprocity, one can write the total absorption cross section as

$$\sigma_C = \sum_{M_0 S_1} (\hat{J}_0 \cdot \hat{\sigma}_1)^{-1} \cdot \sigma_C(\alpha; J_0 M_0, \sigma_1 S_1; \mathbf{k}) \quad (27)$$

$$\begin{aligned} &= (2\pi/k)^2 \sum (\hat{J}_0 \cdot \hat{\sigma}_1)^{-1} T_{l_i j_i} |Y_{l_i}^{\mu_i}(\mathbf{k})|^2 \\ &\times |\langle j_1 m_1 | l_1 \sigma_1 \mu_1 S_1 \rangle \langle J_1 M_1 | J_0 j_1 M_0 m_1 \rangle|^2, \end{aligned} \quad (28)$$

with summation over  $j_1, l_1, \mu_1, J_1, M_1, M_0, S_1$ . On carrying out the summation over  $M_1, M_0, S_1$ , and  $\mu_1$  in steps, viz.,

$$\sum_{M_1 M_0 (\mu_1, S_1 \text{ const})} |\langle J_1 M_1 | J_0 j_1 M_0 m_1 \rangle|^2 = \hat{J}_1^2 / j_1^2, \quad (29)$$

$$\sum_{S_1 (\mu_1 \text{ const})} |\langle j_1 m_1 | l_1 \sigma_1 \mu_1 S_1 \rangle|^2 = j_1^2 / l_1^2, \quad (30)$$

$$\sum_{\mu_1} |Y_{l_i}^{\mu_i}(\mathbf{k})|^2 = l_i^2 / 4\pi, \quad (31)$$

Eq. (28) reduces to

$$\sigma_C = \pi \lambda^2 \sum_{J_1 l_i j_i} \hat{J}_1^2 (\hat{J}_0 \cdot \hat{\sigma}_1)^{-1} T_{l_i j_i}. \quad (32)$$

Finally, noting that  $\mathbf{J}_1 = \mathbf{J}_0 + \mathbf{j}_1$  it follows that

$$\sum_{J_1} \hat{J}_1^2 = \hat{J}_0^2 \cdot j_1^2, \quad (33)$$

whence

$$\sigma_C = \pi \lambda^2 \sum_{l_i j_i} (j_i^2 / \hat{\sigma}_1^2) T_{l_i j_i}. \quad (34)$$

This reduces, of course, to the usual form

$$\sigma_C = \pi \lambda^2 \sum_{l_i} l_i^2 T_{l_i} \quad (35)$$

when spin-orbit coupling is neglected, for then  $T_{l_i j_i} \rightarrow T_{l_i}$  and since  $\mathbf{j}_1 = \mathbf{l}_1 + \boldsymbol{\sigma}_1$  the sum over  $j_1$  in Eq. (34) can be carried out to yield the result (35), on noting that  $\sum_{j_1} \hat{J}_1^2 = l_i^2 \cdot \hat{\sigma}_1^2$ .

These preliminary considerations enable us now to embark upon formulation of angular correlation theory taking cognizance of spin-orbit interaction.

### 3. THEORETICAL CROSS SECTIONS FOR CN MECHANISM

#### A. Angular Correlation Theory for CN Mechanism (with spin-orbit interaction)

We generalize the current formulation of CN correlation theory as due to Satchler<sup>11,12</sup> following upon the basic approach of Biedenharn and Rose<sup>1</sup> by replacing standard transmission coefficients  $T_l$  by the generalized penetrabilities  $T_{lj}$ . The treatment applies generally to  $(\mathfrak{N}, \mathfrak{N}'\gamma)$  reactions for spin- $\frac{1}{2}$  particles  $\mathfrak{N}, \mathfrak{N}'$  (not necessarily identical) and incorporates an important correction to preceding formulations in that certain interference terms that had previously been erroneously included in the summation are here excluded. This error, which has but recently been detected, invalidates previous calculations of angular correlation<sup>12,13,22-24</sup> for inelastic scattering with the exception of those in Ref. 14, of which more detailed mention will be made at a later stage. It should be mentioned that the alternative approach of combining  $(p, \gamma\gamma)$  correlation parameters as tabulated by Ferguson and Rutledge<sup>25</sup> with suitable particle parameters to obtain values for  $(p, p'\gamma)$  correlation remains valid when interferences are omitted.

In the generalized model of the preceding section, the scattering matrix elements  $\eta_{lj}$  were taken to correspond to the average of the actual  $S$ -matrix elements,

$$\eta_{jl} \equiv \langle S_{aj'l, ajl}^J \rangle, \quad (36)$$

wherein the latter are nonzero only if the  $j$ 's are numerically the same, e.g., formally

$$\langle S_{aj'l', ajl}^J \rangle = 0 \quad \text{if } j \neq j' \text{ or } l \neq l'. \quad (37)$$

The evaluation of the correlation function thus involves incoherent summation over partial waves having not only the same value of  $l$  but the same total angular momentum  $j$  also, viz., it excludes "mixed- $j$ " values  $l + \frac{1}{2}, l - \frac{1}{2}$ . It is typographically convenient and less liable to induce confusion in the calculations if one changes the notation at this stage and writes  $T_{lj}$  as either  $T_l^{(+)}$  or  $T_l^{(-)}$  according as  $j = l \pm \frac{1}{2}$ .

<sup>22</sup> S. Prêtre, H. R. Brugger, and M. P. Steiger, *Helv. Phys. Acta* **33**, 583 (1960).

<sup>23</sup> F. D. Seward, *Phys. Rev.* **114**, 514 (1959).

<sup>24</sup> H. Taketani and W. P. Alford, *Nucl. Phys.* **32**, 430 (1962).

<sup>25</sup> A. J. Ferguson and A. R. Rutledge, Chalk River Report CRP-615, 1957 (unpublished), revised 1962 (CRP-615, AECL-420, revised) (unpublished).

On neglecting spin-orbit interaction, one obtains the usual transmission coefficients  $T_i$  from the above by weighted averaging,

$$T_i = (l^2)^{-1}[(l+1)T_i^{(+)} + lT_i^{(-)}], \quad (38)$$

whence for s waves,  $T_0^{(+)} = T_0^{(-)} = T_0$ . This weighting can be seen to follow from the definition of operators  $\Omega_i^{(+)}$  and  $\Omega_i^{(-)}$  which select the states  $j^{(\pm)} = l \pm \frac{1}{2}$  and  $j^{(-)} = l - \frac{1}{2}$ , respectively, and which may be written

$$\Omega_i^{(+)} = (l^2)^{-1}(l+1 + \boldsymbol{\sigma} \cdot \mathbf{l}); \quad \Omega_i^{(-)} = (l^2)^{-1}(l - \boldsymbol{\sigma} \cdot \mathbf{l}), \quad (39)$$

where  $\boldsymbol{\sigma}$  is the Pauli spin operator of the incident nucleon. Thus,  $\boldsymbol{\sigma} \cdot \mathbf{l} = l$  if spin and orbital momentum are parallel and  $\boldsymbol{\sigma} \cdot \mathbf{l} = -l-1$  if antiparallel. Hence, for  $j^{(+)}$  one finds  $\Omega_i^{(+)} = 1$ ,  $\Omega_i^{(-)} = 0$ , and for  $j^{(-)}$  the converse.

At this stage it may be remarked that the exclusion of "mixed- $j$ " interference terms invalidates not only past calculations of the correlation function, but also influences certain expressions derived therefrom, for example, the derivation of the angular *distribution* of inelastically scattered nucleons by integrating the correlation function over the unobserved  $\gamma$  radiation angle (see Sec. 3B). Calculation of the  $\gamma$  distribution is, of course, unaffected thereby, as will explicitly be shown later.

To derive the double-differential cross section, we now follow Satchler's treatment<sup>11</sup> in considering a reaction sequence of the form  $J_0$  ( $j_i^{(\pm)} = l_i \pm \frac{1}{2}$ )  $J_1$  ( $j_2^{(\pm)} = l_2 \pm \frac{1}{2}$ )  $J_2$  ( $L, L'$ )  $J_3 = J_0$  for the inelastic scattering process. This new notation will henceforth be employed throughout: The  $J$  are nuclear spins,  $j_i^{(\pm)}$ ,  $j_2^{(\pm)}$  are, respectively, total angular momenta of incident and emergent nucleons associated with population of a CN level of spin-parity  $J_1 \pi_1$  under conditions such that the statistical assumption can be deemed to be satisfied. The emergent  $\gamma$  radiation may be of mixed multipolarity  $L$  and  $L'$  in general, with mixing ratio  $\Delta$  and it is assumed that there are no intermediate unobserved radiations, whose presence would otherwise introduce additional normalized Racah functions into the correlation function of the type

$$U_\kappa(L_r J_r J_{r+1}) = (-)^{J_r + J_{r+1} - L_r} \hat{J}_r \cdot \hat{J}_{r+1} \times W(J_r J_r J_{r+1} J_{r+1}; \kappa L_r), \quad (40)$$

wherein the phase factor has been corrected from that quoted by Satchler. Each step of the over-all process furnishes a "linking term" with summation

index  $\mu$ ,  $\nu$ , and  $\lambda$ , respectively, in building up the absolute double-differential cross section,

$$\frac{d^2\sigma}{d\Omega_1 d\Omega_2} \sim W(\theta_1, \theta_2, \varphi) = \text{const} \sum g A_\mu(J_0 J_1) \times R_{\mu\nu\lambda}(J_1 J_2) A_\lambda(J_2 J_3) S_{\mu\nu\lambda}(\theta_1, \theta_2, \varphi) \quad (41)$$

with the summation extended over  $\mu$ ,  $\nu$ ,  $\lambda$  and the various angular momenta involved [of which one is finally left with summation over the momenta  $J_1$  and  $j_2^{(\pm)}$ ]. Biedenharn<sup>3</sup> has given a simple account of the derivation of such linking terms in function of tabulated parameters (e.g., the  $F_\nu$  functions of Biedenharn and Rose<sup>1</sup> or Ferentz and Rosenzweig<sup>26</sup> for  $\gamma$ -ray transitions and the analogous  $\eta_\nu$  functions of Satchler<sup>27</sup> for nucleon transitions). The correlation function thus consists of a sum of the product of such terms weighted by the respective  $g$  factor (the statistical spin factor) as the numerical coefficient of the "Legendre hyperpolynomial"  $S_{\mu\nu\lambda}(\theta_1, \theta_2, \varphi)$ , which contains the entire angular dependence of the correlation function.<sup>28,29</sup>

The explicit form of each term in Eq. (41) is as follows:

(i) The  $g$  factor, which takes account of the multiplicity of spin values entering into the process, figures implicitly in the Hauser-Feshbach treatment of inelastic scattering and has the value

$$g = \hat{J}_1^2 (\hat{s}^2 \cdot \hat{J}_0^2)^{-1} = \frac{1}{2} \hat{J}_1^2 / \hat{J}_0^2, \quad (42)$$

since for nucleons the spin  $s = \frac{1}{2}$ .

(ii) The term dependent on the spins of the first transition is

$$A_\mu(J_0 J_1) = \sum_{j_i^{(\pm)}} |B(j_i^{(\pm)})|^2 \eta_\mu(j_i^{(\pm)}, j_i^{(\pm)}) J_0 J_1 \delta_{(\pm)} \quad (43) \\ = \sum_{j_i^{(\pm)}} |B(j_i^{(\pm)})|^2 (-)^{J_0 - J_1 - \frac{1}{2}} \hat{J}_1^2 j_1^{2(\pm)} \delta_{(\pm)} \\ \times \langle \mu 0 | j_1^{(\pm)}, j_1^{(\pm)} \frac{1}{2} - \frac{1}{2} \rangle W(J_1 J_1 j_1^{(\pm)}, j_1^{(\pm)}; \mu J_0), \quad (44)$$

where  $B(j_i^{(\pm)})$  is a reduced matrix element which is real. The symbol  $\delta_{(\pm)}$  confines the summation to terms where the pairs of  $j$  values are numerically equal, e.g., an incoherent sum of terms with  $j_i^{(+)}$  throughout added to terms with  $j_i^{(-)}$  throughout, with *omission* of mixed terms of the type  $j_i^{(+)} j_i^{(-)}$ .

<sup>26</sup> M. Ferentz and N. Rosenzweig, Argonne Report ANL-5324, 1955 (unpublished).

<sup>27</sup> G. R. Satchler, Proc. Phys. Soc. (London) **A66**, 1081 (1953).

<sup>28</sup> M. E. Rose, Oak Ridge Report ORNL-2516, 1958 (unpublished).

<sup>29</sup> A. J. MacFarlane, Nucl. Phys. **38**, 504 (1962).

(iii) Analogously for the  $\gamma$  transition, assumed to be of mixed multipolarity  $L, L'$  with mixing ratio defined by

$$\Delta^2 \equiv \frac{(J_3 \| L' \| J_2)^2}{(J_3 \| L \| J_2)^2}, \quad (45)$$

the spin-dependent term is

$$A_\lambda(J_2 J_3) = [F_\lambda(LLJ_3J_2) + 2\Delta F_\lambda(LL'J_3J_2) + \Delta^2 F_\lambda(L'L'J_3J_2)]/[1 + \Delta^2], \quad (46)$$

wherein it may be emphasized firstly that the  $F_\lambda$  are always so written that the spin of the intermediate (decaying) state appears last, and secondly that the above  $F_\lambda$  are generalized to take account of mixed multipolarity, with the normalization  $F_0(LL'J_3J_2) = 1$ . Explicitly, the  $F_\lambda$  have the form<sup>3</sup>

$$F_\lambda(LL'J_3J_2) = (-)^{J_3 - J_2 - 1} \hat{L} \hat{L}' \hat{J}_2 \langle \lambda 0 | LL' 1 - 1 \rangle \times W(J_2 J_2 LL'; \lambda J_3). \quad (47)$$

(iv) The coupling term connecting initial and final steps is

$$R_{\mu\nu\lambda}(J_1 J_2) = \sum_{j_2^{(\pm)}} |B(j_2^{(\pm)})|^2 (-)^{j_2^{(\pm)} - \frac{1}{2}} \times \langle \nu 0 | j_2^{(\pm)} j_2^{(\pm)} \frac{1}{2} - \frac{1}{2} \rangle \hat{J}_1 \hat{J}_2 \hat{J}_2^{2(\pm)} \delta_{(\pm)} \times X(J_1 J_1 \mu; j_2^{(\pm)} j_2^{(\pm)} \nu; J_2 J_2 \lambda) \quad (48)$$

in which the final member is a Fano  $X$  coefficient, identical with a Wigner  $9-j$  symbol but written in the above manner for typographical convenience. The  $\delta_{(\pm)}$  operator now restricts the permissible (incoherent) combination of values of  $j_2^{(\pm)}$ : The absence of "mixed- $j$ " interference terms renders the expression slightly more simple than that quoted by Satchler.

In Eqs. (44) and (48), the reduced matrix elements  $B(j)$  represent scattering amplitudes which can be treated by continuum theory on the basis of two underlying assumptions. One first makes the statistical assumption that interferences between CN states, as also between incoming and outgoing partial waves, effectively average to zero; in passing, it should be mentioned that Satchler's expression at the top right of p. 1199 in Ref. 12 should be emended to exclude "mixed- $j$ " interferences, so that in his notation it should read

$$\langle S(J_1; j_2 l_2; j_1 l_1) S^*(J'_1; j'_2 l'_2; j'_1 l'_1) \rangle_{av} = \bar{S}(J_1; j_2 l_2; j_1 l_1) \times \bar{S}^*(J'_1; j'_2 l'_2; j'_1 l'_1) \delta(J_1 J'_1) \delta(j_2 j'_2) \delta(l_1 l'_1) \delta(l_2 l'_2). \quad (49)$$

One secondly assumes that the average transition amplitudes depend only on the transmission co-

efficients  $T_i^{(\pm)}(E)$  at the nucleon energy  $E$  in the c.m. system, whence

$$|B(j_1^{(\pm)})|^2 |B(j_2^{(\pm)})|^2 \rightarrow \tau \equiv T_{i_1}^{(\pm)}(E_1) T_{i_2}^{(\pm)}(E_2) / \sum_{i_1 E} T_{i_1}^{(\pm)}(E) \quad (50)$$

with the summation  $\sum'$  extended over all open channels (including that for elastic scattering) by which the particular compound state  $J_1 \pi_1$  can decay. For typographical convenience, the symbol  $\tau$  will henceforth be employed to denote the oft-recurring expression (50). It is stressed that as used in the above context, the energy  $E$  refers to the energy of the particle in the c.m. system, for example,

$$E_1 = E_{1 \text{ lab}} [M_A / (M_A + M_a)]^2, \quad (51)$$

and *not* to the *total* energy in the c.m. system

$$E_{c.m.} = E_{1 \text{ lab}} M_A / (M_A + M_a) \quad (52)$$

though the difference is usually but slight.

(v) The angular-dependent term  $S_{\mu\nu\lambda}$  is discussed in fuller detail in the Appendix; as shown there, it can be reduced to

$$S_{\mu\nu\lambda}(\theta_1, \theta_2, \varphi) = 4\pi (\hat{\mu}/\hat{\lambda}) \sum_m (-)^m \langle \lambda m | \mu \nu 0 m \rangle \times Y_\nu^{-m}(\theta_1, 0) Y_\lambda^m(\theta_2, \varphi) \quad (53)$$

with  $m$  a summation index running over negative and positive integer values up to the lesser of  $\nu, \lambda$ . This term determines the symmetries of the CN correlation function<sup>17</sup> and on integration over  $\Omega_1$  or  $\Omega_2$  reduces to a simple Legendre polynomial which determines the angular dependence of the angular *distribution* (see Sec. 3B). Explicit values of  $S_{\mu\nu\lambda}$  for various combinations of  $\mu, \nu, \lambda \leq 4$  are given in the Appendix. The indices  $\mu, \nu, \lambda$  take on positive even values in CN correlation theory (when no polarization measurements are simultaneously effected).

The expressions of subsections (i)–(v) can now be substituted into the over-all correlation function (41), which after simplification assumes the form

$$W(\theta_1, \theta_2, \varphi) = \text{const}' \sum [(-)^{J_0 - J_1 - J_2 + J_3 + j_2^{(\pm)}} \times (\hat{J}_1)^4 (\hat{j}_1^{(\pm)})^2 (\hat{j}_2^{(\pm)})^2 \delta_{(\pm)} [\langle \mu 0 | j_1^{(\pm)} j_1^{(\pm)} \frac{1}{2} - \frac{1}{2} \rangle \times \langle \nu 0 | j_2^{(\pm)} j_2^{(\pm)} \frac{1}{2} - \frac{1}{2} \rangle] [W(J_1 J_1 j_1^{(\pm)} j_1^{(\pm)}; \mu J_0)] \times [\hat{L}^2 \langle \lambda 0 | LL 1 - 1 \rangle W(J_2 J_2 LL; \lambda J_3) + 2\Delta \hat{L} \hat{L}' \langle \lambda 0 | LL' 1 - 1 \rangle W(J_2 J_2 LL'; \lambda J_3) + \Delta^2 (\hat{L}')^2 \langle \lambda 0 | L'L' 1 - 1 \rangle W(J_2 J_2 L'L'; \lambda J_3)] \times (1 + \Delta^2)^{-1} \times X(J_1 J_1 \mu; j_2^{(\pm)} j_2^{(\pm)} \nu; J_2 J_2 \lambda) \times \tau \times S_{\mu\nu\lambda}(\theta_1, \theta_2, \varphi), \quad (54)$$

wherein the factor  $(\hat{J}_2)^2/2(\hat{J}_0)^2$  has been absorbed into the constant (hence the prime on the new constant)

and the summation extends over all permitted values of  $\mu, \nu, \lambda, J_1, j_1^{(\pm)}, j_2^{(\pm)}$ . The values are restricted by triangle relations which must be obeyed by the following triads:

$$\begin{aligned} & (j_1^{(\pm)} l_1 \frac{1}{2}), (j_2^{(\pm)} l_2 \frac{1}{2}), (LL'1), (j_1^{(\pm)} J_1 J_0), (J_1 j_2^{(\pm)} J_2), \\ & (J_2 L J_3), (J_2 L' J_3), (j_1^{(\pm)} j_1^{(\pm)} \mu), (J_1 J_1 \mu), (j_2^{(\pm)} j_2^{(\pm)} \nu), \\ & (J_2 J_2 \lambda), (LL\lambda), [(LL'\lambda)], (L'L'\lambda), (\mu\nu\lambda), \end{aligned}$$

wherein the relation in square brackets above applies only if  $\lambda \neq 0$ .

If the multipolarity of the  $\gamma$  transition is pure, then  $L = L', \Delta = 0$ , and the correlation (54) reduces considerably. The value of the constant is arbitrary for a correlation function, which merely expresses the *relative probability* of emission in directions  $\theta_1, \theta_2$  at an azimuth  $\varphi$ , and can accordingly be taken either as unity or, as in the convention employed in construction of correlation surfaces (see Sec. 6), such as to normalize the correlation function to

$$W(\theta_1 = \frac{1}{2} \pi, \theta_2 = \frac{1}{2} \pi, \varphi) = 1. \quad (55)$$

If, however, one expresses the correlation as an absolute double-differential cross section, the constant takes on the numerical value

$$\text{const}' \equiv \frac{(\hat{J}_2)^2}{2(\hat{J}_0)^2} \cdot \text{const} = \frac{\lambda^2}{4} \cdot \frac{(\hat{J}_2)^2}{(\hat{J}_0)^2} \cdot \frac{1}{4\pi} = \frac{\lambda^2}{32\pi} \cdot \frac{(\hat{J}_2)^2}{(\hat{J}_0)^2}, \quad (56)$$

where  $\lambda$  is the reduced wavelength of the incident nucleon (in the c.m. system).

Since all the correlation studies analyzed in Sec. 7 have been confined to even-even target nuclei having a  $0^+$  ground state and  $2^+$  first excited state it is of interest to deduce the double-differential cross section for this special case. This follows directly from (54) and (56) on substituting  $J_0 = J_3 = 0, j_1 = J_1, J_2 = L = 2, \Delta = 0$ , and remembering  $\mu, \nu, \lambda$  to be even,

$$\begin{aligned} W(\theta_1, \theta_2, \varphi) \Big|_{0^+ - 2^+}^{\text{CN}} & \sim \frac{d^2 \sigma}{d\Omega_1 d\Omega_2} \Big|_{0^+ - 2^+}^{\text{CN}} \\ & = \frac{5\lambda^2}{32\pi} \sum \delta_{(\pm)} N C X \tau S_{\mu\nu\lambda} \text{ mb sr}^{-2} \quad (57) \end{aligned}$$

$$= \frac{10.3150}{E_1} \sum \delta_{(\pm)} N C X \tau \cdot S_{\mu\nu\lambda} \text{ mb sr}^{-2}, \quad (58)$$

with  $E_1$  the c.m. energy of the incident nucleon in MeV, the summation extended over  $\mu, \nu, \lambda, J_1, j_2^{(\pm)}$ , and the following abbreviations:

$$N \equiv (-)^{J_1 + j_2^{(\pm)}} (\hat{J}_1)^4 (\hat{J}_2^{(\pm)})^2, \quad (59)$$

$$C \equiv \langle \mu 0 | J_1 J_1 \frac{1}{2} - \frac{1}{2} \rangle \langle \nu 0 | j_2^{(\pm)} j_2^{(\pm)} \frac{1}{2} - \frac{1}{2} \rangle \langle \lambda 0 | 2 2 1 - 1 \rangle, \quad (60)$$

$$X \equiv X(J_1 J_1 \mu; j_2^{(\pm)} j_2^{(\pm)} \nu; 2 2 \lambda), \quad (61)$$

$$\tau \equiv T_{i_1}^{(\pm)}(E_1) T_{i_2}^{(\pm)}(E_2) / \sum_{j_1 E} T_{i_1}^{(\pm)}(E). \quad (62)$$

For each combination of summation parameters permitted by the triangle relations above, the coefficient of the, in itself, quite complicated  $S_{\mu\nu\lambda}$  term involves basically the product of three Clebsch-Gordan coefficients and one 9- $j$  symbol, which have been tabulated in published reports only for fairly low angular momenta.<sup>30-34</sup> It is understandable, therefore, that in the past numerical evaluation of the correlation function by hand has been restricted to  $s$ -,  $p$ -, and  $d$ -incoming and outgoing waves (for  $l_1, l_2 \leq 2$ , there are 59 such permissible combinations; previously when mixed- $j$  terms were still erroneously included the number of combinations was 109). Because of the rapid increase in the number of combinations with rising orbital momentum, as illustrated in Table I, the correlation function for

TABLE I. The number of product terms to be summed over in the correlation function in terms of the highest orbital momentum considered, for nucleons undergoing compound inelastic scattering to the first excited state ( $2^+$ ) of  $e$ -target nuclei.

$l_1, l_2 \leq l_{\text{max}}$ No. of $J_1, j_2^{(\pm)}$ groups	0	1	2	3	4	5	6	7	8	9
No. of product terms	0	3	11	21	31	41	51	61	71	81
	0	10	59	178	383	677	1063	1538	2103	2758

higher partial waves has to be computed electronically, with the program coded to evaluate all the requisite Racah functions and the  $S_{\mu\nu\lambda}$  automatically over a predetermined range of momenta and angles.

It appears opportune at this stage to quote the results of hand calculations of the double-differential cross section for  $e$ - $e$  target nuclei and momenta  $l_1, l_2 \leq 2$  in terms of "measured" transmission coefficients  $T_i$  which do not take spin-orbit interaction into account. With the notation

<sup>30</sup> A. Simon, Oak Ridge Report ORNL-1718, 1954 (unpublished).

<sup>31</sup> K. Smith and J. W. Stevenson, Argonne Report ANL-5776, 1957 (unpublished).

<sup>32</sup> K. Smith, Argonne Report ANL-5860, 1958 (unpublished), Parts I and II.

<sup>33</sup> M. Rotenberg, R. Bivins, N. Metropolis, and J. K. Wooten, Jr., *The 3-j and 6-j Symbols* (Technology Press, Cambridge, Massachusetts, 1959).

<sup>34</sup> J. M. Kennedy, B. J. Sears, and W. T. Sharp, Chalk River Report CRT-569, 1954 (unpublished).

$$\begin{aligned}
 \tau^{(1)} &\equiv \frac{T_0(E_1) \cdot T_2(E_2)}{T_0(E_1) + 2T_2(E_2)}, \\
 \tau^{(2)} &\equiv \frac{T_1(E_1) \cdot T_1(E_2)}{T_1(E_1) + T_1(E_2)}, \\
 \tau^{(3)} &\equiv \frac{T_1(E_1) \cdot T_1(E_2)}{T_1(E_1) + 2T_1(E_2)}, \\
 \tau^{(4)} &\equiv \frac{T_2(E_1) \cdot T_0(E_2)}{T_2(E_1) + T_0(E_2) + 2T_2(E_2)}, \\
 \tau^{(5)} &\equiv \frac{T_2(E_1) \cdot T_2(E_2)}{T_2(E_1) + T_0(E_2) + 2T_2(E_2)}, \quad (63)
 \end{aligned}$$

for the  $\tau$  terms (exit channels being confined to those leading to the ground and first excited states of the target nucleus only) and

$$\begin{aligned}
 x &\equiv \cos \theta_1, \quad y \equiv \cos \theta_2, \\
 z &\equiv \sin \theta_1 \cos \theta_1 \sin \theta_2 \cos \theta_2 = xy[(1-x^2)(1-y^2)]^{1/2}, \quad (64)
 \end{aligned}$$

$$\begin{aligned}
 \omega &\equiv \cos(\mathbf{k}_1, \mathbf{k}_2) = \cos \theta_1 \cos \theta_2 + \sin \theta_1 \sin \theta_2 \cos \varphi \\
 &= xy + (z/xy) \cos \varphi, \quad (65)
 \end{aligned}$$

for the angular terms employed for brevity, one obtains the following expressions which yield numerical values in perfect accord with those obtained by electronic computation:

$$\begin{aligned}
 W(\theta_1, \theta_2, \varphi) &\Big|_{0^+ - 2^+}^{\text{CN}} \sim \frac{d^2 \sigma}{d\Omega_1 d\Omega_2} \Big|_{0^+ - 2^+}^{\text{CN}} \\
 &= (E_1)^{-1} \{ \tau^{(1)} [8.2520 + 4.4207 P_2(\omega) \\
 &\quad - 2.3577 P_4(\omega)] + \tau^{(2)} [4.1260 + 2.0630 P_2(\omega)] \\
 &\quad + \tau^{(3)} [16.5041 - 4.9512 P_2(x) + 4.1260 P_2(y) \\
 &\quad - 0.8821 S_{222} - 1.5781 S_{224}] \\
 &\quad + \tau^{(4)} [20.6301 + 11.1992 P_2(y) - 7.0732 P_4(y)] \\
 &\quad + \tau^{(5)} [41.2602 - 5.2628 P_2(\omega) + 0.8421 P_4(\omega) \\
 &\quad - 5.8944 P_2(x) - 5.3049 P_4(x) - 2.9472 P_2(y) \\
 &\quad + 3.5366 P_4(y) - 4.4495 S_{222} - 1.8403 S_{224} \\
 &\quad + 1.3803 S_{242} + 0.0402 S_{244} + 1.6822 S_{422} \\
 &\quad + 0.6032 S_{424} - 0.4524 S_{442} - 1.3840 S_{444}] \}. \quad (66)
 \end{aligned}$$

The exclusion of "mixed- $j$ " interference terms causes this to differ both in normalization and in numerical magnitude from the corresponding expression quoted by Seward (p. 524 of Ref. 23). On substituting analytical values for the  $S_{\mu\nu\lambda}$  as given in the Appendix with  $\varphi = 0$ , this reduces further to

$$\begin{aligned}
 W(\theta_1, \theta_2, 0) &\Big|_{0^+ - 2^+}^{\text{CN}} \sim \frac{d^2 \sigma}{d\Omega_1 d\Omega_2} \Big|_{0^+ - 2^+}^{\text{CN}} \\
 &= (E_1)^{-1} \{ x^4 y^4 [-82.5204 \tau^{(1)} - 25.0503 \tau^{(5)}] \\
 &\quad + x^4 y^2 [+82.5204 \tau^{(1)} + 53.7847 \tau^{(5)}]
 \end{aligned}$$

$$\begin{aligned}
 &+ x^2 y^4 [+82.5204 \tau^{(1)} - 49.5122 \tau^{(3)} \\
 &\quad - 56.7121 \tau^{(5)}] + x^4 [-10.3151 \tau^{(1)} \\
 &\quad - 42.3651 \tau^{(5)}] + y^4 [-10.3151 \tau^{(1)} \\
 &\quad + 24.7561 \tau^{(3)} - 30.9451 \tau^{(4)} + 40.5233 \tau^{(5)}] \\
 &\quad + x^2 y^2 [-72.2053 \tau^{(1)} + 6.1890 \tau^{(2)} + 49.5122 \tau^{(3)} \\
 &\quad + 40.5233 \tau^{(5)}] + x^2 [+5.1575 \tau^{(1)} - 3.0945 \tau^{(2)} \\
 &\quad - 12.3781 \tau^{(3)} + 25.0503 \tau^{(5)}] + y^2 [+5.1575 \tau^{(1)} \\
 &\quad - 3.0945 \tau^{(2)} - 18.5671 \tau^{(3)} + 43.3232 \tau^{(4)} \\
 &\quad - 34.6289 \tau^{(5)}] + [+10.3151 \tau^{(1)} + 6.1890 \tau^{(2)} \\
 &\quad + 18.5671 \tau^{(3)} + 12.3781 \tau^{(4)} + 35.7342 \tau^{(5)}] \\
 &\quad + x^2 y^2 z [-82.5204 \tau^{(1)} - 25.0503 \tau^{(5)}] \\
 &\quad + x^2 z [+41.2602 \tau^{(1)} + 41.2602 \tau^{(5)}] \\
 &\quad + y^2 z [+41.2602 \tau^{(1)} - 49.5122 \tau^{(3)} \\
 &\quad - 69.2581 \tau^{(5)}] + z [-10.3151 \tau^{(1)} + 6.1890 \tau^{(2)} \\
 &\quad + 24.7561 \tau^{(3)} + 16.2095 \tau^{(5)}] \} \text{ mb sr}^{-2}. \quad (67)
 \end{aligned}$$

This equation is a renormalized form of the expression cited in the Appendix to Ref. 14, wherein the latter took cognizance of exclusion of "mixed- $j$ " interference terms and tacitly corrected an error in a tabulation by Rose<sup>28</sup> which had previously<sup>13</sup> led to a wrong value of  $S_{444}$ . The formula, thus, replaces that previously published by Sheldon.<sup>13</sup> When  $\varphi = \pi$ , as is the case when the de-excitation  $\gamma$  radiation emerges in the scattering plane on the *opposite* side of the incident axis to the inelastically scattered nucleons, the correlation is given numerically from Eq. (67) on replacing either  $\theta_1$  or  $\theta_2$  (but not both) by the supplementary angle, i.e.,  $z \rightarrow -z$ . The corresponding expression for an arbitrary azimuth  $\varphi$  is too involved to be reproduced here, but is directly calculable in any given case from the values of  $S_{\mu\nu\lambda}$  listed in the Appendix.

For the special case when  $\varphi = \frac{1}{2}\pi$ , the double-differential cross section is

$$\begin{aligned}
 W(\theta_1, \theta_2, \frac{1}{2}\pi) &\Big|_{0^+ - 2^+}^{\text{CN}} \sim \frac{d^2 \sigma}{d\Omega_1 d\Omega_2} \Big|_{0^+ - 2^+}^{\text{CN}} \\
 &= (E_1)^{-1} \{ x^4 y^4 [-10.3151 \tau^{(1)} - 142.9374 \tau^{(5)}] \\
 &\quad + x^4 y^2 [+179.0399 \tau^{(5)}] + x^2 y^4 [+90.6259 \tau^{(5)}] \\
 &\quad + x^4 [-49.7333 \tau^{(5)}] + y^4 [-24.7561 \tau^{(3)} \\
 &\quad - 30.9451 \tau^{(4)} + 11.0516 \tau^{(5)}] \\
 &\quad + x^2 y^2 [+15.4726 \tau^{(1)} + 3.0945 \tau^{(2)} \\
 &\quad + 24.7561 \tau^{(3)} - 92.8362 \tau^{(5)}] \\
 &\quad + x^2 [-12.3781 \tau^{(3)} + 11.0519 \tau^{(5)}] \\
 &\quad + y^2 [+6.1890 \tau^{(3)} + 43.3232 \tau^{(4)} - 26.5242 \tau^{(5)}] \\
 &\quad + [+5.1575 \tau^{(1)} + 3.0945 \tau^{(2)} + 18.5671 \tau^{(3)} \\
 &\quad + 12.3781 \tau^{(4)} + 57.1011 \tau^{(5)}] \} \text{ mb sr}^{-2}. \quad (68)
 \end{aligned}$$

From this, the expressions for the correlation when one of the counters detecting the outgoing radiation is arranged to be perpendicular to the incident beam can directly be obtained, viz., the  $n'$ - or  $p'$ -perpendicular correlation

$$W(\frac{1}{2}\pi, \theta_2, \frac{1}{2}\pi) \sim \frac{d^2\sigma}{d\Omega_1 d\Omega_2} (\theta_1 = \varphi = \frac{1}{2}\pi) \Big|_{0^+ - 2^+}^{\text{CN}}$$

follows on setting  $x = 0$ ;  
and the  $\gamma$ -perpendicular correlation

$$W(\theta_1, \frac{1}{2}\pi, \frac{1}{2}\pi) \sim \frac{d^2\sigma}{d\Omega_1 d\Omega_2} (\theta_2 = \varphi = \frac{1}{2}\pi) \Big|_{0^+ - 2^+}^{\text{CN}}$$

follows on setting  $y = 0$ .

It should be mentioned that the expressions so derived replace the numerically incorrect formulas (3) and (4) on p. 810 of Ref. 13 (but do not influence the conclusions drawn there).

### B. Angular Distribution for CN Mechanism (with spin-orbit interaction)

It is interesting to follow the somewhat circuitous method of integrating the angular correlation over the unobserved radiation directions to obtain the angular distribution and total cross section for inelastic nucleon scattering. Agreement of the results with the corresponding expressions provided by straightforward Hauser-Feshbach theory<sup>18</sup> provides some check of the correctness of the correlation expressions from which one starts.

To derive the nucleon distribution, one integrates the general correlation formula (41) over the  $\gamma$  radiation angle  $\theta_2$ , noting in the first place that

$$\int S_{\mu\nu\lambda}(\theta_1, \theta_2, \varphi) d\Omega_2 = \delta_{\mu\nu} \delta_{\lambda 0} \delta_{m_0} 4\pi \hat{\nu} P_\nu(\cos \theta_1), \quad (69)$$

since

$$S_{\nu 0}(\theta_1, \theta_2, \varphi) = \hat{\nu} P_\nu(\cos \theta_1). \quad (70)$$

The influence of the Kronecker  $\delta$ 's on the remaining terms of Eq. (41) is as follows:

$$A_\mu(J_0 J_1) \rightarrow \sum_{j_1^{(\pm)}} |B(j_1^{(\pm)})|^2 \delta_{(\pm)} \eta_\nu(j_1^{(\pm)} j_1^{(\pm)} J_0 J_1), \quad (71)$$

$$R_{\mu\nu\lambda}(J_1 J_2) \rightarrow \sum_{j_2^{(\pm)}} |B(j_2^{(\pm)})|^2 \delta_{(\pm)} (\hat{\nu})^{-1} \eta_\nu(j_2^{(\pm)} j_2^{(\pm)} J_2 J_1), \quad (72)$$

$$A_\lambda(J_2 J_3) \rightarrow F_0 = 1. \quad (73)$$

Hence, on substitution, one obtains

$$\frac{d\sigma}{d\Omega_1} = \int \frac{d^2\sigma}{d\Omega_1 d\Omega_2} d\Omega_2 = \text{const} \sum g \eta_\nu(j_1^{(\pm)} j_1^{(\pm)} J_0 J_1) \times \eta_\nu(j_2^{(\pm)} j_2^{(\pm)} J_2 J_1) 4\pi \delta_{(\pm)} \tau P_\nu(\cos \theta_1), \quad (74)$$

wherein the  $\delta_{(\pm)}$  acts to prevent mixed- $j_1$  and mixed- $j_2$

interferences. Thus, combining the above with Eqs. (42) and (56), one finally obtains the nucleon angular distribution in the Hauser-Feshbach form, generalized to include spin-orbit interaction,

$$\frac{d\sigma}{d\Omega_1} = (\lambda^2/8) \sum [(\hat{J}_1)^2 / (\hat{J}_0)^2] \eta_\nu(j_1^{(\pm)} j_1^{(\pm)} J_0 J_1) \times \eta_\nu(j_2^{(\pm)} j_2^{(\pm)} J_2 J_1) \delta_{(\pm)} \tau P_\nu(x), \quad (75)$$

with the summation extended over all permitted values of  $\nu$ ,  $J_1$ , and  $j_2^{(\pm)}$  (and thus inherently also over  $j_1^{(\pm)}$ ,  $l_1$ , and  $l_2$ ), with exclusion of "mixed- $j$ " terms as an additional physical requirement.

In the derivation of the  $\gamma$  angular distribution, the latter condition automatically follows from the Racah algebra, as one would expect. The integration procedure is analogous to the above, and one has

$$\int S_{\mu\nu\lambda}(\theta_1, \theta_2, \varphi) d\Omega_1 = \delta_{\mu\lambda} \delta_{\nu 0} \delta_{m_0} 4\pi \hat{\lambda} P_\lambda(\cos \theta_2), \quad (76)$$

so that

$$A_\mu(J_0 J_1) \rightarrow \sum_{j_1^{(\pm)}} |B(j_1^{(\pm)})|^2 \eta_\lambda(j_1^{(\pm)} j_1^{(\pm)} J_0 J_1) \delta_{(\pm)}, \quad (77)$$

$$R_{\mu\nu\lambda}(J_1 J_2) \rightarrow \sum_{j_2^{(\pm)}} |B(j_2^{(\pm)})|^2 \delta_{(\pm)} (-)^{j_2^{(\pm)} - J_1 - J_2} \times (\hat{J}_1 \hat{J}_2 / \hat{\lambda}) W(J_1 J_1 J_2 J_2; \lambda j_2^{(\pm)}), \quad (78)$$

$$A_\lambda(J_2 J_3) \rightarrow F_\lambda(J_3 J_2) \equiv [F_\lambda(LLJ_3 J_2) + 2\Delta F_\lambda(LL'J_3 J_2) + \Delta^2 F_\lambda(L'L'J_3 J_2)](1 + \Delta^2)^{-1}, \quad (79)$$

whence finally

$$\frac{d\sigma}{d\Omega_2} = \int \frac{d^2\sigma}{d\Omega_1 d\Omega_2} d\Omega_1 = \frac{\lambda^2}{8} \sum (-)^{j_2^{(\pm)} - J_1 - J_2} \times (\hat{J}_1)^3 (\hat{J}_2) / (\hat{J}_0)^2 \delta_{(\pm)} \eta_\lambda(j_1^{(\pm)} j_1^{(\pm)} J_0 J_1) F_\lambda(J_3 J_2) W \times (J_1 J_1 J_2 J_2; \lambda j_2^{(\pm)}) \tau P_\lambda(y), \quad (80)$$

with the summation over all permitted values of  $\lambda$ ,  $J_1$ , and  $j_2^{(\pm)}$ . The inelastic scattering transition ( $J_1 \rightarrow J_2$ ) thus acts as a "gate" for information pertaining to the  $\gamma$  distribution even though the scattered nucleons are not observed. When the reduced wavelength  $\lambda$  is expressed in cm, the angular distributions have the dimension  $\text{cm}^2 \cdot \text{sr}^{-1}$ .

For the special case of  $e-e$  target nuclei with a  $0+$  ground state and  $2+$  excited state, and when orbital angular momenta are restricted to  $l_1, l_2 \leq 2$ , the expressions can be simplified considerably. For the nucleon distribution, one obtains

$$W(\theta_1) \sim \frac{d\sigma}{d\Omega_1} \Big|_{0^+ - 2^+}^{\text{CN}} = (E_1)^{-1} \{x^4 [-291.497 \tau^{(5)}] + x^2 [-93.279 \tau^{(3)} + 138.808 \tau^{(6)}] + [+103.644 \tau^{(1)} + 51.822 \tau^{(2)} + 238.381 \tau^{(3)} + 259.110 \tau^{(4)} + 530.249 \tau^{(5)}] \} \text{mb sr}^{-1}, \quad (81)$$

and for the  $\gamma$  distribution

$$\begin{aligned}
 W(\theta_2) \sim \frac{d\sigma}{d\Omega_2} \Big|_{0^+ \pm 2^+}^{\text{CN}} &= (E_1)^{-1} \{ y^4 [-388.664 \tau^{(4)} \\
 &+ 194.332 \tau^{(5)} + y^2 [+77.733 \tau^{(3)} + 544.130 \tau^{(4)} \\
 &- 222.095 \tau^{(5)} + [+103.644 \tau^{(1)} + 51.822 \tau^{(2)} \\
 &+ 181.377 \tau^{(3)} + 155.466 \tau^{(4)} \\
 &+ 553.384 \tau^{(5)}] \} \text{ mb sr}^{-1}. \quad (82)
 \end{aligned}$$

It may be mentioned that the relatively tedious derivation of these expressions can be obviated by employing the following "short-cut prescription" once the angular correlation has been evaluated in the form (66). The differential cross section can then straightway be written down:

$d\sigma/d\Omega_1$  follows on multiplying (66) by  $4\pi$  and setting  $P_\nu(\omega) = P_\nu(y) = S_{\mu\nu\lambda} = 0$  therein, with  $(\mu, \nu \neq 0, \lambda = 0)$ ,

$d\sigma/d\Omega_2$  follows on multiplying (66) by  $4\pi$  and setting  $P_\lambda(\omega) = P_\lambda(x) = S_{\mu\nu\lambda} = 0$  with  $(\mu, \lambda \neq 0, \nu = 0)$ .

Theoretical substantiation of this procedure is provided by the fact that

$$\frac{d\sigma}{d\Omega_1} = 4\pi \frac{d^2\sigma}{d\Omega_1 d\Omega_2} \Big|_{\lambda=0} \quad \text{and} \quad \frac{d\sigma}{d\Omega_2} = 4\pi \frac{d^2\sigma}{d\Omega_1 d\Omega_2} \Big|_{\nu=0}, \quad (83)$$

as can directly be verified by carrying out the requisite Racah algebra. The factor of  $4\pi$  as "norm" arises from integration over the angles of the unobserved radiation.

It is of interest to remark that the angular distributions are not identical with the corresponding perpendicular correlations, even when normalized to unity at  $90^\circ$ , although they display very similar angular dependence. This point, already considered,<sup>35</sup> is illustrated graphically in Fig. 34 of the present paper (see Sec. 7E).

### C. Total Inelastic Scattering Cross Section for CN Mechanism (with spin-orbit interaction)

The integration procedure can be carried one step further as a means of obtaining the total inelastic cross section from the distribution function,

$$\sigma = \int \frac{d\sigma}{d\Omega_1} d\Omega_1. \quad (84)$$

One notes that

$$\int P_\nu(\cos \theta_1) d\Omega_1 = \delta_{\nu 0} 4\pi, \quad (85)$$

<sup>35</sup> E. Sheldon, Nucl. Phys. **37**, 302 (1962).

whence

$$\eta_\nu(j_1^{(\pm)} j_1^{(\pm)} J_0 J_1) \eta_\nu(j_2^{(\pm)} j_2^{(\pm)} J_2 J_1) \delta_{(\pm)} \rightarrow \eta_0 \eta_0 = 1, \quad (86)$$

so that

$$\sigma = \frac{1}{2} \pi \lambda^2 \sum_{J_1} [(\hat{J}_1)^2 / (\hat{J}_0)^2] \tau. \quad (87)$$

For momenta  $l_1, l_2 \leq 2$  and  $e-e$  nuclei, this reduces to

$$\begin{aligned}
 \sigma &= (E_1)^{-1} \{ 646.82 \tau^{(1)} + 646.82 \tau^{(2)} + 1293.64 \tau^{(3)} \\
 &+ 3234.10 \tau^{(4)} + 3234.10 \tau^{(5)} \} \text{ mb}. \quad (88)
 \end{aligned}$$

One can readily show that the same results ensue from integration over the  $\gamma$  radiation angle,

$$\sigma = \int \frac{d\sigma}{d\Omega_2} d\Omega_2. \quad (89)$$

### 4. ANGULAR CORRELATION THEORY FOR DI MECHANISM

Since the DWDI treatment of scattering (albeit without the inclusion of spin-orbit coupling) leading to evaluation of the absolute double-differential cross section for nucleon inelastic scattering has recently been published together with computational details in a report by Bassel, Drisko, and Satchler,<sup>16</sup> the present section will be confined to a bare outline of the DWDI approach followed by the requisite details for determination of the double-differential cross section. Apart from the above excellent report, detailed accounts of the application of distorted-wave DI theory have been given by Tobocman<sup>36,37</sup> and by Levinson and Banerjee<sup>38-40</sup>: the above formulation, however, has the additional merit of yielding an absolute quantitative result in the sense that it permits absolute evaluation of the coefficients in the well-known, hitherto arbitrarily normalized correlation expression

$$\begin{aligned}
 W(\theta_1, \theta_2, \pi) \Big|_{\text{DWDI}} \sim &P + Q \sin^2 2(\theta_2 - \theta') \\
 &+ R \sin^2 (\theta_2 - \theta''), \quad (90)
 \end{aligned}$$

wherein the  $\theta_1$  dependence is contained within the entities  $P, Q, R, \theta', \theta''$ . The formula has here been referred to the  $\varphi = \pi$  plane, with the angles  $\theta'$  and  $\theta''$  taken as positive; it could equally well have been referred analytically unchanged to the  $\varphi = 0$  plane

<sup>36</sup> W. Tobocman, *Theory of Direct Nuclear Reactions* (Oxford University Press, Oxford, England, 1961).

<sup>37</sup> G. R. Satchler and W. Tobocman, Phys. Rev. **118**, 1566 (1960).

<sup>38</sup> C. A. Levinson and M. K. Banerjee, Ann. Phys. **2**, 471 (1957); **3**, 67 (1958).

<sup>39</sup> M. K. Banerjee and C. A. Levinson, Ann. Phys. **2**, 499 (1957).

<sup>40</sup> C. A. Levinson, in *Nuclear Spectroscopy*, edited by F. Ajzenberg-Selove (Academic Press Inc., New York, 1960), Part B, p. 670.

with  $\theta'$  and  $\theta''$  taken as *negative* (as in Ref. 17), or alternatively written in the form

$$W(\theta_1, \theta_2, 0) \Big|^{DWDI} \sim P + Q \sin^2 2(\theta_2 + \theta') + R \sin^2 (\theta_2 + \theta''), \quad (91)$$

where now  $\theta'$  and  $\theta''$  are taken as *positive*. It is, of course, clear that

$$W(\theta_1, \theta_2, 0) \Big|^{DWDI} = W(\theta_1, \pi - \theta_2, \pi) \Big|^{DWDI} \neq W(\theta_1, \theta_2, \pi) \Big|^{DWDI}. \quad (92)$$

Further DWDI symmetries will be discussed later; it suffices for the present to mention that it is permissible to add  $\pm \frac{1}{2} \pi$  to  $\theta'$  and  $\pm \pi$  to  $\theta''$  without influencing the correlation.

The result analogous to Eq. (90) as deduced by Satchler *et al.* for inelastic scattering of nucleons on  $e-e$  target nuclei with orbital momentum transfer  $l = 2$  is

$$\frac{d^2 \sigma}{d\Omega_1 d\Omega_2} \Big|_{0^+ - 2^+}^{DWDI} \sim W(\theta_1, \theta_2, \pi) \sim [(\alpha + y\beta) + (1 - \frac{2}{3}y) \times \sin^2 2(\theta_2 - \theta') + y\gamma \sin^2 (\theta_2 - \theta'')], \quad (93)$$

where  $y$ , the ratio of spin-flip to non-spin-flip intensity, represents the only indeterminate parameter at the present stage of DWDI theory. For scattering of spinless particles, such as  $\alpha$  particles, one would have  $y = 0$  and the simple expression

$$\frac{d^2 \sigma}{d\Omega_1 d\Omega_2} \Big|_{y=0}^{DWDI} \sim W(\theta_1, \theta_2, \pi) \Big|_{y=0}^{DWDI} = N[\alpha + \sin^2 2(\theta_2 - \theta')]. \quad (94)$$

The terms  $\alpha$ ,  $\beta$ ,  $\gamma$  can be computed numerically from DWDI codes which evaluate statistical tensors and their phases  $\theta'$ ,  $\theta''$  from transition amplitudes which lie at the basis of DWDI theory. For the present analysis, the IBM 7090 code "SALLY" compiled at the Oak Ridge National Laboratory was employed to evaluate these quantities in function of the scattering angle  $\theta_1$  and these in turn were fed into the DWDI correlation program "MARILYN," coded to calculate the double-differential cross section numerically. The only drawback of the code "SALLY," which itself evaluates the differential cross section  $d\sigma/d\Omega_1$  in function of  $\theta_1$ , lies in the fact that it does not incorporate spin-orbit coupling. A program to obviate this is, at present, in the process of compilation.

Omitting any assumptions as to the reaction mechanism, one can write the angular correlation in terms of normalized spherical harmonics  $C_{kq}(\theta_2, \varphi) = (4\pi)^{\frac{1}{2}} (\hat{k})^{-1} Y_k^q(\theta_2, \varphi)$  such that  $C_{00} = 1$  as

$$W(\theta_1, \theta_2, \varphi) = \sum_{kq} a_{kq}(\theta_1) C_{kq}(\theta_2, \varphi), \quad (95)$$

wherein since  $W$  is real, the  $a_{kq}$  have the symmetry  $a_{kq} = (-)^q a_{k-q}^*$  and vanish for odd values of  $k$  when the  $\gamma$  transition is between states of definite parity. In the coordinate system employed here, with  $z$  axis along  $\mathbf{k}_0$ ,  $y$  axis along  $\mathbf{k}_0 \times \mathbf{k}_1$ , and  $x$  axis in the scattering plane (where  $\mathbf{k}_0$  and  $\mathbf{k}_1$  represent propagation vectors of the incident and scattered particle, respectively), the  $a_{kq}$  are real in order that the azimuthal symmetry  $W(\theta_1, \theta_2, \varphi) = W(\theta_1, \theta_2, -\varphi)$  be preserved. For a DWDI scattering mechanism, the coefficients  $a_{kq}$  can be separated further into three factors,

$$a_{kq}(\theta_1) = b_k \cdot F_k(J_3 J_2) \cdot d_{kq}(\theta_1), \quad (96)$$

where  $b_k$  is a coefficient which depends on the momentum transfer  $\mathbf{j} = \mathbf{1} + \mathbf{s}$  to the target nucleus, with  $\mathbf{s} = \mathbf{0}$  for nucleon scattering,

$$b_k = (-)^{J_0 - J_2} \hat{l}^2 \hat{J}_2 \langle k0 || U00 \rangle W(l J_2 J_2; k J_0). \quad (97)$$

The  $\gamma$ -transition link  $F_k(J_3 J_2)$  has been defined by Eqs. (46), (47), and (79). The term  $d_{kq}(\theta_1)$  is a normalized statistical tensor described in detail elsewhere,<sup>15,37,41</sup> viz.,

$$d_{kq}(\theta_1) = [(-)^q \langle k0 || U00 \rangle]^{-1} \rho_{kq}(l_j, l_j) / \rho_{00}(l_j, l_j), \quad (98)$$

such that  $d_{00} = 1$ . One then normalizes to  $a_{00} = 1$ . Satchler *et al.*<sup>15</sup> used a different coordinate system (characterized here by a "tilde") and expressed the correlation parameters  $\alpha$ ,  $\beta$ ,  $\gamma$ ,  $\theta'$ ,  $\theta''$  in terms of the values of the statistical tensors  $\tilde{d}_{kq}$  in that system, wherein  $\mathbf{k}_0$  was chosen as  $\tilde{x}$  axis and  $\mathbf{k}_0 \times \mathbf{k}_1$  as  $\tilde{z}$  axis:

$$\alpha = [0.17430(1 - \tilde{d}_{20}) / |\tilde{d}_{44}|] - \frac{1}{2}, \quad (99)$$

$$\beta = [0.34867(1 + 0.81652|\tilde{d}_{22}|) / |\tilde{d}_{44}|] + \frac{1}{3}, \quad (100)$$

$$\gamma = -0.56932|\tilde{d}_{22}| / |\tilde{d}_{44}|. \quad (101)$$

At  $\tilde{\theta}_1 = 0^\circ$  or  $180^\circ$ , these revert to their plane-wave DI values,

$$\alpha = 0, \quad \beta = \frac{4}{3}, \quad \gamma = -\frac{2}{3}. \quad (102)$$

The angles  $\theta'$  and  $\theta''$  (in our system) were expressed as phase angles,

$$\tilde{d}_{22} = |\tilde{d}_{22}| \exp(-2i\theta''), \quad (103)$$

$$\tilde{d}_{44} = |\tilde{d}_{44}| \exp(-4i\theta'), \quad (104)$$

and computed in terms of the scattering angle  $\theta_1$ .

The double-differential cross section can now be evaluated absolutely; for simplicity we assume the spin-flip intensity to be zero, so that the correlation is of the form (94). The value of  $N$  follows on noting

<sup>41</sup> B. Buck and P. E. Hodgson, *Phil. Mag.* **6**, 1371 (1961).

that the actual expression for  $W$  is, as can be shown,

$$W(\theta_1, \theta_2, \pi) \Big|_{\nu=0}^{\text{DWDI}} = [(5/8)(1 - \tilde{d}_{20}) - (45/14)^{\frac{1}{2}} |\tilde{d}_{44}|] \\ + (90/7)^{\frac{1}{2}} |\tilde{d}_{44}| \sin^2 2(\theta_2 - \theta'), \quad (105)$$

that is,

$$W(\theta_1, \theta_2, \pi) \Big|_{\nu=0}^{\text{DWDI}} = (90/7)^{\frac{1}{2}} |\tilde{d}_{44}| \\ \times \left\{ \frac{1}{2} \left[ \frac{(35)^{\frac{1}{2}} (1 - \tilde{d}_{20})}{12\sqrt{2} |\tilde{d}_{44}|} - 1 \right] + \sin^2 2(\theta_2 - \theta') \right\}, \quad (106)$$

which determines the value of  $N$  as

$$N = (90/7)^{\frac{1}{2}} |\tilde{d}_{44}| = 3.5858 |\tilde{d}_{44}|. \quad (107)$$

The double-differential cross section is related to the correlation as follows:

$$\frac{d^2\sigma}{d\Omega_1 d\Omega_2} (\varphi = \pi) \Big|_{\nu=0}^{\text{DWDI}} = c \cdot \frac{d\sigma}{d\Omega_1} \cdot W(\theta_1, \theta_2, \pi) \Big|_{\nu=0}^{\text{DWDI}}, \quad (108)$$

where the constant  $c$  is given from

$$\frac{d\sigma}{d\Omega_1} = \int \frac{d^2\sigma}{d\Omega_1 d\Omega_2} \cdot d\Omega_2 = c \frac{d\sigma}{d\Omega_1} \int W \cdot d\Omega_2 \\ = c \frac{d\sigma}{d\Omega_1} \int \sum a_{kq} C_{kq}(\theta_2, \varphi) = 4\pi c a_{00} \frac{d\sigma}{d\Omega_1}, \quad (109)$$

as

$$c = (4\pi)^{-1}, \quad (110)$$

since  $a_{00} = 1$ .

It only remains to note that the code "SALLY" evaluates a quantity  $\sigma(\theta_1)$  which is related to the nucleon scattering differential cross section,

$$\frac{d\sigma}{d\Omega_1} = (V\beta_D r_0 A^{\frac{1}{3}})^2 (5093a^2)^{-1} \cdot \sigma(\theta_1) \text{ mb sr}^{-1}. \quad (111)$$

Here,  $V$  is the real optical potential in MeV,  $\beta_D$  is the nuclear deformation parameter,  $r_0 A^{\frac{1}{3}}$  the nuclear radius, and  $a$  the diffuseness of the real optical potential well. Substituting Eqs. (93), (94), (107), (110), and (111) in (108), we finally arrive at the relation

$$\frac{d^2\sigma}{d\Omega_1 d\Omega_2} (\varphi = \pi) \Big|_{0^+ - 2^+}^{\text{DWDI}} = 5.6025 \times 10^{-5} |\tilde{d}_{44}| \\ \times (V\beta_D r_0 A^{\frac{1}{3}}/a)^2 \sigma(\theta_1) [(\alpha + y\beta) + (1 - \frac{2}{3}y) \\ \times \sin^2 2(\theta_2 - \theta') + y\gamma \sin^2(\theta_2 - \theta'')] \text{ mb sr}^{-2}, \quad (112)$$

expressing the double-differential cross section in terms of nuclear constants and computed parameters. The latter then represent the input for the code "MARILYN," which for a given  $\theta_1$  and for selected values of the relative spin-flip intensity  $y$  numerically evaluates the double-differential cross section for a range of values of  $\theta_2$ .

The quantitative evaluation of the double-differential cross section for the DWDI as well as for the CN mechanism offers a means of attempting to combine the respective predictions of these two theories in order to investigate correlation behaviour in the intermediate energy region. One thereby encounters the problem of the possibility of interference between CN and DI mechanisms, the extent of which is basically governed by the sharpness of the beam energy, a factor which cannot *a priori* be incorporated in the theoretical treatment. In the paper of Chase, Wilets, and Edmonds,<sup>20</sup> an excitation function was constructed by simple addition of CN and DI cross sections, thereby assuming interference to be absent; this simplifying assumption was also made by Satchler and Sheldon<sup>14</sup> in analyzing the  $\text{Ni}^{58}(p, p'\gamma)$  correlation measurements of Taketani and Alford<sup>25</sup> at  $E_p = 5.73 \text{ MeV}_{\text{c.m.}}$  (see Fig. 54). An alternative method of combination is to introduce a phase factor  $\epsilon$  (which varies with experimental conditions) and to define the net cross section as

$$\sigma = |\sigma_{\text{CN}}^{\frac{1}{2}} + e^{i\epsilon} \sigma_{\text{DI}}^{\frac{1}{2}}|^2. \quad (113)$$

Austern<sup>42</sup> has summarized the present status of these theoretical approaches; in the approach of Sano *et al.*,<sup>43</sup> choice of a suitable potential matrix obviates interferences between CN and DI in the formalism.

The DWDI angular distribution of  $\gamma$  radiation can be elucidated from Eq. (95) on averaging over the nucleon angular distribution,

$$W(\theta_2) = \sum_{k \text{ even}} \langle d_{k0} \rangle P_k(\cos \theta_2), \\ = \sum_{k \text{ even}} b_k F_k(J_3 J_2) \langle d_{k0} \rangle P_k(\cos \theta_2), \quad (114)$$

where  $\langle d_{k0} \rangle$ , the value of the tensor  $d_{k0}$  averaged over the nucleon distribution, cannot easily be derived from the present theory, though Satchler and Tobocman<sup>37</sup> have indicated how it may be estimated. On averaging in azimuth around the incident beam, the  $d_{kq}$  with nonzero  $q$  vanish, of course. Equation (114) indicates that the  $\gamma$  distribution for the DWDI mechanism is, as for the CN mechanism, symmetrical about  $\theta_2 = \frac{1}{2}\pi$ , since the Legendre polynomials run over *even* values of  $k$ .

It may also be remarked that for nucleon inelastic scattering, as for other direct interactions, the re-

<sup>42</sup> N. Austern, in *Selected Topics in Nuclear Theory*, edited by F. Janouch (International Atomic Energy Agency, Vienna, 1963). See also S. Yoshida, in *Proceedings of the International Conference on Nuclear Structure, Kingston*, edited by D. A. Bromley and E. W. Vogt (University of Toronto Press, Toronto, Canada, 1960), p. 336.

<sup>43</sup> M. Sano, S. Yoshida, and T. Terasawa, *Nucl. Phys.* **6**, 20 (1958).

mark of Ferguson *et al.*,<sup>44</sup> suggesting that nucleon distribution measurements could, in certain cases, be facilitated by detecting the desired nucleon group in coincidence with de-excitation  $\gamma$  rays emitted perpendicular to the reaction plane, since the distribution when only one  $l$ -value contributes is identical to the perpendicular correlation, has to be restricted.

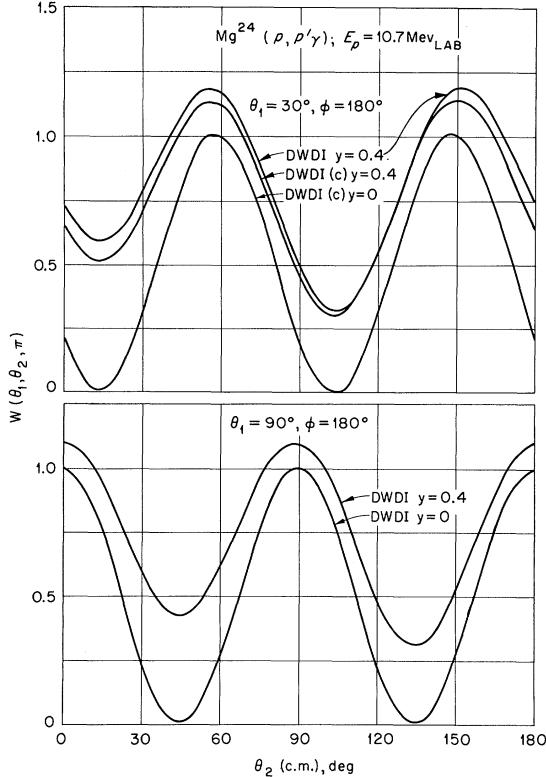


Fig. 2. Distorted-wave direct interaction correlation functions for the reaction  $Mg^{24}(p, p'\gamma)Q - 1.368 \text{ MeV}$  at an incident proton energy of 10.7 MeV. Comparison between theoretical results with and without consideration of spin-flip and those for strong-coupling theory.

The same reasons as those which prompted the comment of Satchler and Toboeman<sup>37</sup> in the case of deuteron stripping apply to DWDI nucleon scattering, with the result that the above statement holds only for  $l = 0$  or 1 but not for  $l \geq 2$ . In the "tilde" coordinate system the correlation can be written as

$$W(\tilde{\theta}_1, \tilde{\theta}_2, \tilde{\varphi}) = \sum_{kq} b_k \cdot F_k(J_3 J_2) \cdot \tilde{d}_{kq} C_{kq}(\tilde{\theta}_2, \tilde{\varphi}), \quad (115)$$

which, for the perpendicular correlation where  $\tilde{\theta}_2 = 0$ , reduces to

$$W(\tilde{\theta}_1, \tilde{\theta}_2 = 0, \tilde{\varphi}) = \sum_k b_k \cdot F_k(J_3 J_2) \tilde{d}_{k0} \quad (116)$$

<sup>44</sup> A. J. Ferguson, H. E. Gove, A. E. Litherland, and R. Batchelor, *Bull. Am. Phys. Soc.* **5**, 45 (1960).

on expanding the spherical harmonic  $C_{kq}(\theta_2, \tilde{\varphi})$  in terms of Legendre functions, of which the  $q = 0$  term becomes unity on setting  $\theta_2 = 0$  and the remainder vanish. Now, only for  $l = 0$  or  $l = 1$  are the  $\tilde{d}_{k0}$  independent of scattering angle (the tensors assume their plane-wave values  $\tilde{d}_{00} = 1$ ,  $\tilde{d}_{20} = -\frac{1}{2}$ ). The values of  $\tilde{d}_{k0}$  for  $l = 2$  transfers of orbital momentum are given explicitly in the report of Satchler *et al.*<sup>15</sup>; inserting them into Eq. (116) renders it  $\theta_1$ -dependent. In the latter case, the perpendicular correlation is given by the noncoincidence distribution modulated by the  $\theta_1$ -dependent expression (116). This offers a means of measuring the  $\tilde{d}_{k0}$  in function of  $\theta_1$  for comparison with theory, though no such measurements have so far been carried out at energies where the DI mechanism would be expected to prevail.

It should also be mentioned that as a check on the correlation parameters furnished by the code "SALLY" (omitting consideration of spin-orbit interaction) a set of computations was undertaken to evaluate these for inelastic proton scattering on  $Mg^{24}$  at energies between 5 and 17 MeV using a strong-coupling computer program by Buck which includes spin-orbit coupling for deformed nuclei. Results for 10.7 MeV, as shown in Figs. 2 and 19, were found to be practically identical with those from "SALLY." The distinction between this approach and the normal DWDI treatment lies in the fact that the former does *not* treat the residual interaction of the incident particle with the target nucleus as a perturbation; in consequence, the inelastic scattering can, as it is in fact often found to do, appreciably influence the elastic cross sections. Buck has given<sup>10</sup> details of the theoretical treatment and set up a code which strongly couples a  $0+$  ground state to a  $2+$  first excited state to furnish tensor parameters which can be used as input for "MARILYN." Since his code evaluates the inelastic differential cross section  $d\sigma/d\Omega_1$  directly, the normalization of the double-differential cross section is simplified, namely,

$$\begin{aligned} \frac{d^2\sigma}{d\Omega_1 d\Omega_2}(\varphi = \pi) \Big|_{0^+ - 2^+}^{\text{str. coupl.}} &= c \cdot \frac{d\sigma}{d\Omega_1} \cdot W(\theta_1, \theta_2, \pi) \quad (117) \\ &= 0.2854 |\tilde{d}_{44}| (d\sigma/d\Omega_1) [(\alpha + y\beta) + (1 - \frac{2}{3}y) \\ &\quad \times \sin^2(\theta_2 - \theta') + y\gamma \sin^2(\theta_2 - \theta'')] \text{ mb sr}^{-2}. \quad (118) \end{aligned}$$

Although the coupled equations approach yielded correlation results in excellent agreement with the normal DWDI treatment, the fit to experimental results was found to be poor: only in one instance

was there even fair agreement between experiment and theory. This is depicted in Fig. 3 for a relative spin-flip intensity of  $y = 0.45$ . The measurements are those of Braid, Yntema, and Zeidman,<sup>45</sup> who also studied correlations with the proton counter fixed at  $\theta_1 = 30^\circ$  and  $60^\circ$  (additional measurements at  $\theta_1 = 120^\circ$  and  $150^\circ$  have been mentioned<sup>46</sup> but not illustrated). At these angles the theoretical fit is poor—far worse than the “semiempirical” fit obtained with arbitrarily selected parameters introduced into the DWDI correlation expression, as depicted in Fig. 4.

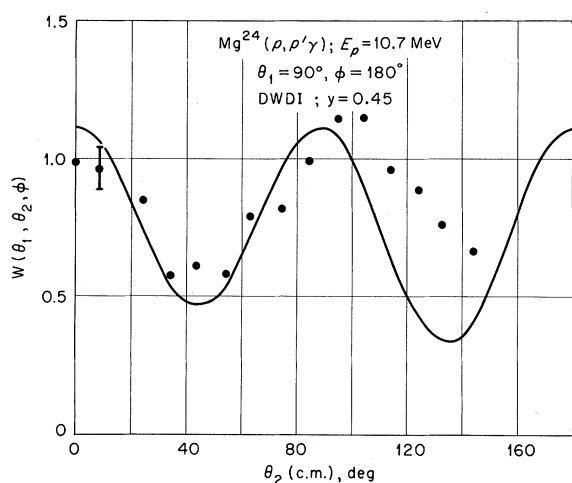


Fig. 3. Comparison of the experimental results of Braid, Yntema, and Zeidman (Ref. 45) for  $Mg^{24}(p, p'\gamma)$  at 10.7 MeV with the theoretical correlation function including spin-flip for  $\theta_1 = 90^\circ$ .

The positions of maxima and minima in the DWDI correlation are, of course, determined by  $\theta'$  and  $\theta''$ ; the poor fitting of experimental results arises essentially from disagreement between the computed angles and those arbitrarily selected to give an empirical fit. In Figs. 2 and 4, for instance, the theoretical values of  $\theta'$  and  $\theta''$  are for  $\theta_1 = 30^\circ$ , respectively,  $14^\circ$  and  $12^\circ$ ; for  $\theta_1 = 60^\circ$ , respectively,  $29^\circ$  and  $29^\circ$ ; and for  $\theta_1 = 90^\circ$ , respectively,  $45^\circ$  and  $43^\circ$ . The relative amplitude of the peaks, on the other hand, can be varied by altering the (at present) unknown magnitude  $y$  of spin-flip intensity; Fig. 5

<sup>45</sup> T. H. Braid, J. L. Yntema, and B. Zeidman, *Bull. Am. Phys. Soc.* **6**, 37 (1961).

<sup>46</sup> T. H. Braid, J. L. Yntema, and B. Zeidman, in *Proceedings of the Rutherford Jubilee International Conference*, edited by J. E. Birko (Heywood and Company, Ltd., Manchester, England, 1962), p. 519.

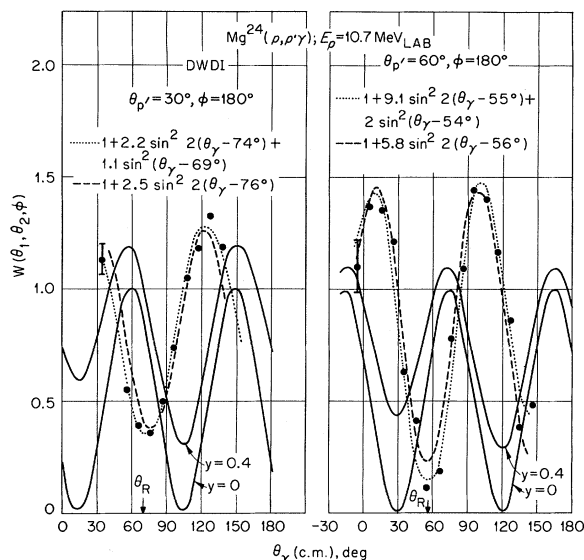


Fig. 4. Comparison between semiempirical and absolute theoretical DWDI fits to the results of Braid, Yntema, and Zeidman (Ref. 45) at  $\theta_1 = 30^\circ$  and  $60^\circ$ . In both cases curves with and without spin-flip terms are shown.

provides an illustration of the influence of relative spin-flip intensity upon the DWDI correlation. Had the DWDI correlation graphs had phases in accord with the measured correlation, one would have had the means at hand to determine the magnitude  $y$  empirically by elucidating the values which furnish closest agreement with experiment. It should also be possible to determine this experimentally from the scattering of polarised nucleon beams from aligned targets. However, in the absence of such results,  $y$

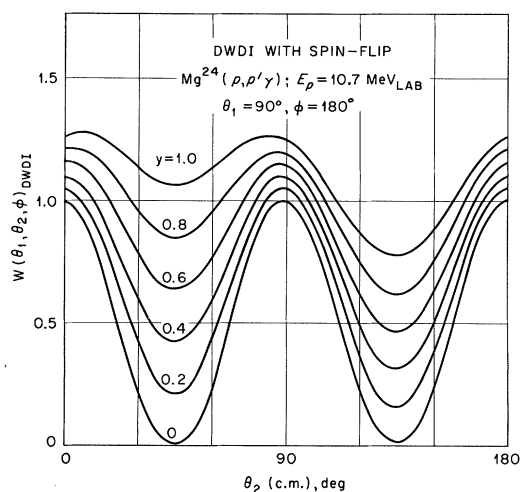


Fig. 5. Influence of the relative magnitude of spin-flip upon the DWDI correlation function at  $\theta_1 = 90^\circ$  for the reaction  $Mg^{24}(p, p'\gamma)$  at 10.7 MeV.

was arbitrarily taken as zero and 0.4 throughout the present analysis. There are indications of the manner in which it may vary with scattering angle. Satchler *et al.*<sup>47</sup> have considered the possibility of spin-independent excitations showing some collective enhancement, while this is generally negligible for spin-flip transitions, and in consequence having a different effective interaction matrix element between initial and final nuclear states. On constructing the ratio  $R_1(\theta_1)$  of differential cross sections for "single-particle" transitions (those in which the angular momentum transfer is due to single-particle transitions between nuclear orbits induced by a zero-range two-body force; the matrix element then peaks within the nucleus) to that for "collective" transitions (surface coupling described by an optical potential), one obtains an indication of the possible differences between spin-flip and spin-independent distributions in function of the scattering angle. This ratio could then be interpreted as the variation of  $y$  with  $\theta_1$ . It has been evaluated<sup>47</sup> for the  $\text{Mg}^{24}(p, p'\gamma)$  reaction at 16.6 MeV for  $l = 2$  momentum transfer and is reproduced as Fig. 6.

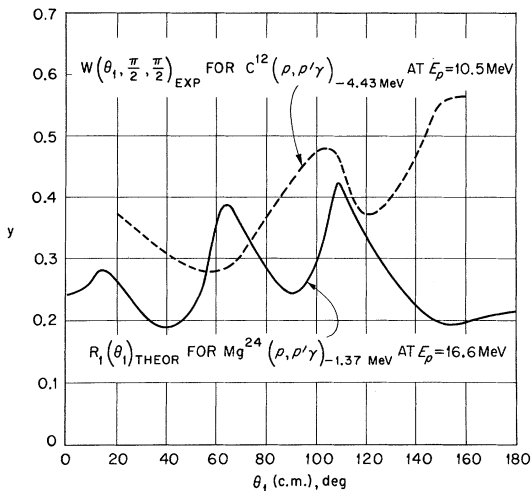


FIG. 6. Estimated relative magnitude of the spin-flip magnitude for inelastic proton scattering on  $\text{C}^{12}$  ( $Q = -4.43$  MeV) at 10.5 MeV and on  $\text{Mg}^{24}$  ( $Q = -1.368$  MeV) at 16.6 MeV.

Satchler's spin-flip ratio fluctuates about a rough mean of 0.3, in reasonably good agreement with the experimental results of Schmidt, Gerhart, and Kolasinski<sup>48</sup> for the spin-flip magnitude in the  $\text{C}^{12}(p, p'\gamma)_{Q = -4.43}$  MeV reaction at  $E_p = 10.5$  MeV<sub>lab</sub>,

<sup>47</sup> G. R. Satchler, R. M. Drisko, and R. H. Bassel, *Bull. Am. Phys. Soc.* **6**, 66 (1961).

<sup>48</sup> F. H. Schmidt, J. B. Gerhart, and W. A. Kolasinski, *Bull. Am. Phys. Soc.* **7**, 60 (1962).

which has also been included in Fig. 6. Employing a basically different approach to derive an estimate of the magnitude of  $y$ , these authors obtained values ranging from 0.28 to 0.58, fluctuating about a mean of 0.4. Noting that for the above reaction, emission of de-excitation  $\gamma$  radiation in the direction  $\theta_2 = \varphi = \frac{1}{2}\pi$  can occur only if proton spin-flip takes place,<sup>49</sup> they measured  $\gamma$ -perpendicular correlations for  $\theta_1$  varying from  $20^\circ$  to  $160^\circ$  and interpreted these when appropriately normalized as spin-flip magnitudes in function of  $\theta_1$ , with a possible error of  $\pm 7\%$ . This interpretation rests, of course, on the assumption of pure DWDI mechanism and absence of interference terms in the correlation function for the perpendicular correlation; it should therefore be treated with caution. The results, however, furnish some substantiation that the value of  $y = 0.4$  adopted for the present analysis is not unreasonable.

As a preliminary to presentation of the remaining correlation analysis, some details underlying the calculations are given next.

## 5. EVALUATION OF THE CORRELATION FUNCTION

### A. Choice of Optical Model

As a basis for the numerical evaluation of the correlation function, the nonlocal optical model of Perey and Buck<sup>4</sup> was employed for neutron scattering and the local optical model of Perey<sup>9</sup> for proton scattering unless otherwise stated. The parameters represent results of the most recent analysis of scattering cross sections; the neutron nonlocal potential, in particular, represents a marked fundamental advance upon the various local potentials hitherto proposed,<sup>5-7</sup> and also upon the nonlocal "effective mass approximation" treatment of Wyatt, Wills, and Green,<sup>8</sup> since this approximation can be justified only at low neutron energies. Using an IBM 7090 computer for numerical integration and iteration, Perey and Buck were able to bypass the need for such approximations and, thus, to derive an exact solution to the nonlocal Schrödinger equation for neutron scattering, a spin-orbit term of the Thomas form being included:

$$\left[ \left( \frac{\hbar^2}{2\mu} \right) \nabla^2 + E \right] \psi(\mathbf{r}) + \left\{ \left( \frac{\hbar}{2M_{sc}} \right)^2 (ar)^{-1} \right. \\ \times \left[ \exp \left( \frac{r-R}{a} \right) \right] \left[ 1 + \exp \left( \frac{r-R}{a} \right) \right]^{-2} \\ \left. \times V_{sc} \mathbf{L} \cdot \boldsymbol{\sigma} \right\} \psi(\mathbf{r}) = \int V(\mathbf{r}, \mathbf{r}') \psi(\mathbf{r}') d\mathbf{r}'. \quad (119)$$

<sup>49</sup> A. Bohr, *Nucl. Phys.* **10**, 486 (1959).

By choosing the denominator of the first coefficient in the Thomas term as  $2 M_n c$  in place of the usual  $M_n c$ , the authors obtained a value of 1300 MeV for the real spin-orbit potential  $V_{so}$ , which corresponds to about 7 MeV in the usual normalization. The imaginary spin-orbit potential was, in conformity with current normal practice, taken as zero. The other symbols in Eq. (119) carry their usual significance, with  $\mathbf{r}$  as coordinate vector of the incident and  $\mathbf{r}'$  as coordinate vector of the scattering particle referred to the center of mass of the system. The scattering force is thus treated as a finite-range two-body interaction. For numerical convenience, the symmetrical kernel  $V(\mathbf{r}, \mathbf{r}')$  was split into the product of two functions, the first of which corresponds to the usual optical potential wherein the local coordinate  $\mathbf{r}$  is replaced by a "nonlocal mean" coordinate  $^{50} \frac{1}{2}|\mathbf{r} + \mathbf{r}'|$ , and the second a modifying factor to take account of the nonlocality,

$$V(\mathbf{r}, \mathbf{r}') = U(\frac{1}{2}|\mathbf{r} + \mathbf{r}'|)H(|\mathbf{r} - \mathbf{r}'|/\rho). \quad (120)$$

The function  $H$  involves the range  $\rho$  of the nonlocality and has been taken to be of Gaussian form with the normalization  $\int H d\mathbf{r}' = 1$ ,

$$H\left(\frac{|\mathbf{r} - \mathbf{r}'|}{\rho}\right) = \frac{1}{(\rho\pi^{\frac{1}{2}})^3} \exp\left[-\left(\frac{\mathbf{r} - \mathbf{r}'}{\rho}\right)^2\right]. \quad (121)$$

The complex optical potential was taken as combination of a real Woods-Saxon potential with an imaginary Saxon derivative potential corresponding to surface absorption,

$$U = V\{1 + \exp[(\frac{1}{2}|\mathbf{r} + \mathbf{r}'| - R)/a]\} \\ + 4iW'\{\exp[(\frac{1}{2}|\mathbf{r} + \mathbf{r}'|)/a']\} \\ \times \{1 + \exp[(\frac{1}{2}|\mathbf{r} + \mathbf{r}'|)/a']\}^{-2}. \quad (122)$$

On expanding the wave functions  $\psi(\mathbf{r})$ ,  $\psi(\mathbf{r}')$  and the kernel  $V(\mathbf{r}, \mathbf{r}')$  in partial waves, the authors obtained a radial wave equation which could be solved exactly to obtain scattering phase shifts and, thence, transmission coefficients or theoretical nuclear cross sections. The set of nonlocal optical parameters determined from analysis of experimental angular distributions for the elastic scattering of 7 MeV and 14.5 MeV neutrons on lead<sup>51,52</sup> was found to give universally good agreement between theoretical and experimental cross section, polarization, and strength function results for other target nuclei ranging from

Al to Pb and for other incident energies in the range 0.4–24 MeV when a correction was made for compound-elastic scattering below about 4 MeV. These parameters come out as

$$V = 71 \text{ MeV}, \quad r_0 = 1.22 \text{ F}, \quad a = 0.65 \text{ F}, \quad W' = 15 \\ \text{MeV}, \quad r'_0 = 1.22 \text{ F}, \quad a' = 0.47 \text{ F}, \quad \text{and } V_{so} = 1300 \\ \text{MeV}, \quad \rho = 0.85 \text{ F}.$$

The value of  $\rho$  is in good agreement with current concepts of the range of the two-body force in nuclear matter. It was determined from two simultaneous equations (for the two neutron energies 7 and 14.5 MeV) relating the value of the nonlocal potential depth  $V_{NL}$  to that of the real "equivalent local" potential  $V_L$ , viz., that local potential determined by optical-model search codes empirically to yield the same elastic angular distribution as the nonlocal potential. For an energy  $E$ , the following approximate relation holds,

$$V_L \exp\left[\frac{M_n \rho^2}{2\hbar^2} (E - V_L)\right] = V_{NL}. \quad (123)$$

Although a set of local parameters, based in the main upon those due to Bjorklund and Fernbach,<sup>17</sup> could always be found to give good fits to any given set of experimental data (the "prescription" for the equivalent local neutron optical parameters being  $V = 48 - 0.29 E^{(\text{MeV})}$ ,  $W'_L = 10 \text{ MeV}$ ,  $r_0 = r'_0 = 1.25\text{F}$ ,  $a = 0.65 \text{ F}$ ,  $a' = 0.47 \text{ F}$ ), the fits obtained with the Perey-Buck nonlocal parameters were found throughout to be at least as good as those for a local potential (or for the nonlocal potential of Wyatt, Wills, and Green) and the underlying theoretical approach is fundamentally more satisfying.

At this stage it may be mentioned that insertion of the optical-model parameters of Beyster *et al.*<sup>5</sup> as input in computation of transmission coefficients yielded values of  $T_l$  which did not agree with those tabulated. Since others<sup>53,54</sup> using independent programs corroborate this result (for example, it was found that for Ti and Fe at  $E_n \lesssim 2 \text{ MeV}$  the main effect was to render computed values of  $T_0$  larger by 10–30% and  $T_2$  larger by 20–50% than the listed values), Beyster penetrabilities cannot be regarded as internally consistent and have, therefore, not been used in this paper.

Up to the present, analysis of proton distributions has not advanced sufficiently to yield a set of nonlocal potential parameters for protons, but the fol-

<sup>50</sup> Perey and Buck actually used the form  $\frac{1}{2}|\mathbf{r}| + \frac{1}{2}|\mathbf{r}'|$ , which is a fairly good approximation to the above.

<sup>51</sup> R. J. Howerton, University of California Report UCRL-5573, 1961 (unpublished).

<sup>52</sup> D. J. Hughes and R. B. Schwartz, *Neutron Cross Sections*, Brookhaven Report BNL-325 (2nd ed.) (1958).

<sup>53</sup> D. M. Van Patter, N. Nath, S. M. Schafroth, S. S. Malik, and M. A. Rothman, *Phys. Rev.* **128**, 1246 (1962).

<sup>54</sup> E. H. Auerbach (private communication).

lowing local potential as proposed by Perey<sup>9</sup> has mainly been used in the present calculations:  $V_L = 46.7 - 0.32 E^{(\text{MeV})} + Z A^{-\frac{1}{2}} \text{MeV}$ ,  $W'_L = 11 \text{ MeV}$ ,  $r_0 = r'_0 = 1.25 \text{ F}$ ,  $a = 0.65 \text{ F}$ ,  $a' = 0.47 \text{ F}$ .

These parameters were selected on the basis of an analysis of 35 elastic scattering distributions in the energy range 9 to 22 MeV for target nuclei ranging from Al to Au ( $Z/A^{\frac{1}{2}} = 4$  to 14) and were found also to give good agreement with experimental polarization data.

In order to provide comparison with previously published correlation analysis which employed a Preskitt-Alford optical potential<sup>55</sup> for protons, a few of the present calculations also based themselves upon this choice of parameters. The results were found to be practically identical with those for a Perey potential. The Preskitt-Alford potential involves *volume* absorption and is characterized by the following parameters:

$$V = 50 \text{ MeV}, W = 5 \text{ MeV}, r_0 = 1.33 \text{ F}, a = 0.4 \text{ F}.$$

It has been found to give good fits to 43 experimental elastic distributions for protons ranging from 3.5 to 6.5 MeV incident upon the nuclei V, Cr, Fe, Co, and has accordingly been used in past correlation analysis by Seward<sup>23</sup> for Co and Sheldon<sup>13,14,35</sup> for Cr and Fe.

### B. Transmission Coefficients

Transmission coefficients, which were required for evaluation of the  $\tau$  terms in the CN correlation expression, were obtained for neutron scattering from tables by Perey and Buck and for proton scattering from computed scattering amplitudes. A subroutine of the code "SALLY" which calculates the real and imaginary parts of the partial-wave elastic scattering amplitudes  $G_l = e^{iK_l} \sin K_l$  for the  $l$ th partial wave was adapted to compute and print out "average" transmission coefficients  $T_l$  directly, where

$$T_l = 4(\text{Im } G_l - |G_l|^2). \quad (124)$$

Alternatively, if the generalized  $T_l^{(\pm)}$  were required, they were calculated by hand from corresponding generalized amplitudes  $G_l^{(+)}$  and  $G_l^{(-)}$  obtained as output from codes (such as the strong-coupling code) which took account of spin-orbit interaction.

### C. CN Correlation Functions

As preliminary to more extensive coding, a fairly simple computer program termed "ETHEL," for evaluating the CN correlation function in the scattering plane ( $\varphi = 0$ ), was first compiled for  $l_1, l_2 \leq 2$  and the normalization  $W(\frac{1}{2}\pi, \frac{1}{2}\pi, 0) = 1$ . Using "aver-

age" transmission coefficients  $T_l$  as input data, it evaluated the terms  $\tau^{(1)}$  to  $\tau^{(6)}$  with the application of which it then computed  $W(\frac{1}{2}\pi, \frac{1}{2}\pi, 0)$  using the expression (67) and stored the latter as norm. It subsequently computed and printed out for each value of  $\theta_1$  and  $\theta_2$  from  $0^\circ$  to  $180^\circ$  in  $5^\circ$  steps the numerical value of  $W(\theta_1, \theta_2, 0)$ , normalized as a result of division by the norm. The possibility of checking systematically each step of the coding and numerical computation against hand calculations and tabulations rendered this rapid ( $< \frac{1}{2}$  min) code useful not only in its own right, but as a standard for checking others.

In particular, it paved the way for the generalized CN correlation code "ERICA" which was compiled to take account of arbitrarily high orbital momenta when the requisite  $T_l^{(\pm)}$  incorporating spin-orbit interaction had been fed in as output, and permitted variation of azimuth  $\varphi$  as well as of  $\theta_1$  and  $\theta_2$  in arbitrary steps. The latter code incorporated the option of obtaining print-out (or automatic curve plotting) of either the double-differential cross section or the correlation function normalized to unity when  $\theta_1 = \theta_2 = \frac{1}{2}\pi$  for given azimuth  $\varphi$ . Thereby, use was made of the basic expression (58); the code not only determined the permissible sets of parameters and momenta to be summed over by application of triangle relations and for each of these evaluated the requisite  $\tau$  term and  $S_{\mu\nu\lambda}$ , etc., from built-in subroutines for calculation of all necessary Racah functions omitting unnecessary repetition, but also made use of the relations (75) and (80) for computing and printing out the angular distributions at option either normalized to unity at  $\theta = \frac{1}{2}\pi$  or absolutely as differential cross sections. The running time of this code varied per case according to one's selection of the maximum orbital momenta and whether or not one availed oneself of automatic curve plotting facilities. Times ranged from about  $\frac{1}{2}$  min to over 30 min per case.

Finally, mention should be made of the code "PENNY" which for orbital momenta  $l_1, l_2 \leq 2$  evaluated CN angular correlations for  $\theta_1, \theta_2 = 0^\circ$  ( $5^\circ$ )  $180^\circ$  in the  $\varphi = \frac{1}{2}\pi$  plane [thus, in particular, the "perpendicular correlations"  $W(\theta_1, \frac{1}{2}\pi, \frac{1}{2}\pi)$  and  $W(\frac{1}{2}\pi, \theta_2, \frac{1}{2}\pi)$ ] from the expression (68), using "average"  $T_l$  as input. It also printed out the angular distributions, calculated from Eqs. (81) and (82), and the total inelastic cross section  $\sigma$  evaluated from Eq. (88). At option, the above could be expressed either in absolute or normalized form. Running time averaged  $\frac{1}{2}$  min per case.

It is important to note that all the above codes

<sup>55</sup> C. A. Preskitt and W. P. Alford, Phys. Rev. **115**, 389 (1959).

refer to inelastic scattering to the first level (2+) of even-even nuclei (g.s. 0+) and that whereas the internally consistent codes "ETHEL" and "PENNY" could throughout rigorously be checked against hand calculations, checking of "ERICA" could be undertaken only for conclusive results with  $l_1, l_2 \leq 2$ . For higher momenta, only tabulation and subroutines could be tested by fairly thorough spot checks in the reasonable hope that no extraneous errors enter on extension of established computer procedures.

## 6. ANGULAR CORRELATION SURFACES

A concise method of representing information on the angular variation of the theoretical correlation function over the entire range of angles at a given azimuth is in the form of a correlation surface,<sup>22,35</sup> this being a contour map of equivalued  $W$  in terms of the emission angles  $\theta_1$  and  $\theta_2$  at a given  $\varphi$ , normalized for convenience of comparison to  $W = 1$  at  $\theta_1 = \theta_2 = \frac{1}{2}\pi$ . Correlation curves for given counter settings can directly be obtained from the requisite sections in the surface, even such curves as correspond to simultaneous displacement of nucleon and  $\gamma$ -counter settings. For example, one might select, from such surfaces, sequences of counter settings corresponding to loci of steepest variation or alternatively follow a contour line to test constancy in the correlation function.

The correlation surfaces which are here depicted provide for the even-even nuclei  $\text{Mg}^{24}$  and  $\text{Fe}^{56}$  an over-all picture of correlation behavior in the scattering plane ( $\varphi = 0$ ) for

- (a) CN mechanism as one incorporates higher partial waves. (See Figs. 7 to 9.)
- (b) DI mechanism as one progresses from the plane-wave approximation to distorted-wave calculations, without and with spin-flip considerations. (See Figs. 10 to 12.)

The first example of CN surfaces concerns the  $\text{Mg}^{24}(n, n'\gamma)$   $Q = -1.368$  MeV reaction at  $E_n = 3.35$  MeV<sub>lab</sub>. The radical alteration in the contours on going from the  $l_{\text{max}} = 1$  correlation to higher partial waves is a feature common to all investigated CN correlations, whereas thereafter the change in over-all appearance is less drastic, so that one might infer that the  $l_{\text{max}} = 3$  surface represents essentially the ultimate correlation behavior. The angular dependence of sections in this surface for the three fixed  $\gamma$ -counter settings  $\theta_2 = 25^\circ, 35^\circ, 45^\circ$  have been drawn in Fig. 13 for comparison with the measurements of Brugger, Niewodniczanski, and Steiger.<sup>56</sup> It is per-

haps of interest to compare the  $l \leq 2$  surface with those (the first of such contour representations) published for the slightly higher incident energy  $E_n = 3.45$  MeV<sub>c.m.</sub> by Prêtre, Brugger, and Steiger (Fig. 2 of Ref. 22), wherein the difference from the present results is in the main due to the present exclusion of mixed- $j$  interference terms, which leads to a "smoothing-out" of the correlation function (see Fig. 1 of Ref. 14). The present peak-to-valley ratio is 2.2, whereas that for the surface of Prêtre *et al.* exceeds 2.4.

In view of the evidence which is presented in Secs. 7 and 8, the nucleus  $\text{Mg}^{24}$  would seem to be too light for analysis on the basis of the statistical model (the continuum assumption of random phase is unlikely to be fulfilled), whereas good agreement between theory and experiment obtains for the heavier nuclei in the iron region. It is, therefore, probably more meaningful to present correlation results for the reaction  $\text{Fe}^{56}(n, n'\gamma)$   $Q = -0.845$  MeV, as shown in Fig. 8 for neutron scattering at 2.05 MeV<sub>lab</sub>. In this case, the appearance of the surface does not tend to "stabilize" as one progresses to higher  $l$  values, and again the unique form of the  $l \leq 1$  surface stands out. The present  $l \leq 2$  surface may be compared with that previously published by Sheldon (Fig. 3 of Ref. 13) to illustrate the effect of exclusion of mixed- $j$  interferences and selection of a different optical model. The former involves generalized transmission coefficients  $T\{\pm\}$  for a Perey-Buck surface-absorption potential, whereas the latter used Beyster  $T_i$  corresponding to volume absorption.

To illustrate over-all CN correlation behavior for proton scattering, the group of surfaces shown in Fig. 9 involve the  $\text{Fe}^{56}(p, p'\gamma)$   $Q = -0.845$  MeV reaction at  $E_p = 4.22$  MeV<sub>c.m.</sub>. Again the marked transition from  $l \leq 1$  to higher orbital momenta stands out, and again the surfaces do not tend to "stabilize" in appearance as the limiting momenta are increased, but rather to "oscillate" between forms characteristic of even- $l_{\text{max}}$  and odd- $l_{\text{max}}$  cutoff momenta. Sections in these surfaces for  $\theta_1 = 90^\circ$  and  $130^\circ$  are shown in Fig. 49.

The manner in which the resultant correlation surface for momenta  $l \leq 2$  ensues from composition of the resonance correlation surfaces for various levels  $J_1, \pi_1$  of the compound nucleus has been depicted in Ref. 35; unfortunately, the over-all surface depicted therein had been erroneously taken over from an earlier publication<sup>13</sup> in which exclusion of mixed- $j$  interference terms from the correlation calculation had not been recognized and, therefore, differs in appearance from the  $l \leq 2$  surface shown here. In

<sup>56</sup> H. R. Brugger, T. Niewodniczanski, and M. P. Steiger, *Helv. Phys. Acta* **35**, 3 (1962).

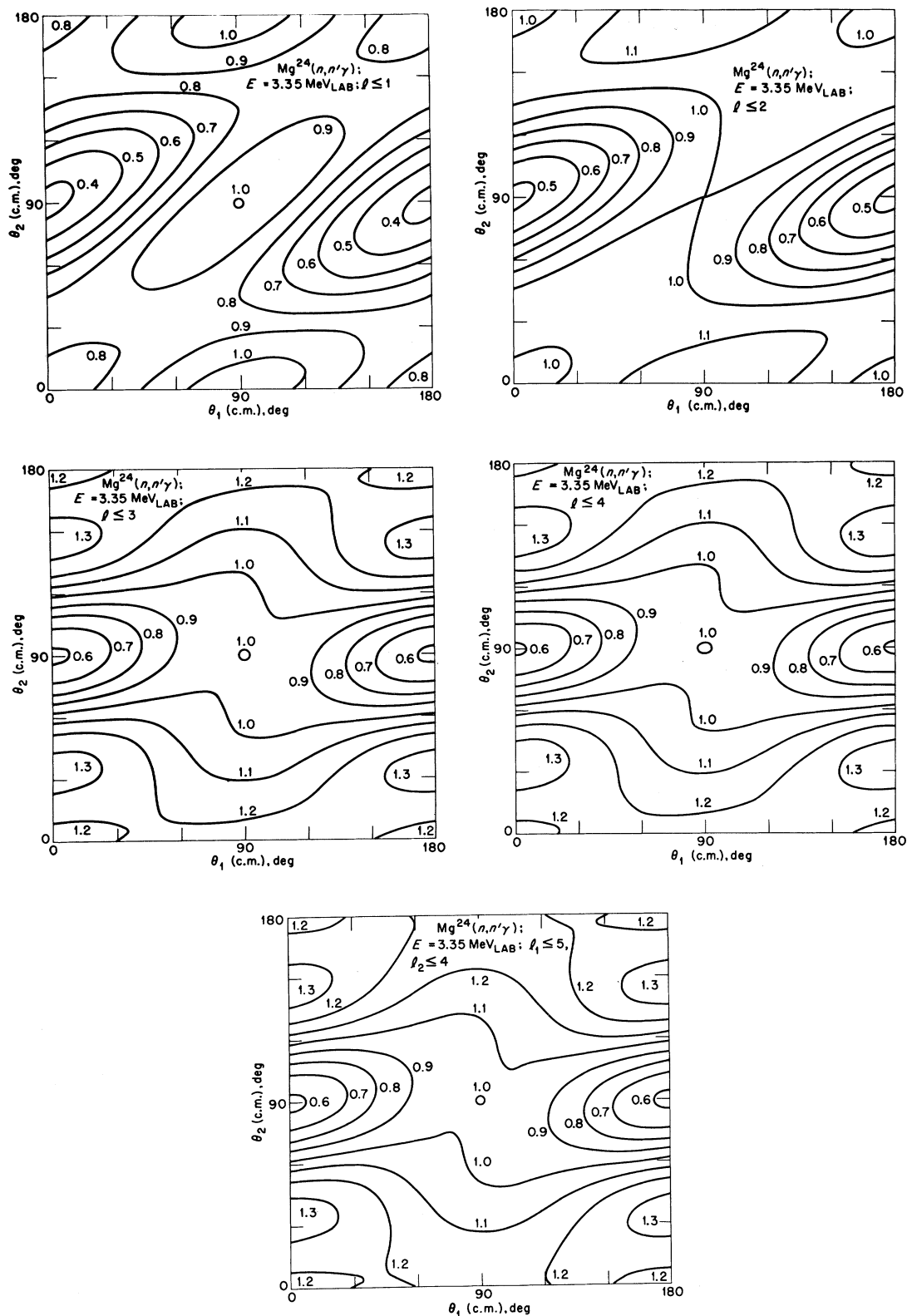


FIG. 7. Influence of particle orbital momentum upon correlation surfaces for the  $Mg^{24}(n,n'\gamma)$  reaction ( $Q = -1.368 \text{ MeV}$ ) at  $3.35 \text{ MeV}_{\text{lab}}$ , calculated for the CN mechanism using a Perey-Buck nonlocal optical potential.

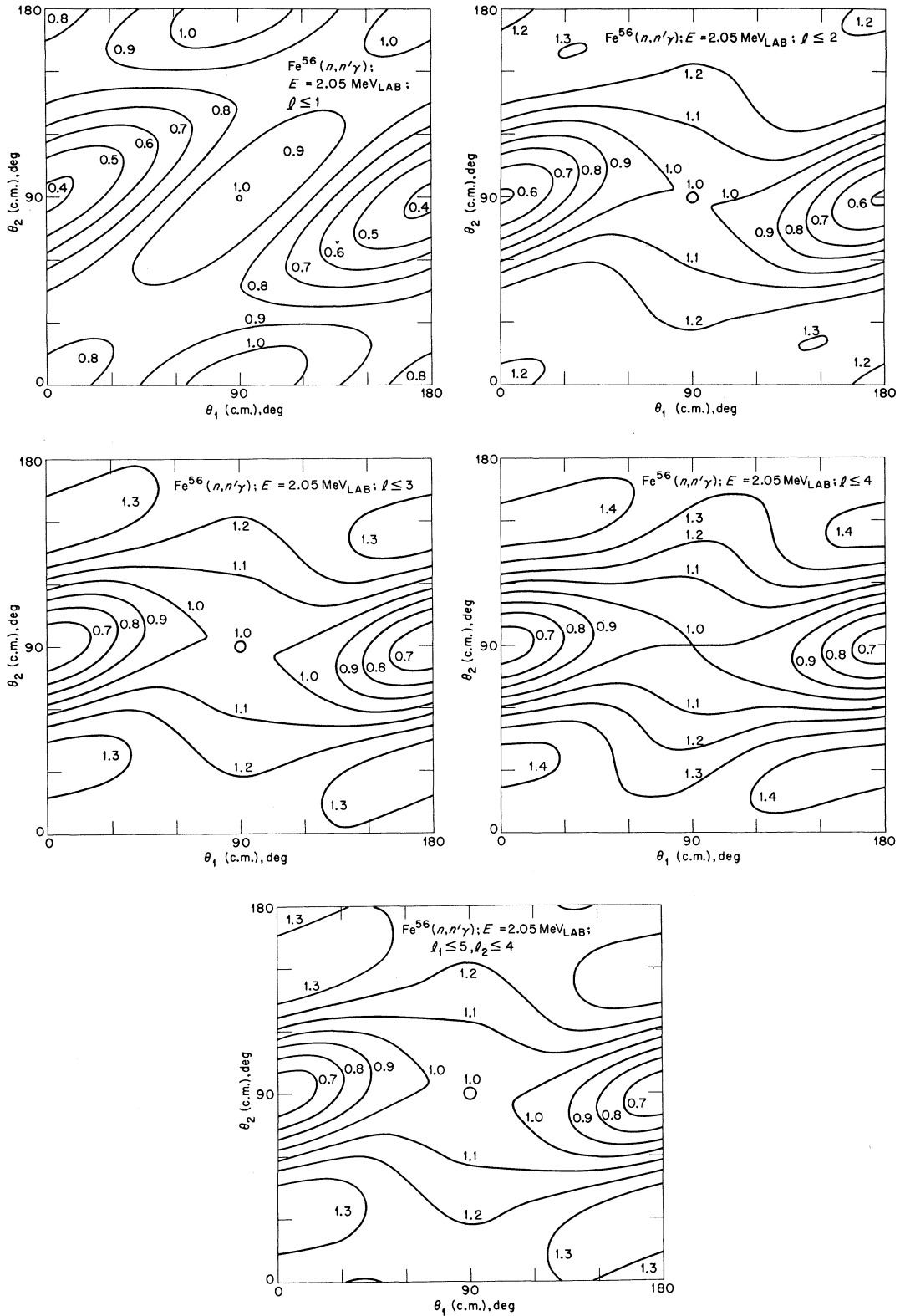


FIG. 8. Influence of higher partial waves upon the correlation surfaces for the  $Fe^{56}(n,n'\gamma)$  reaction ( $Q = -0.845 \text{ MeV}$ ) at  $2.05 \text{ MeV}_{\text{lab}}$ , calculated for the CN mechanism using a Perey nonlocal optical potential including spin-orbit interaction.

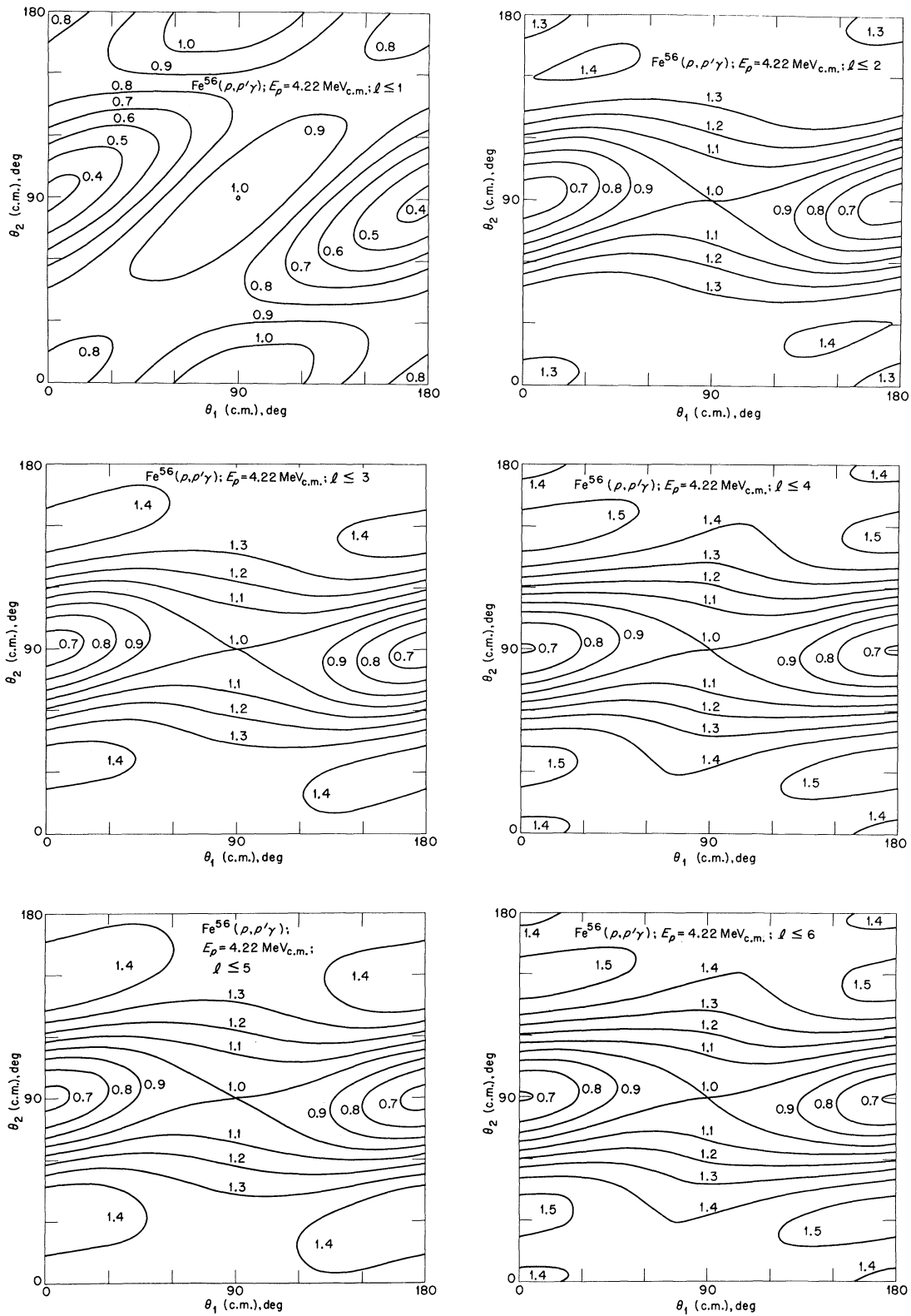


FIG. 9. Illustration of the variation of correlation contours in correlation surfaces for the  $Fe^{56}(p,p'\gamma)$  reaction ( $Q = -0.845$  MeV) at 4.22 MeV c.m. upon inclusion of higher partial waves. The surfaces have been computed for a CN mechanism using Preskitt-Alford transmission coefficients and normalized to unity at  $\theta_1 = \theta_2 = 90^\circ$ ,  $\varphi = 0^\circ$ . This normalization results in surfaces for "odd- $l_{max}$ " displaying a form which differs slightly from that characteristic of "even- $l_{max}$ " surfaces, an effect which occurs for (normalized) correlation functions but not for absolute double-differential cross sections.

the present analysis, as before, a Preskitt-Alford volume-absorption optical potential yielding "mean"  $T_i$  independent of spin-orbit interaction is employed. Computations based upon a Perey potential for protons were found to yield almost identical results, which have, therefore, not been reproduced here.

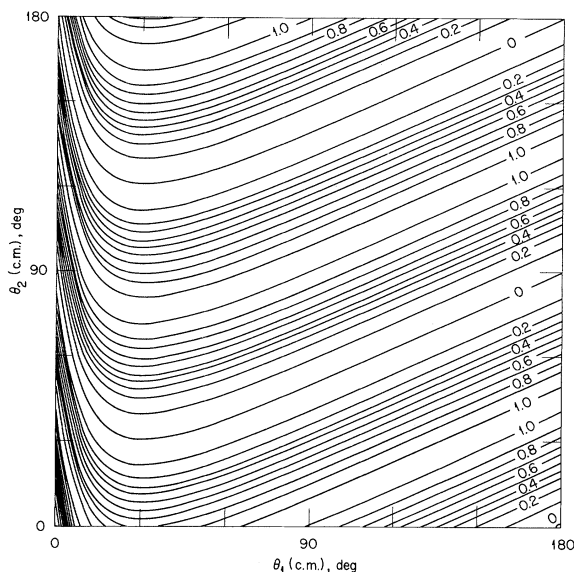


Fig. 10. Plane-wave DI correlation surface for the  $\text{Ni}^{58}(p,p'\gamma)$  reaction ( $Q = -1.45$  MeV) at  $5.73$  MeV<sub>c.m.</sub> in the  $\varphi = 0^\circ$  plane.

Correlation surfaces for the DI mechanism display markedly different appearance; the three surfaces shown here refer to the  $\text{Ni}^{58}(p,p'\gamma)_{Q=-1.45}$  MeV reaction at  $E_p = 5.73$  MeV<sub>c.m.</sub> and contrast the correlation characteristics of the simple plane-wave DI theory with those for DWDI theories, in each instance referred to the  $\varphi = 0$  plane and based upon a modified Perey potential ( $V = 44$  MeV,  $W' = 11$  MeV,  $r_0 = 1.35$  F,  $a = 0.65$  F,  $r'_0 = 1.25$  F,  $a' = 0.47$  F) due to Satchler. The plane-wave surface, Fig. 10, consists essentially of suitably displaced curves of the classical laboratory recoil angle  $\theta_R$  in function of the scattering angle  $\theta_1$  (the basic curve is that for  $W = 0$ ), based upon the following reasoning: The PWDI correlation function is of the form

$$W(\theta_1, \theta_2, \pi) = Q \sin^2 2(\theta_2 - \theta_R). \quad (125)$$

Hence, in the  $\varphi = \pi$  plane,  $W$  vanishes when  $\theta_2 = \theta_R$ . Accordingly, the plot of  $\theta_2 = \theta_R$  against  $\theta_1$  represents the  $W = 0$  contour in this plane. To normalize the surface to unity at the center, it suffices to note that

$$\tan \theta_R = (\cos \theta_1 - k)^{-1} \sin \theta_1 \quad (126)$$

with

$$k = (1 - E^* \mu^{-1} E^{-1})^{-\frac{1}{2}}, \quad (127)$$

where  $E^*$  is the energy of the first excited level of the target nucleus,  $E$  the c.m. energy of the incident nucleon, and  $\mu$  the reduced mass of the system. Thus, for  $\theta_1 = \frac{1}{2} \pi$ ,

$$\theta_R^{(\frac{1}{2}\pi)} = \tan^{-1}(-1/k) \quad (128)$$

and from Eq. (125),

$$W(\frac{1}{2}\pi, \frac{1}{2}\pi, \pi) = Q \sin^2 2\theta_R^{(\frac{1}{2}\pi)} = 1, \quad (129)$$

whence the desired normalization ensues on setting

$$Q = (k^2 + 1)^2 / 4k^2. \quad (130)$$

Further, since  $\theta_R = 0$  when  $\theta_1 = 0$  the correlation function for the latter special case takes the form

$$W(0, \theta_2, \pi) = Q \sin^2 2\theta_2. \quad (131)$$

From this relation with  $Q$  given by Eq. (130), the values of  $\theta_2$  for given values of  $W$  can be determined. These then give the intercepts on the ordinate for contours of  $W$  in steps of  $\Delta W = 0.1$ . The pattern for the lower half-plane,  $\theta_2 = 0$  to  $\frac{1}{2} \pi$  is identical with that for the upper,  $\theta_2 = \frac{1}{2} \pi$  to  $\pi$  in accordance with the symmetry

$$W(\theta_1, \theta_2, \pi) = W(\theta_1, \frac{1}{2}\pi + \theta_2, \pi). \quad (132)$$

From the PWDI surface in the  $\varphi = \pi$  plane, that for the  $\varphi = 0$  plane then follows on inversion since

$$W(\theta_1, \theta_2, \pi) = W(\theta_1, \pi - \theta_2, 0). \quad (133)$$

It should be pointed out that by omitting this final step, Prêtre *et al.*<sup>22</sup> inadvertently referred their PWDI surface for the  $\text{Fe}^{56}(n, n'\gamma)$  reaction at  $E_n = 3.30$  MeV<sub>c.m.</sub> to the  $\varphi = \pi$  plane.

The DI surface in Fig. 11 has been constructed from computation with codes "SALLY" and "MARILYN" assuming spin-flip to be zero for the reaction  $\text{Ni}^{58}(p, p'\gamma)$  at  $E_p = 5.73$  MeV<sub>c.m.</sub>. There is an appreciable increase in the peak-to-valley ratio and a radically different dependence upon  $\theta_1$ , especially in the neighborhood of  $\theta_1 = \frac{1}{2} \pi$ . The identical appearance of the upper half-plane to the lower half-plane illustrates a characteristic DI symmetry which could furnish information on the presence of spin-flip in a given scattering process.

The general expression

$$W(\theta_1, \theta_2, \pi) = P + Q \sin^2 2(\theta_2 - \theta') + R \sin^2 (\theta_2 - \theta'') \quad (134)$$

is numerically different from that with  $\theta_2$  replaced by  $\frac{1}{2}\pi + \theta_2$ , viz.,

$$W(\theta_1, \theta_2 + \frac{1}{2}\pi, \pi) = (P + R) + Q \sin^2 2(\theta_2 - \theta') - R \sin^2 (\theta_2 - \theta'). \quad (135)$$

Invariance for  $\theta_2 \rightarrow \frac{1}{2}\pi + \theta_2$  obtains only when  $R = 0$  (i.e., DWDI *without* spin-flip) or when  $P = R = 0$  (plane-wave DI), but *not* in the general case of

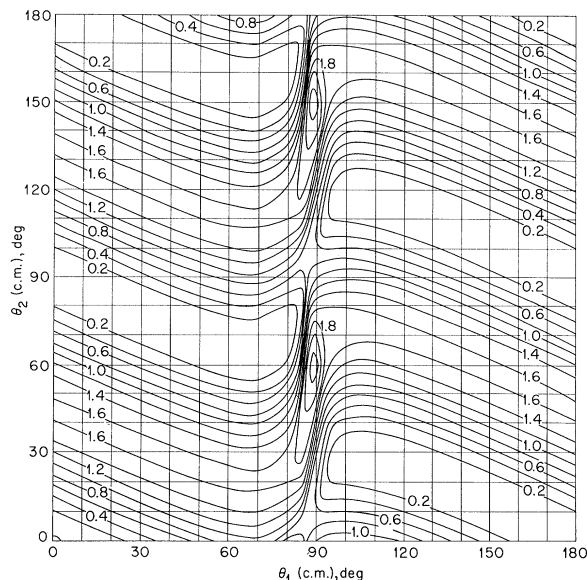


FIG. 11. DWDI surface *without* spin-flip for the  $\text{Ni}^{58}(p, p'\gamma)$  reaction at  $5.73 \text{ MeV}_{\text{c.m.}}$ , calculated using a modified Perey potential.

DWDI *with* spin-flip. The study of such symmetries as an experimental means of identifying the presence of spin-flip is, however, made difficult by the small magnitude of the asymmetry, which can be seen either from the DWDI correlation curves in Sec. 7 or the correlation surface for DWDI with a constant relative spin-flip intensity, Fig. 12. The normalization in Figs. 11 and 12 has been effected upon the respective DWDI correlation functions and not upon the absolute double-differential cross section since the latter peaks strongly in the forward scattering direction under the influence of the angular distribution factor. As already discussed, the assumption that  $y$  does not change with  $\theta_1$  is possibly unrealistic, but for illustration the reasonable constant magnitude  $y = 0.4$  has been chosen for the  $\text{Ni}^{58}(p, p'\gamma)$  reaction at  $E_p = 5.73 \text{ MeV}_{\text{c.m.}}$  to show the over-all influence of spin-flip upon the correlation function. Not only do the left and right half-planes differ [as is the case with all DI surfaces, since  $W(\theta_1, \theta_2, 0) \neq W(\frac{1}{2}\pi + \theta_1, \theta_2, 0) \neq W(\pi - \theta_1, \theta_2, 0)$ ], but also

the upper and lower half-planes [ $W(\theta_1, \theta_2, 0) \neq W(\theta_1, \frac{1}{2}\pi + \theta_2, 0) \neq W(\theta_1, \pi - \theta_2, 0)$ ]. The peak-to-valley ratio is reduced by the inclusion of spin-flip; comparison of Figs. 11 and 12 shows that the presence of spin-flip reduces also the amplitude of the  $\theta_2$  dependence of the correlation function. Because of the steepness of the  $\theta_1$  dependence around  $\theta_1 = \frac{1}{2}\pi$  the contour steps there had to be increased to  $\Delta W = 0.2$  and are shown dashed; the shape of a further contour for  $W = 1.2$  lying between  $\theta_1 = 85^\circ$  and  $90^\circ$  could not be established precisely from the computer output, and it has, therefore, been omitted.

## 7. ANGULAR CORRELATION ANALYSIS FOR INELASTIC NUCLEON SCATTERING

Measurements of the correlation function for inelastic neutron and proton scattering have been published for the low and medium energy range for nuclei ranging from  $\text{Li}^7$  to  $\text{Ni}^{60}$  (preliminary results exist also for proton scattering on the isotopes  $\text{Zn}^{64,66,68}$  by the Zürich group). No analysis has here been attempted for elements lighter than  $\text{Mg}^{24}$  since one can neither feel confidence in the choice of optical

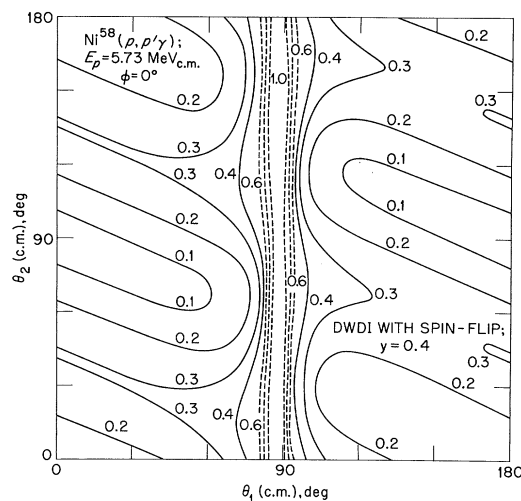


FIG. 12. Influence of *inclusion* of spin-flip of relative intensity  $y = 0.4$  for the  $\text{Ni}^{58}(p, p'\gamma)$  reaction at  $5.73 \text{ MeV}_{\text{c.m.}}$  in the  $\phi = 0^\circ$  plane. For representational convenience the normalization in Figs. 11 and 12 to unity at  $\theta_1 = \theta_2 = 90^\circ$  has been effected upon the appropriate correlation function [expression (93)] rather than upon the double-differential cross section [expressions (108) and (112)], since the latter peaks strongly at forward scattering angles  $\theta_1$ .

potential nor in the statistical assumption. Indeed, systematic theoretical analysis indicates that the latter becomes valid for incident energies around 6 MeV only for target nuclei with  $A \gtrsim 40$ . Of the target nuclei examined in this section, viz.,  $\text{Mg}^{24}$ ,  $\text{Si}^{28}$ ,

$S^{32}$ ,  $Ti^{48}$ ,  $Cr^{52}$ ,  $Fe^{56}$ ,  $Ni^{58,60}$ ,  $Zn^{64,66,68}$ , good CN theoretical fits to measured correlations could be attained only for the nuclei  $Ti^{48}$  and beyond, the quality of fit improving with increasing mass number. In many cases, DWDI correlation curves have also been included in the figures for comparison, but in no instance were the latter in satisfactory agreement with the experimental angular dependence. For the fairly low incident energies considered here, the absolute DWDI double-differential cross section proved to be far smaller in magnitude than that for a CN mechanism. Except in rare instances, experimentally measured coincidences have not been expressed in publications as absolute double-differential cross sections; in the present analysis they have, therefore, been normalized arbitrarily. For comparison with the theoretical curves, it is, therefore, necessary to examine relative slopes and amplitudes, and also positions of maxima and minima to establish the extent of agreement between theory and experiment. Even where the double-differential cross section has been measured absolutely, the error limits are so much larger than otherwise that direct qualitative comparison is still somewhat inconclusive.

For each target element in the subsections which follow is given a list of the experimental work analyzed, arranged in order of increasing incident energy. Some purely theoretical curves are also included to illustrate such behavior as the azimuthal dependence or the  $l$  dependence of the CN correlation function, and combination of CN + DI characteristics.

#### A. $Mg^{24}$ , $Q = -1.368$ MeV

$E(\text{MeV})_{\text{lab}}$	$\mathcal{N}$	$\theta_1$	$\theta_2$	Authors
3.5	$n$		$25^\circ, 35^\circ, 45^\circ$	Brugger <i>et al.</i> <sup>56</sup>
3.5	$n$	$35^\circ$ and $145^\circ$ $50^\circ$ and $130^\circ$		Niewodniczanski and Steiger <sup>57</sup>
5.41	$p$	$45^\circ, 90^\circ, 120^\circ$		Lackner <i>et al.</i> <sup>58</sup> Seward <sup>23</sup>
6.2	$p$	$70^\circ, 90^\circ, 120^\circ$		Lackner <i>et al.</i> <sup>58</sup>
6.66	$p$	$45^\circ, 75^\circ, 105^\circ$		Seward <sup>23</sup>
7.01	$p$	$45^\circ, 60^\circ, 90^\circ,$ $135^\circ$		Seward <sup>23</sup>
7.3	$p$		$30^\circ, 90^\circ$	Gove and Hedgran <sup>59</sup>
10.7	$p$	$30^\circ, 60^\circ, 90^\circ$ $(120^\circ, 150^\circ)$		Braid <i>et al.</i> <sup>45,46</sup>
16.6	$p$	$30^\circ, 42.5^\circ$ $70^\circ, 95^\circ, 120^\circ$ $150^\circ$		Yoshiki <sup>60</sup>

<sup>57</sup> T. Niewodniczanski and M. P. Steiger, in Proceedings of the International Symposium on Direct Interactions and Nuclear Reaction Mechanisms, Padua, 1962 (to be published) and private communication.

<sup>58</sup> H. A. Lackner, G. F. Dell, and H. J. Hausman, Phys. Rev. **114**, 560 (1959).

<sup>59</sup> H. E. Gove and A. Hedgran, Phys. Rev. **86**, 574 (1952).

<sup>60</sup> H. Yoshiki, Phys. Rev. **117**, 773 (1960).

With the exception of  $C^{12}$ , on which some early coincidence measurements were undertaken<sup>61-63,39</sup> but which falls outside the purview of the present analysis, the nucleus  $Mg^{24}$  represents the target on which the first correlation investigations were carried out, both for neutron<sup>56</sup> and for proton<sup>59</sup> scattering. The neutron studies by Brugger *et al.* of the Zürich group at  $3.35 \text{ MeV}_{\text{c.m.}}$  ( $=3.5 \text{ MeV}_{\text{lab}}$ ) appeared to provide remarkably good substantiation of the predictions of statistical CN theory. However, at that time, the latter was evaluated with inclusion of mixed- $j$  interference terms and the use of a numerically incorrect  $S_{444}$  term. On recalculating the correlation function for the present analysis using a Perey-Buck potential in place of the questionable Beyster potential then employed, the  $\theta_2$  angular dependence was found to be drastically different and to yield no agreement with the experimental points. The tendency for the double-differential cross section to increase above  $\theta_2 = \frac{1}{2} \pi$ , particularly when higher partial waves are taken into account, as shown in Fig. 13, contrasts the trend of Brugger's measurements. On the other hand, later neutron measurements to examine the  $\theta_2$  dependence of the correlation by Niewodniczanski and Steiger<sup>57</sup> at 3.5 MeV, which corresponds with a valley in the excitation function for this reaction, yielded results in quite good agreement with CN theory, as shown in Fig. 14. A particular feature of these measurements lies in the selection of supplementary angles for study of the CN correlation symmetry

$$W(\theta_1, \theta_2, 0) = W(\pi - \theta_1, \pi - \theta_2, 0), \quad (136)$$

which the results did not quite satisfactorily verify, probably because of the inapplicability of the statistical assumption. Whereas each individual set of results follows the theoretical trend very closely, the use of a single norm to normalize all four sets causes the points for forward neutron angles  $\theta_1$  to lie too high, and those for backward angles too low. The fact that for a pair of supplementary angles, the points lying closest to  $\theta_2 = \frac{1}{2} \pi$  do not even approximately agree in numerical magnitude may point to a systematic experimental error. On the other hand, if the discrepancy is valid—and it occurs also for  $Fe^{56}$  ( $n, n' \gamma$ ) correlation measurements at  $E_n = 2.05 \text{ MeV}_{\text{lab}}$  (see Figs. 44, 45, 46), albeit in smaller measure—a partial breakdown of the pure CN theory is indi-

<sup>61</sup> R. B. Theus, A. H. Aitken, and L. A. Beach, Bull. Am. Phys. Soc. **5**, 45 (1960).

<sup>62</sup> G. Deconninck and A. Martegani, Nucl. Phys. **21**, 33 (1960).

<sup>63</sup> R. Sherr and W. F. Hornyak, Bull. Am. Phys. Soc. **1**, 197 (1956).

cated, a consequence either of invalidity of the random-phase hypothesis or of interference between CN and DI mechanisms. It should also be noted that for  $Mg^{24}$  the differential cross sections (especially for the DI mechanism) change very markedly with energy

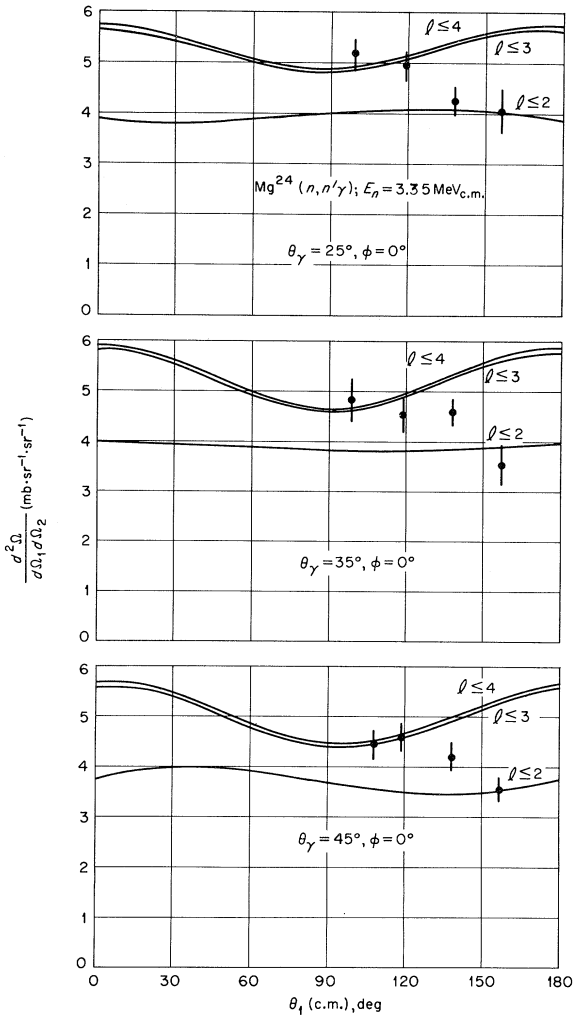


FIG. 13. Comparison of the  $\theta_1$  dependence of experimental results by Brugger *et al.* (Ref. 56) for inelastic neutron scattering on  $Mg^{24}$  at 3.35 MeV<sub>c.m.</sub> with predictions of CN theory for  $\theta_2 = 25^\circ, 35^\circ, 45^\circ$ .

in this region, suggesting that the make-up of the compound system changes rather abruptly with changes in incident energy, the resultant scattering mechanism being a highly energy-dependent impure CN process.

Proton correlation studies upon  $Mg^{24}$  have been made at energies of 5.41 MeV and upward. At 5.4 MeV, two groups carried out measurements which have been combined in Fig. 15, and compared with

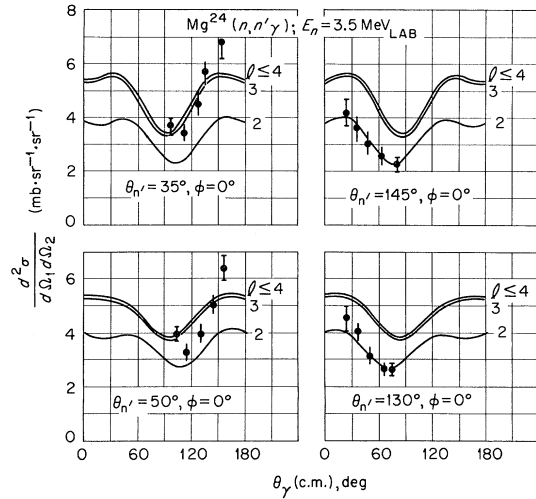


FIG. 14. Comparison between experimental and CN theoretical correlation results for the  $Mg^{24}(n,n'\gamma)$  reaction ( $Q = -1.368$  MeV) at 3.5 MeV<sub>lab.</sub> The points as measured by Niewodniczanski and Steiger (Ref. 57) have been normalized by a single factor for all four curves.

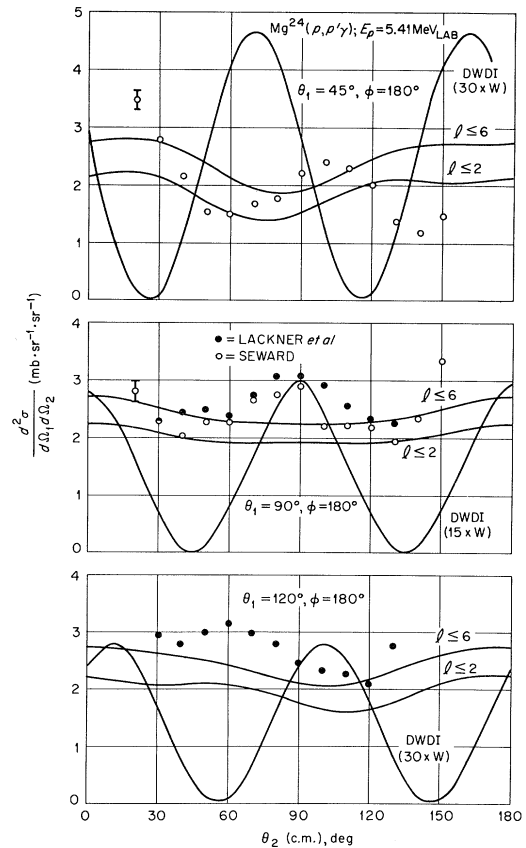


FIG. 15. Analysis of the correlation results of Lackner *et al.* (Ref. 58) and of Seward (Ref. 23) for  $Mg^{24}(p,p'\gamma)$  at  $E_p = 5.4$  MeV<sub>lab.</sub> Neither CN nor DI correlation curves yield a satisfactory fit.

the predictions of CN and DWDI theory (without spin-flip). It is clear that neither theory offers a good fit, though the measurements themselves appear to be quite consistent.

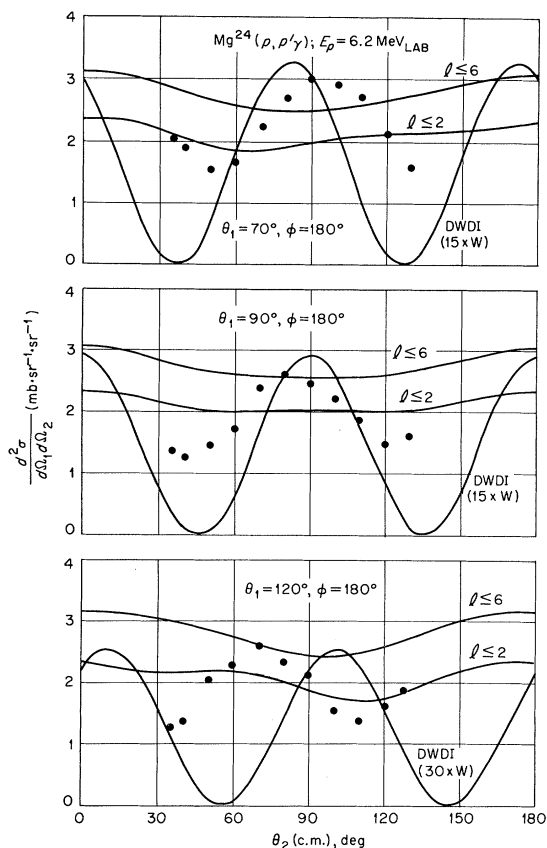


Fig. 16. Analysis of correlation results for  $Mg^{24}(p, p'\gamma)$  at 6.2 MeV<sub>lab</sub> by Lackner *et al.* (Ref. 58), wherein the arbitrarily normalized experimental points appear to show some accord with DWDI theoretical predictions at  $\theta_1 = 70^\circ$  and  $90^\circ$ .

A further set of measurements by Lackner *et al.* at 6.2 MeV, illustrated in Fig. 16, appears to show some affinity with the DWDI mechanism, as do also measurements at 6.66 MeV by Seward (Fig. 17). Particularly for the scattering angle  $\theta_1 = 75^\circ$ , the DWDI curve with spin-flip intensity  $y = 0.4$  has a structure closely resembling that of the experimental data, though at the other angles,  $\theta_1 = 45^\circ$  and  $105^\circ$  the fit is appreciably poorer. This may be compared with Fig. 19, which contrasts theoretical and experimental results for an incident energy of 10.7 MeV and wherein a fair measure of agreement obtains for  $\theta_1 = 90^\circ$  but worsens for lower  $\theta_1$ .

The measurements at 7.3 MeV by Gove and Hedgran, as depicted in Fig. 18, are interesting in that they represent the pioneer (1952) experimental studies in the correlation field in which the  $\theta_1$  dependence of the correlation was studied. Results are unfortunately too sparse and too scattered for any decisive conclusions to be drawn.

Attention has already been drawn to the measurements of Braid *et al.* at 10.7 MeV. As can be seen

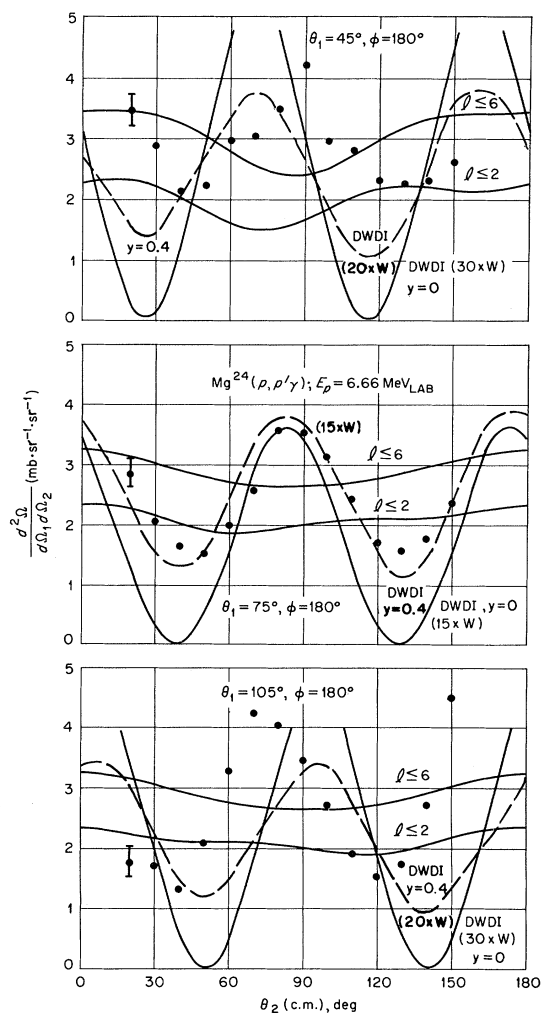


Fig. 17. Correlation results for  $Mg^{24}(p, p'\gamma)$  at 6.66 MeV<sub>lab</sub> by Seward (Ref. 23). Again the structure of the observed  $\theta_2$  dependence is rather more in keeping with predominance of a DI mechanism.

from Fig. 19, the results suggest an impure DWDI mechanism; the theoretical curves marked "DWDI (c)" were computed using parameters from the strong-coupling code, which includes spin-orbit interaction.

Finally, the results of Yoshiki at 16.6 MeV, depicted in Fig. 20 suggest a DWDI mechanism, but again, even at this relatively high incident energy, display very marked deviation from theoretical predictions. Yoshiki also took some measurements to test symmetry characteristics, viz.,

$$W(\theta_1, \theta_2, 0) = W(\theta_1, \pi - \theta_2, \pi) \equiv W(\theta_1, \theta_2 - \pi, 0), \quad (137)$$

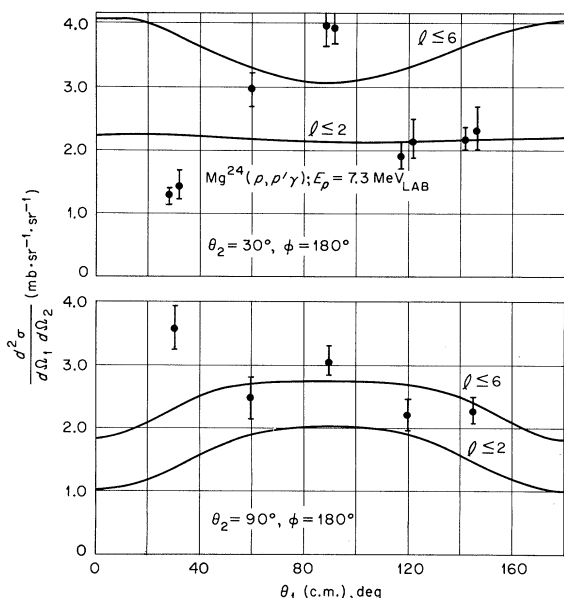


Fig. 18. Results for  $Mg^{24}(p, p'\gamma)$  at 7.3 MeV<sub>lab</sub> by Gove and Hedgran (Ref. 59) compared with theoretical CN curves at  $\theta_2 = 30^\circ$  and  $90^\circ$ .

and these are shown in Fig. 21. The measurements tend to display such symmetry, but they are not in concord with theoretical correlation curves.

### B. $Si^{28}$ , $Q = -1.78$ MeV

$E_p$ (MeV) <sub>lab</sub>	$\mathfrak{N}$	$\theta_1$	Authors
5.8	$p$	$60^\circ, 90^\circ$	Bowsher <i>et al.</i> <sup>64</sup>
5.86	$p$	$45^\circ, 90^\circ, 135^\circ$	Taketani and Alford <sup>24</sup>
6.2	$p$	$90^\circ$	Bowsher <i>et al.</i> <sup>64</sup>
6.3	$p$	$60^\circ, 90^\circ$	Bowsher <i>et al.</i> <sup>64</sup>
6.5	$p$	$60^\circ$	Bowsher <i>et al.</i> <sup>64</sup>
6.5(7.0?)	$p$	$60^\circ, 90^\circ, 120^\circ, 140^\circ$	Hausman <i>et al.</i> <sup>65</sup>
6.7	$p$	$37^\circ, 60^\circ, 90^\circ, 120^\circ$	Bowsher <i>et al.</i> <sup>64</sup>
6.94	$p$	$45^\circ, 90^\circ, 135^\circ$	Taketani and Alford <sup>24</sup>
7.0	$p$	$37^\circ, 60^\circ, 90^\circ, 120^\circ$	Bowsher <i>et al.</i> <sup>64</sup>

<sup>64</sup> H. F. Bowsher, G. F. Dell, and H. J. Hausman, Phys. Rev. 121, 1504 (1961).

<sup>65</sup> H. J. Hausman, G. F. Dell, and H. F. Bowsher, Phys. Rev. 118, 1237 (1960).

The lack of agreement between theory and experiment found for  $Mg^{24}$  obtains also for  $Si^{28}$ , a target nucleus for which to date no neutron scattering correlation results exist and for which no investigations of the  $\theta_1$  dependence of the correlation function have been undertaken. Published data is confined to a

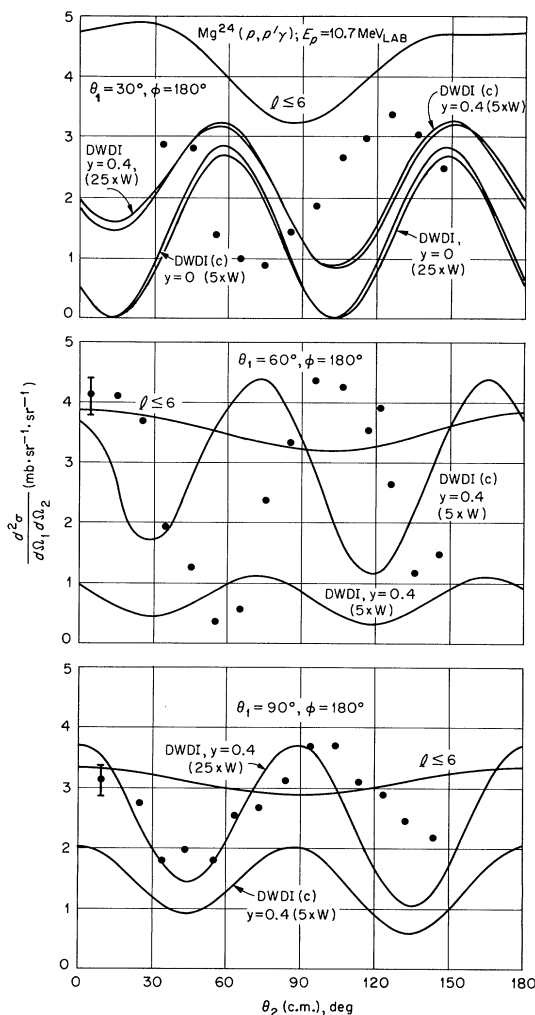


Fig. 19. CN, DWDI (with and without spin-flip) and strong-coupling DI (with and without spin-flip) curves compared with the experimental results of Braid *et al.* (Ref. 45) at  $\theta_1 = 30^\circ, 60^\circ$  and  $90^\circ$  for the  $Mg^{24}(p, p'\gamma)$  reaction at 10.7 MeV<sub>lab</sub>. The  $\theta_1 = 30^\circ$  analysis shows the strong structural similarity of normal DWDI curves to those employing the strong-coupling approach.

rather narrow energy region, within which results of the Rochester group under Alford agree quite closely with compatible results of the Ohio group under Hausman. The latter data are fairly extensive and to some extent confusing. For ease of comparison in the present analysis, data have been combined in three

groups, the first of which collates the 5.8 MeV<sub>lab</sub> and 5.86 MeV<sub>lab</sub> (=5.66 MeV<sub>c.m.</sub>) measurements, the second the 6.2-, 6.3-, and 6.5-MeV measurements, and the third the 6.7-, 6.94-MeV<sub>lab</sub> (=6.7 MeV<sub>c.m.</sub>), and 7.0-MeV results, these being compared, respectively, with CN theoretical predictions for 5.86 MeV, 6.5 MeV, and 6.9 MeV<sub>lab</sub> including partial waves up to  $l \leq 6$ . A point of discrepancy exists in that results published by Hausman *et al.* for an energy

The Ohio group employed three different Si<sup>28</sup> targets in form of quartz fibres; the last-mentioned results were obtained with Target 1. These differ qualitatively from results using Target 2 at the same energy of 7.0 MeV, but concur with the single set

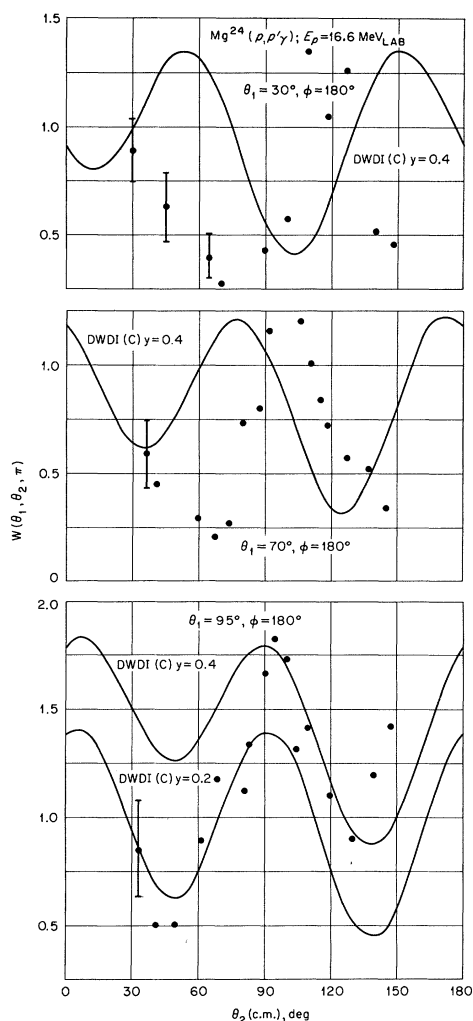


FIG. 20. Strong-coupling DI analysis (with spin-flip and spin-orbit interaction) of Yoshiki's results (Ref. 60) for the  $Mg^{24}(p, p'\gamma)$  reaction at 16.6 MeV<sub>lab</sub>. The solid curves are correlation functions of the form (118).

for 6.5 MeV have been reproduced by Bowsher *et al.* for an energy of 7.0 MeV—from the text of the latter paper one infers the higher energy to be appropriate and, hence, these data have been incorporated in the *third* rather than the second group.

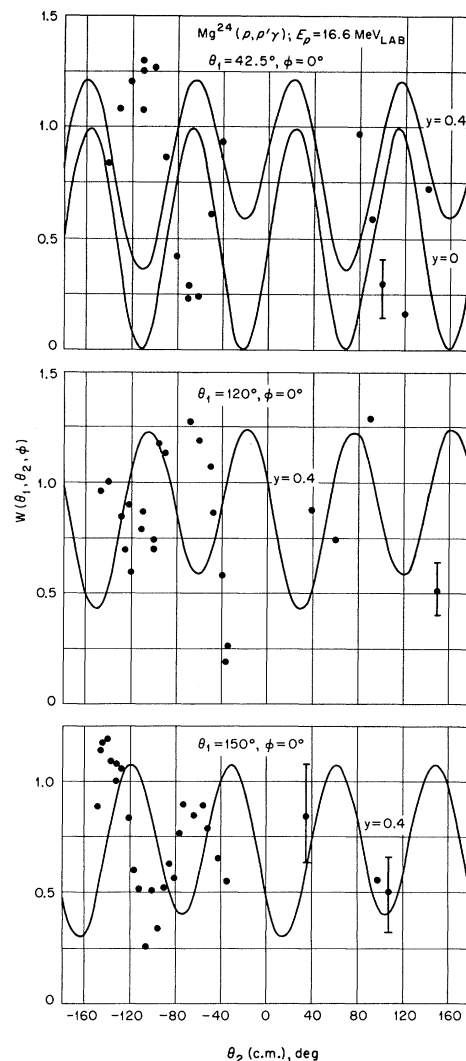


FIG. 21. Symmetry properties of the DI correlation function for  $Mg^{24}(p, p'\gamma)$  at 16.6 MeV: the points represent the measurements of Yoshiki (Ref. 60) and the curves the (normalized) correlation function in the  $\phi = 0^\circ$  plane for a Perey potential ( $V = 46$  MeV,  $r_0 = 1.25$  F,  $a = 0.65$  F,  $W' = 10.5$  MeV,  $r_0' = 1.25$  F,  $a' = 0.47$  F).

( $\theta_1 = 60^\circ$ ) of measurements for Target 3 at that energy. Apart from a further set of results at  $\theta_1 = 60^\circ$  for  $E_p = 6.5$  MeV with Target 3, all other measurements were taken using Target 2. Data from each of the various targets have been graphically distinguished in the present analysis and normalized

arbitrarily in each instance for purpose of comparison.

Figure 22 shows the degree of consistency between measurements of the Rochester and Ohio groups at 5.8 MeV and at the same time the marked disparity with theoretical predictions. It will further be noted that data for the supplementary angles  $\theta_1 = 45^\circ$  and  $135^\circ$  do not display reflection symmetry.

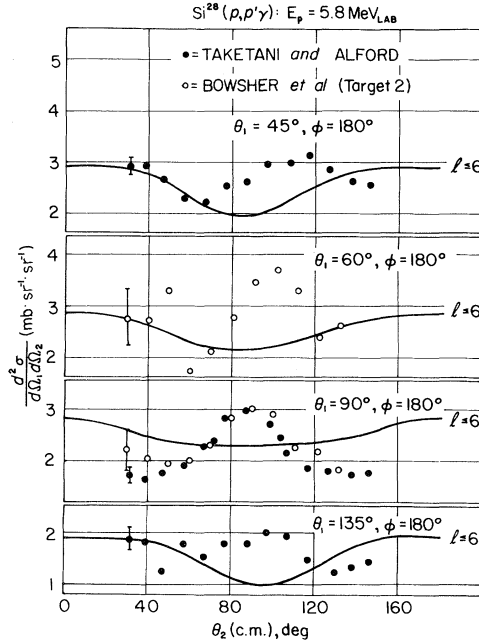


FIG. 22. Comparison of the experimental results of the Rochester (Ref. 24) and Ohio (Ref. 64) groups for the  $\text{Si}^{28}(p,p'\gamma)$  reaction ( $Q = -1.78$  MeV) at 5.8 MeV<sub>lab</sub> with the predicted  $\theta_2$  dependence of the CN double-differential cross section.

Results at the intermediate energies around 6.4 MeV as depicted for Targets 2 and 3 in Fig. 23 are in gross disaccord with theory, though reasonably consistent in their over-all trend. The solid points representing data for 6.3 MeV lie appreciably below the others for  $\theta_1 = 60^\circ$  because of their having been normalized by the same factor as was used for the 6.3-MeV results at  $\theta_1 = 90^\circ$  rather than having been adjusted separately. Thereby they illustrate the fact that over-all agreement between separate sets of data does not obtain when the batch of data for a given target and energy is treated as an entity and multiplied by a common norm; rather, it is necessary to select a suitable norm separately for each ensemble of points for any given angle, target, and energy. This rather unsatisfactory procedure has, accordingly, had to be applied to the results of the Ohio group

in the present analysis, and may be contrasted with the results obtained by the Zürich neutron group for  $\text{Mg}^{24}$  and  $\text{Fe}^{56}$  (Figs. 14 and 44–46) which have in each instance been multiplied by a single over-all norm.

In Fig. 24, the same norm has been employed for the 6.7-MeV<sub>c.m.</sub> results of the Rochester group at the supplementary angles  $\theta_1 = 45^\circ$  and  $135^\circ$ , of which those for  $135^\circ$  would appear to be in moderately good agreement with theory. Those at  $45^\circ$  are, however, inconsistent with theory and do not display the requisite reflection symmetry, neither the amplitudes nor the positions of maxima and minima agree upon reflection. The points for  $\theta_1 = 90^\circ$  were multiplied by a slightly larger factor in order to centralize them about the theoretical curve; use of the common norm would have reduced them by four-fifths so that, for example, the point for  $\theta_2 = 97^\circ$  would have lain just below the theoretical curve. The experimental peak around  $\theta_2 = 90^\circ$  is in complete contradiction to

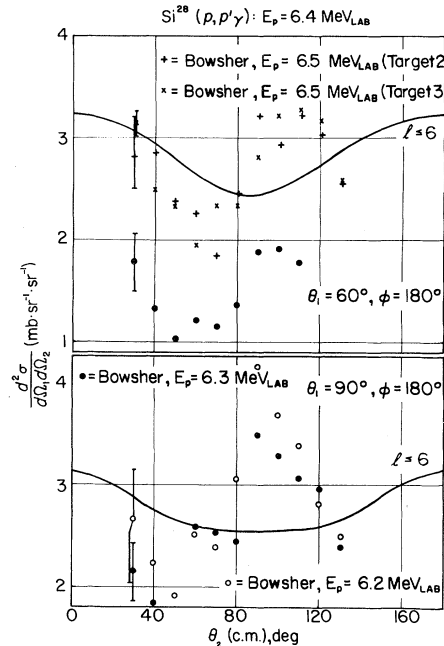


FIG. 23. Analysis of the correlation results of Bowsher *et al.* (Ref. 64) around  $E_p = 6.4$  MeV<sub>lab</sub> for proton scattering on  $\text{Si}^{28}$ .

theory, a feature repeated by the results of Bowsher *et al.* for  $E_p = 6.7$  and 7.0 MeV which are depicted in Fig. 25.

Bowsher *et al.* claim that the symmetry of the correlation function about  $\theta_2 = 90^\circ$  is evidence of a CN mechanism, a conclusion which Sheldon has

shown<sup>17</sup> to be only roughly valid and which in any case is inapplicable to their results since the above symmetry condition requires a *minimum* and not a peak to occur in the correlation function at  $\theta_2 = 90^\circ$ . Indeed, the statement of Bowsher *et al.* that the "6.5-MeV" results of Hausman *et al.* (here included in the 7-MeV data of Fig. 25) can, for all  $\theta_1$ , be fitted by a function of the form

$$W(\theta_1, \theta_2, \pi) = P + Q \sin^2 2(\theta_2 - 90^\circ) \quad (138)$$

is in disaccord with the facts. The symmetry angle lies at  $\theta' = 47^\circ$  but not  $90^\circ$ . The postulation of a CN resonance would not yield correlation functions

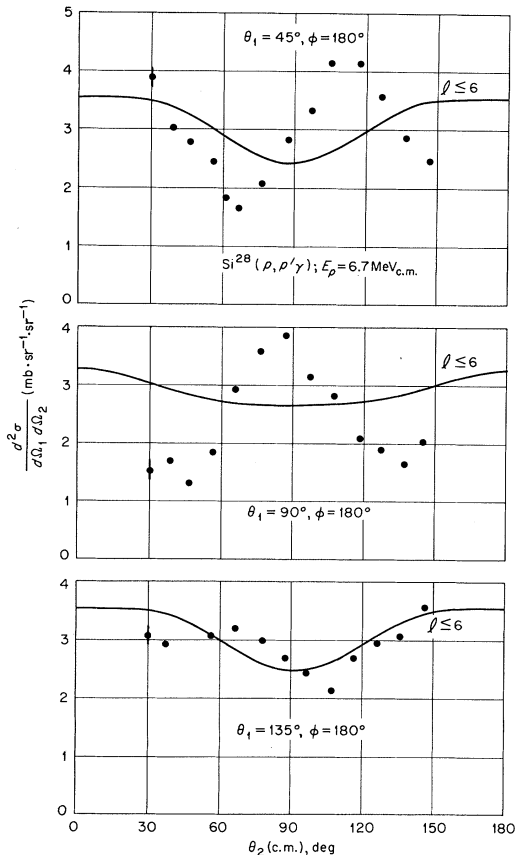


FIG. 24. Comparison between the results of the Rochester group (Ref. 24) for 6.7-MeV<sub>c.m.</sub> protons scattered on Si<sup>28</sup> and the predictions of CN theory.

having a  $\theta_2$  dependence similar to that of the experimental data. The conclusion of these authors that one can infer a CN mechanism proceeding by way of a resonance due to a predominant set of CN levels which become populated by 7-MeV protons (a resonance which does not occur at the lower incident

energies and, therefore, permits the DI mechanism to supercede there), is thus untenable. A noteworthy, albeit confusing, feature of their results is the fact that measurements taken at the same energy but with a different target (No. 2) failed to display the "90° symmetry"—the symmetry, in fact, varied

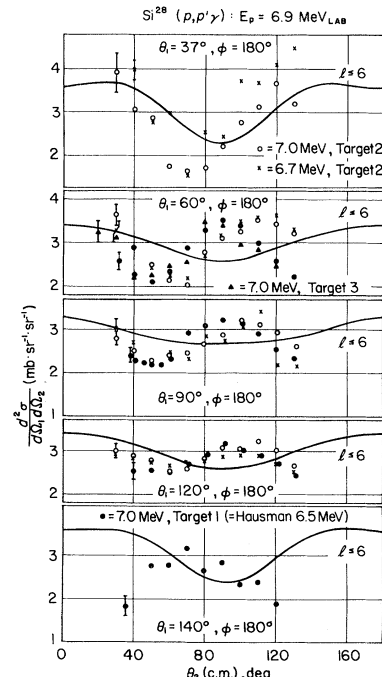


FIG. 25. Experimental results (arbitrarily normalized) of the Ohio group (Refs. 64, 65) around 6.9 MeV<sub>lab</sub> for the Si<sup>28</sup>( $p, p'\gamma$ ) reaction contrasted with the theoretical CN  $\theta_2$  dependence of the double-differential cross section.

with  $\theta_1$  (the symmetry angle  $\theta'$  decreased as  $\theta_1$  went from  $37^\circ$  to  $90^\circ$  and then increased for  $\theta_1 = 120^\circ$ )—while the single set of observations with Target 3 for this energy at  $\theta_1 = 60^\circ$  again revealed no "90° symmetry." These differences of behavior were attributed by the authors to differences in beam energy straggling for targets of apparently different thicknesses, although no further experimental evidence to vindicate this claim was presented. Their final statement that the number of coincidences for "90° symmetric" correlation measurements was approximately double that for the remaining runs would be in rough quantitative agreement with the ratio of theoretical double-differential cross sections for the CN and DI mechanisms. The theoretical ratio proves to be appreciably larger; for example, at 7 MeV and  $\theta_1 = 60^\circ$ , a maximum of the DWDI double-differential cross section

occurs at  $\theta_2 = 76^\circ$  and has the value  $1.08 \text{ mb sr}^{-1} \text{ sr}^{-1}$ . The corresponding theoretical CN double-differential cross section is  $2.84 \text{ mb sr}^{-1} \text{ sr}^{-1}$ , and is, thus, roughly 2.6 times as large as for DWDI. In general, the theoretical ratio is larger than this, however, even when taken at the maxima of the DWDI correlation, as can be seen from Table II. From comparison of  $\theta'$  from Table II with the experimental results in Fig. 25, it is evident that only for  $\theta_1 = 120^\circ$  is there fair agreement between experimental and theoretical values of  $\theta_2$  at which the correlation peaks; however, the amplitude of the experimental correlation ( $\approx \frac{4}{3}$ ) is very much less than that predicted theoretically ( $\approx 130$  for  $y = 0$ ). One cannot, therefore, obtain a fit to any of the results of Bowsher *et al.* with the present pure DWDI approach, for which reason the DWDI curves have not been included in Fig. 25. Examination of the experimental results for 6.7 and 7.0 MeV using Target 2, furthermore reveals that the experimental symmetry angle decreases with increasing  $\theta_1$ , whereas the theoretical  $\theta'$  increases appreciably; at  $\theta_1 = 60^\circ$  there is also a rather striking discontinuity in the  $\theta_2$  dependence of the experimental points between  $\theta_2 = 70^\circ$  and  $80^\circ$  which does not, of course, occur for the theoretical correlation function. One may, thus, conclude that neither of the present theoretical CN or DI approaches can be applied to the measured  $\text{Si}^{28}$  correlation functions.

### C. $\text{S}^{32}$ , $Q = -2.25 \text{ MeV}$

$E_p(\text{MeV})_{\text{lab}}$	$\mathcal{N}$	$\theta_1$	Authors
5.7	$p$	$60^\circ, 90^\circ, 120^\circ$	Hulubei <i>et al.</i> <sup>66</sup>
5.8	$p$	$90^\circ, 135^\circ$	Taketani and Alford <sup>24</sup>
6.02	$p$	$60^\circ, 90^\circ, 120^\circ, 150^\circ$	Hulubei <i>et al.</i> <sup>66</sup>
6.2	$p$	$60^\circ, 90^\circ, 120^\circ$	Hulubei <i>et al.</i> <sup>66</sup>
6.34	$p$	$60^\circ, 90^\circ, 120^\circ$	Hulubei <i>et al.</i> <sup>66</sup>
6.5	$p$	$60^\circ, 90^\circ, 120^\circ$	Hausman <i>et al.</i> <sup>65</sup>

<sup>66</sup> H. Hulubei, N. Martalogu, J. Frantz, M. Ivascu, N. Scinteiu, A. Berinde, and I. Neamu, *Phys. Rev.* **126**, 2174 (1962).

TABLE II. Minimum theoretical ratio of CN to DWDI ( $y = 0$ ) double-differential cross sections for  $\text{Si}^{28}(p, p'\gamma)$  at  $E_p = 6.9 \text{ MeV}_{\text{lab}}$ .

$\theta_1$	$10^3\alpha$	$\theta'$	$\theta_2(\text{DWDI} = \text{max})$ $= \theta' \pm 45^\circ$	Corresponding $\frac{d^2\sigma}{d\Omega_1 d\Omega_2} \Big _{\text{DWDI}}$ $y = 0$ ( $\text{mb sr}^{-1} \text{ sr}^{-1}$ )	Corresponding $\frac{d^2\sigma}{d\Omega_1 d\Omega_2} \Big _{\text{CN}}$ ( $\text{mb sr}^{-1} \text{ sr}^{-1}$ )	Minimum Ratio CN DWDI
$35^\circ$	5.0415	$20^\circ$	$65^\circ$	0.753	2.78	3.69
$60^\circ$	1.1767	$31^\circ$	$76^\circ$	1.078	2.63	2.44
$90^\circ$	1.0525	$43^\circ$	$88^\circ$	0.909	2.68	2.95
$120^\circ$	7.8481	$53^\circ$	$98^\circ$	0.363	3.40	9.37
$140^\circ$	0.0897	$54^\circ$	$99^\circ$	0.106	3.57	33.68

No correlation investigations have been undertaken for  $\text{S}^{32}$  with neutrons, nor is any data available on the  $\theta_1$  dependence of the correlation function. However the proton scattering studies tabulated above yield results which begin to show a measure of agreement with the predictions of CN theory.

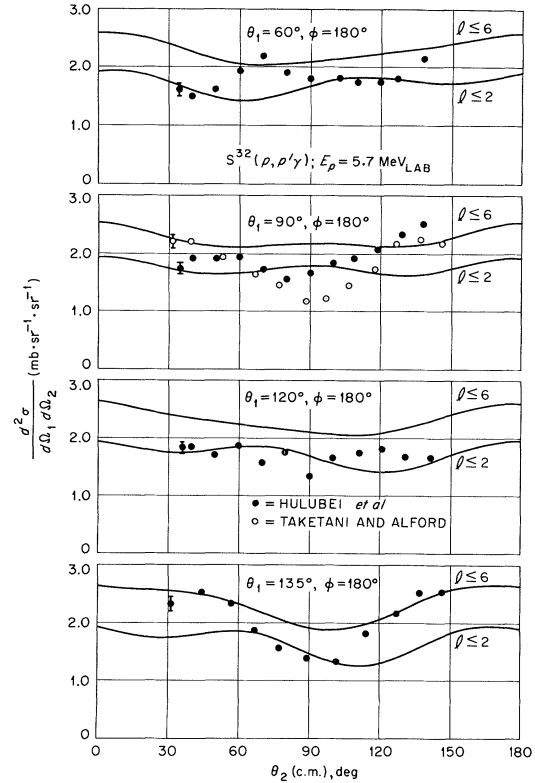


FIG. 26. Comparison for the  $\text{S}^{32}(p, p'\gamma)$  reaction ( $Q = -2.25 \text{ MeV}$ ) around  $5.7 \text{ MeV}_{\text{lab}}$  of the arbitrarily normalized experimental correlation results of the Bucharest (Ref. 66) and Rochester (Ref. 24) groups with the  $\theta_2$  dependence of the CN double-differential cross section.

In view of the proximity of the energies of 5.7 and 5.8 MeV, the results of Hulubei *et al.* and Taketani and Alford have been combined in Fig. 26 and compared with the theoretical double-differential cross

sections at 5.75 MeV. The results of the two groups appear to be mutually compatible and, although, in but imperfect agreement with CN theory, they could not be fitted with absolutely computed DI curves. The sets of results for the supplementary angles  $\theta_1 = 60^\circ$  and  $120^\circ$  roughly substantiate the symmetry property  $W(\theta_1, \theta_2, \pi) = W(\pi - \theta_1, \pi - \theta_2, \pi)$ . However, here this does not furnish a distinguishing criterion between CN and DI mechanisms since study of correlation surfaces reveals this symmetry to be obeyed strictly by CN theory and approximately by DI theory—sufficiently closely to vitiate its use for diagnosis when experimental results display fairly random scatter (as is the case here) and when the latter are expressed as relative (normalized) rather than absolute magnitudes. The theoretical DWDI

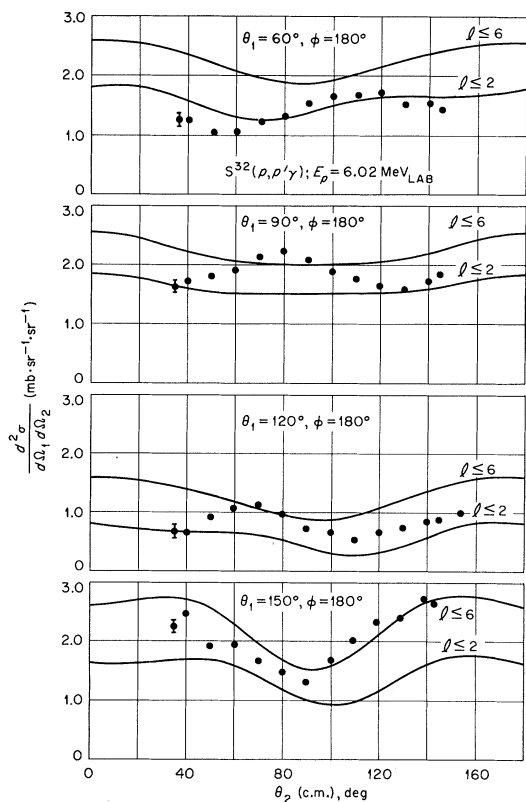


FIG. 27. Correlation results of the Bucharest group (Ref. 66) for  $S^{32}(p, p'\gamma)$  at 6.02 MeV<sub>lab</sub>, in fair agreement with the CN correlation curves for a Perey potential.

correlation functions approximately display the above symmetry, whereas of course the double-differential cross sections do *not*. Figure 27 again shows the fit between experiment and CN theory to be imperfect, but not unreasonable; the aforementioned symmetry holds for measurements at the

supplementary angles  $\theta_1 = 60^\circ$  and  $120^\circ$  which in the present case show less randomness than at the previous energy. Measurements at 6.2 and 6.34 MeV as depicted in Figs. 28 and 29 (wherein they have

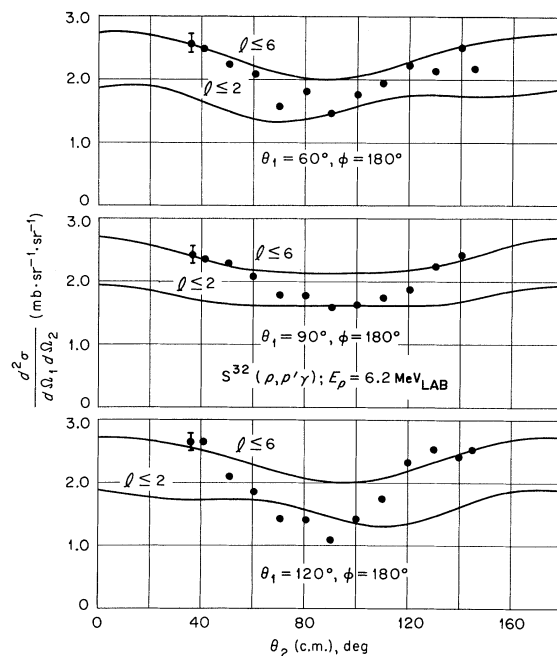


FIG. 28. Correlation analysis for  $S^{32}(p, p'\gamma)$  at 6.2 MeV<sub>lab</sub>: the normalized points of Hulubei *et al.* (Ref. 66) show fair agreement with the CN theoretical curves.

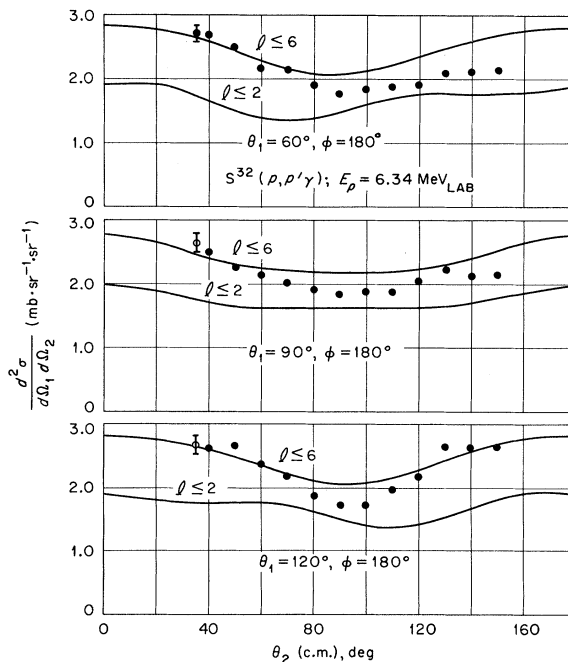


FIG. 29. Correlation analysis for  $S^{32}(p, p'\gamma)$  at 6.34 MeV<sub>lab</sub>: the normalized points of Hulubei *et al.* (Ref. 66) show fair agreement with the CN theoretical curves.

been normalized by the same norm throughout) show very similar  $\theta_2$  dependence, as would be expected, and are in tolerable agreement with the predictions of CN theory. The independent correlation measurements of Hausman *et al.* at 6.5 MeV, as shown in Fig. 30, are in slightly poorer agreement with theory; the results for supplementary angles  $\theta_1 = 60^\circ$  and  $120^\circ$  display discrepancies between the respective symmetry angles, though in their general form an approximate reflective symmetry is evident.

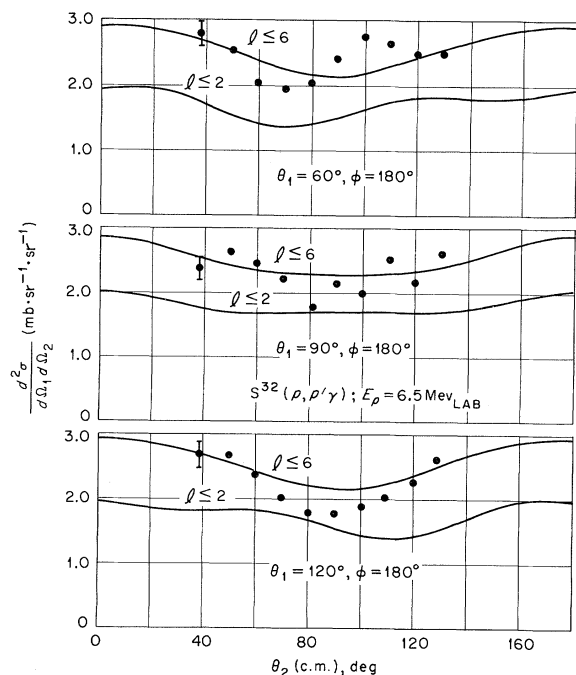


FIG. 30. Correlation analysis for  $S^{32}(p, p'\gamma)$  at 6.5 MeV<sub>lab</sub>: the normalized measurements of Hausman *et al.* (Ref. 65) are in fair agreement with the CN theoretical curves.

#### D. $Ti^{48}$ , $Q = -0.987$ MeV

$E_p(\text{MeV})_{\text{lab}}$	$\pi$	$\theta_1$	Authors
5.84	$p$	$90^\circ, 135^\circ$	Taketani and Alford <sup>24</sup>
6.91	$p$	$90^\circ, 135^\circ$	Taketani and Alford <sup>24</sup>

The sets of correlation measurements taken by Taketani and Alford at 5.72 MeV<sub>c.m.</sub> (=5.84 MeV<sub>lab</sub>) and 6.77 MeV<sub>c.m.</sub> (=6.91 MeV<sub>lab</sub>), shown, respectively, in Figs. 31 and 32, were interpreted by the authors as furnishing evidence for a DI mechanism since DI curves could empirically be fitted to them. However, in the course of the present analysis, it was found that absolutely computed DWDI curves are in disaccord with the experimental  $\theta_2$  dependence,

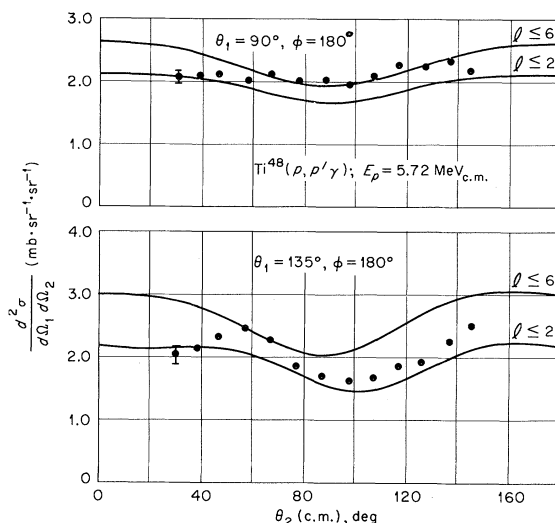


FIG. 31. Comparison between experimental results of the Rochester group (Ref. 24) for inelastic proton scattering on  $Ti^{48}$  ( $Q = -0.987$  MeV) at 5.72 MeV<sub>c.m.</sub> and the theoretical CN curves, which yield a fairly good fit.

particularly for the higher energy, whereas the CN curves shown yield a not unacceptable fit. This evidence, taken in conjunction with estimates of the CN level density as presented in Sec. 8 (Table III) supports the warranty of assuming the continuum hypothesis to be applicable to nuclei with  $A \gtrsim 40$  for incident energies such as the above.

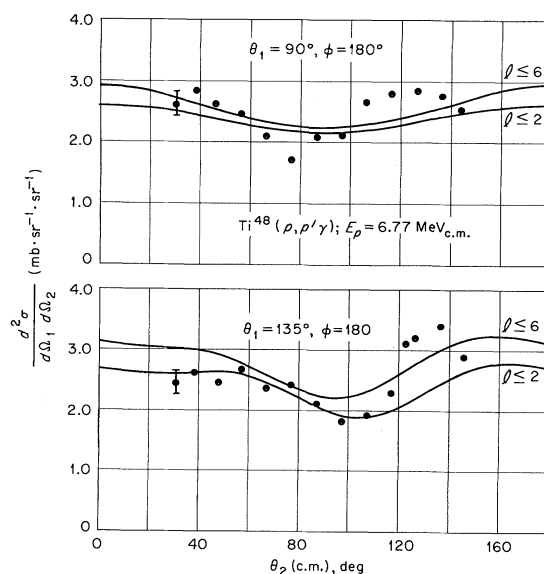


FIG. 32. Measurements at 6.77 MeV<sub>c.m.</sub> for the reaction  $Ti^{48}(p, p'\gamma)$  by the Rochester group (Ref. 24) compared with CN theoretical predictions; discrepancies in fit at this slightly higher energy are most likely due to admixture of DI mechanism.

**E. Cr<sup>52</sup>, Q = -1.433 MeV**

$E_p(\text{MeV})_{\text{lab}}$	$\varpi$	$\theta_1$	Authors
4.1	$p$	$90^\circ(\varphi = 90^\circ)$	Gobbi and Pixley <sup>67</sup>
4.1	$p$	$50^\circ, 90^\circ, 130^\circ$	Gobbi and Pixley <sup>67,68</sup>
5.43	$p$	$45^\circ, 90^\circ$	Seward <sup>23</sup>
5.8	$p$	$45^\circ, 90^\circ, 135^\circ$	Gobbi and Pixley <sup>67</sup>
6.5	$p$	$90^\circ$	Hausman <i>et al.</i> <sup>65</sup>
7.02	$p$	$45^\circ, 90^\circ$	Seward <sup>23</sup>

For protons incident upon the target nucleus Cr<sup>52</sup>, agreement between CN theoretical and measured correlations is remarkably good; the only quantitative disagreement occurs in the analysis of measured double-differential cross sections at 5.8 MeV<sub>lab</sub> for  $\theta_1 = 90^\circ$ , wherein the points display the same  $\theta_2$  dependence as the theoretical curve but differ by a factor of 2 from the predicted absolute magnitude. Measurements at  $\theta_1 = 45^\circ$  and  $135^\circ$ , however, almost attained the theoretical value and will be considered later. Attention is also drawn to the determination of the “ $p'$ -perpendicular correlation” at 4.1 MeV, which will be discussed next.

The results of the Zürich group for the  $p'$ -perpendicular correlation, shown in Fig. 33 normalized

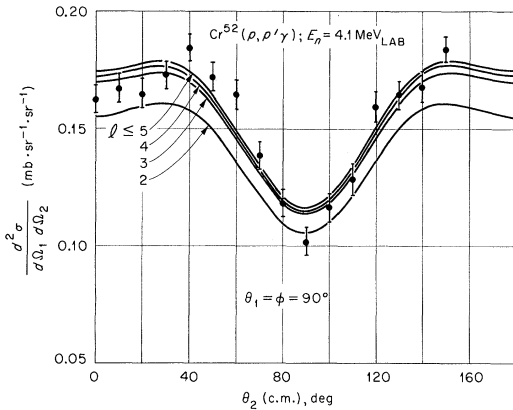


FIG. 33. Normalized  $p' - \gamma$  coincidence measurements of the Zürich group (Ref. 67) with the  $p'$ -counter perpendicular to the  $p - \gamma$  plane for the Cr<sup>52</sup>( $p, p'\gamma$ ) reaction ( $Q = -1.433$  MeV) at 4.1 MeV<sub>lab</sub>, in excellent agreement with CN theoretical predictions using Preskitt-Alford transmission coefficients.

arbitrarily for comparison with the theoretical double-differential cross section, have already been published (with different normalization) together with the  $\gamma$ -ray distribution (Fig. 2 of Ref. 35). The latter figure showed the very good agreement between theory and experiment not only for the  $p'$ -

perpendicular correlation but also for the  $\gamma$  distribution and indicated the corresponding theoretical curves to be similar but not identical. For completeness, this point is illustrated in Fig. 34 for the above pair of curves and also for the pair corresponding to

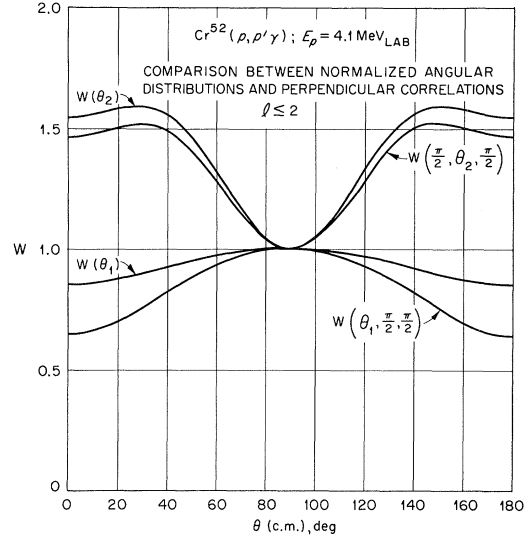


FIG. 34. Illustration of the difference between theoretical CN angular distributions and “perpendicular correlations,” referred to the Cr<sup>52</sup>( $p, p'\gamma$ ) reaction at 4.1 MeV<sub>lab</sub> and normalized to unity at  $90^\circ$ .

the proton distribution and the  $\gamma$  perpendicular correlation, all curves being normalized to unity at  $90^\circ$  in order to display clearly the marked difference in structure.

Excellent agreement between theory and experiment is also found when correlation measurements at 4.1 MeV<sub>lab</sub> are taken in the scattering plane, as can be seen from Fig. 35. Again the points have, as heretofore, been normalized arbitrarily; those obtained at the supplementary angles  $\theta_1 = 50^\circ$  and  $130^\circ$  verify *two* symmetry properties of the CN correlation function, viz.,

$$W(\theta_1, \theta_2, \pi) = W(\pi - \theta_1, \pi - \theta_2, \pi) = W(\pi - \theta_1, \theta_2, 0). \quad (139)$$

The results for  $\theta_1 = 90^\circ$  are in slightly poorer agreement with the theoretical curve in that their amplitude is a little too large and that the dip which they display around  $\theta_2 = 0^\circ$  is not reproduced theoretically. It is interesting that the same effect was found in proton correlation measurements upon Fe<sup>56</sup> at the same energy and at 5.8 MeV (see Figs. 49 and 52), though otherwise the theoretical fit is very satisfactory. There is no *a priori* reason to suspect the validity either of theory or of experiment for forward emission of  $\gamma$  radiation, yet this feature has recur-

<sup>67</sup> B. Gobbi and R. E. Pixley (private communication).

<sup>68</sup> B. Gobbi and R. E. Pixley, *Helv. Phys. Acta* **34**, 802 (1961).

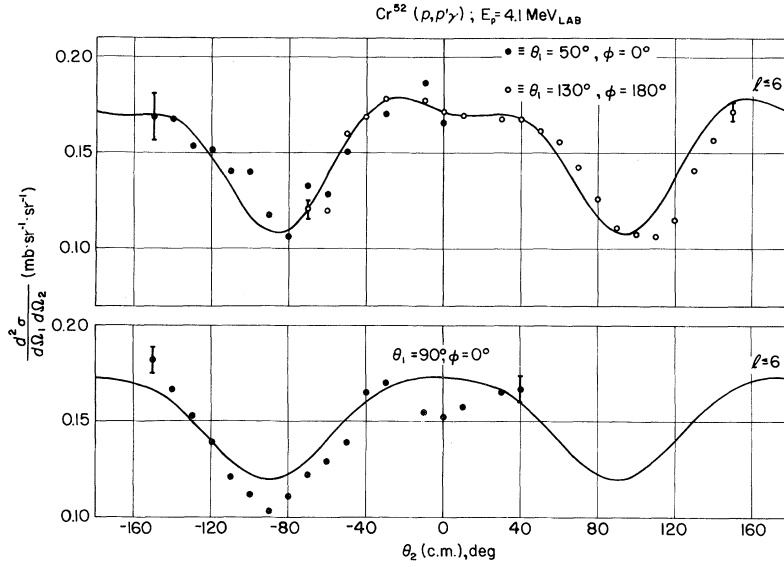


Fig. 35. Experimental results of the Zürich group (Ref. 67) in both scattering half-planes for inelastic proton scattering on  $\text{Cr}^{52}$  at  $4.1 \text{ MeV}_{\text{lab}}$  illustrate the excellent agreement with CN theory including the symmetry predictions of the latter.

rently been observed. It may be that the well-known occurrence of discrepancy between experimental results at forward *proton* angles  $\theta_1$  and optical-model calculations have some bearing upon the above phenomenon.

The correlation measurements at  $5.43 \text{ MeV}$  by Seward of the Rochester group, shown in Fig. 36, were correctly interpreted by him as evidence for the predominance of CN mechanism, though it should

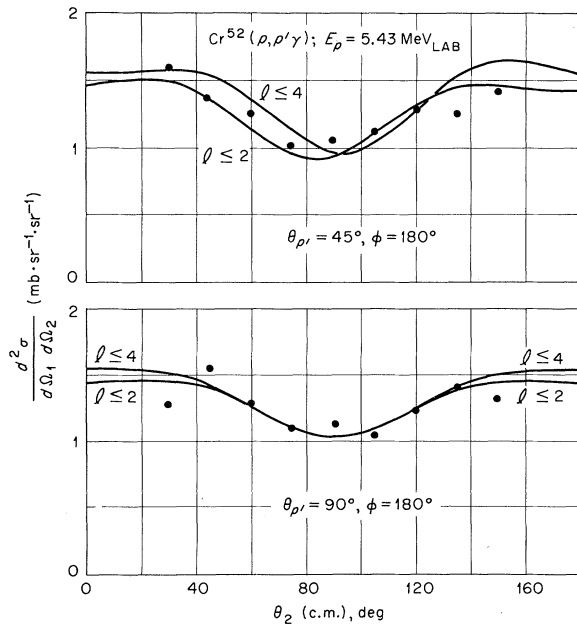


Fig. 36. Experimental results of Seward (Ref. 23) for  $\text{Cr}^{52}$  ( $p, p'\gamma$ ) at  $5.43 \text{ MeV}_{\text{lab}}$ , in very good agreement with CN theory based upon a Preskitt-Alford optical potential.

be noted that his theoretical curves were calculated with incorporation of mixed- $j$  interference terms and, therefore, differ a little from those depicted in Fig. 36. The new theoretical curves provide an equally satisfactory fit to the experimental points.

The results at  $5.8 \text{ MeV}$  shown in Fig. 37 raise an interesting issue in that they depict measured absolute double-differential cross sections which have not been normalized and, therefore, provide a very much more stringent test of CN theory than would otherwise be the case. Not only the qualitative, but also the quantitative, measure of agreement between theory and experiment for the  $\theta_1 = 45^\circ$  and  $135^\circ$  data is very satisfactory, especially on noting that the error limits shown represent observed reproducibilities, whereas the actual over-all accuracy of the measured points is in the order of  $\pm 20\%$ . The study of the  $\theta_2$  dependence over nearly  $360^\circ$  in the scattering plane for supplementary values of  $\theta_1$  furnishes an extensive test of CN correlation symmetries, thereby conferring particular interest upon this batch of results. All the more significant, therefore, is the quantitative disagreement between theoretical and experimental double-differential cross sections for  $\theta_1 = 90^\circ$ , a phenomenon observable also for  $\text{Fe}^{56}$  at the same energy (Fig. 53). A diminution in the cross section might point to onset of DI mechanism, but computations for the latter yield a double-differential cross section of very small magnitude with a minimum at  $\theta_2 \approx \theta' \cong 50^\circ$ , rather like the DWDI curves shown for  $\text{Fe}^{56}$  and, therefore, in marked disagreement with the experimental results. Multiplication of the measured values by the factor

2.15 normalizes them to tally very closely with the CN theoretical curve for  $l \leq 4$ , which suggests that the operative mechanism is nevertheless CN, but modified by slight admixture of DI which particularly influences the  $\theta_1 = 90^\circ$  correlation. Figure 38 shows results of the Ohio group at 6.5 MeV; the experimental points are fairly isotropic and, within error limits, are in rough agreement with CN theory. The authors' statement that CN theory predicts an

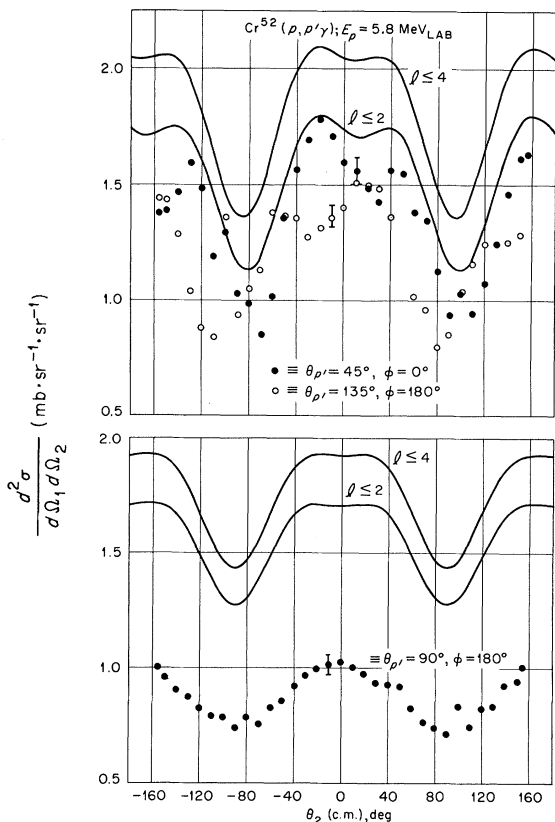


FIG. 37. Experimental absolute measurements of the double-differential cross section for the  $\text{Cr}^{52}(p,p'\gamma)$  reaction at 5.8 MeV<sub>lab</sub> by the Zürich group (Ref. 67) compared with the CN theoretical  $\theta_2$  dependence. The measurements display the same structure as the theoretical curves and reproduce the predicted CN symmetries, but are rather low in magnitude, a consequence either of DI admixture or of the strong energy dependence of the CN double-differential cross section (see Fig. 68).

isotropic correlation is, however, seen to be unsubstantiated by the computed curve, unless interpreted in the loose sense of a small peak-to-valley ratio (the theoretical ratio is about 1.25). The points are rather too few and too scattered to serve as basis for elucidation of mechanism—they are not incompatible with CN theoretical predictions, whereas DWDI theory predicts minima near  $\theta_2 \approx \theta' \cong 40^\circ$  and  $130^\circ$  which are not apparent in the experimental data.

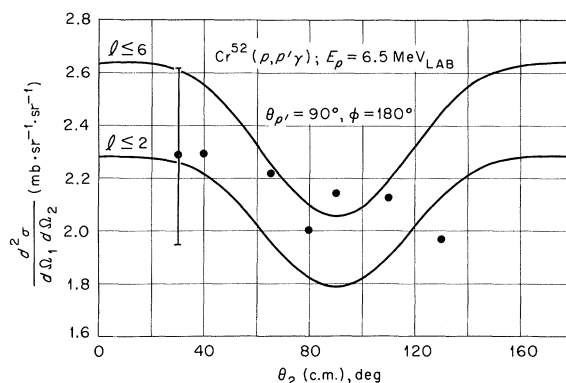


FIG. 38. Normalized experimental points of the Ohio group (Ref. 65) for proton scattering at 6.5 MeV on  $\text{Cr}^{52}$ , compared with CN theory.

Even though Seward empirically fitted curves of DWDI form to his results at 7.02 MeV, depicted in Fig. 39, he observed that even at this energy the CN contribution was probably large and the fit to the  $\theta_1 = 90^\circ$  data meaningless in view of the lack of structure in the  $\theta_2$  dependence: The “ $\text{Cr}^{52}$  correlations at 7 MeV might be interpreted as having a bit of DI in them.” The present analysis indicates the CN mechanism to be predominant and the basic CN theory to furnish a satisfactory fit to the data even though population of target nucleus states higher than the first excited level doubtless occurs. The  $\theta_1 = 90^\circ$  data in particular could not be fitted with

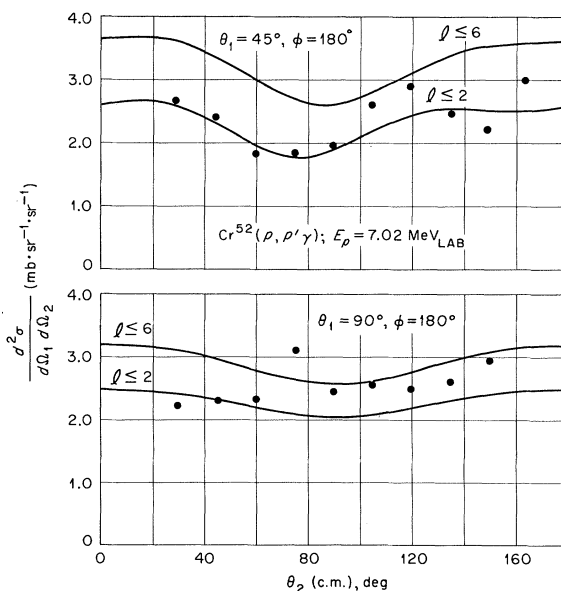


FIG. 39. Normalized experimental results of Seward (Ref. 23) at 7.02 MeV<sub>lab</sub> for  $\text{Cr}^{52}(p,p'\gamma)$ , in good agreement with CN correlation theory based upon a Preskitt-Alford optical potential.

DWDI curves even for large spin-flip intensity since it is practically isotropic, unlike DWDI curves with their strong  $\sin^2$  form, but is well fitted by the shallow CN curves shown.

F. $\text{Fe}^{56}$ , $Q = -0.845 \text{ MeV}$				
$E(\text{MeV})_{\text{lab}}$	$\mathfrak{N}$	$\theta_1$	$\theta_2$	Authors
2.05	$n$	$25^\circ, 35^\circ, 50^\circ,$ $65^\circ, 115^\circ,$ $130^\circ, 145^\circ,$ $155^\circ$	$35^\circ, 50^\circ, 65^\circ,$ $115^\circ, 130^\circ,$ $25^\circ, 145^\circ,$ $155^\circ$	Niewodniczanski and Steiger <sup>57</sup>
4.3	$p$	$90^\circ, 130^\circ$		Gobbi and Pixley <sup>67</sup>
5.8	$p$	$45^\circ, 90^\circ, 135^\circ$		Gobbi and Pixley <sup>67</sup>

The nucleus  $\text{Fe}^{56}$  has been subjected to extensive theoretical and experimental study by the Zürich group. In Sec. 6, correlation surfaces for neutron and

proton scattering have been shown (Figs. 8 and 9), cuts in which constitute some of the correlation curves depicted in the present section. To illustrate the effect of considering higher nucleon orbital momenta and the influence of spin-orbit interaction some theoretical curves are shown which depict the  $\theta_2$  dependence of the correlation in each case. Results have been plotted both in normalized and unnormalized form, namely, as correlation functions, such that  $W(\frac{1}{2}\pi, \frac{1}{2}\pi, \varphi) = 1$ , and as double-differential cross sections in order to indicate the difference in the relative vertical shifts of the curves for various  $l$  values.

Figures 40 and 41 for scattering of 2.05-MeV neutrons at  $\theta_1 = 45^\circ$  and  $90^\circ$ , respectively, show that the effect of including spin-orbit interaction by use of  $T_i^{(\pm)}$  penetrabilities in place of the normal  $T_i$  is very slight in comparison with inclusion of higher partial

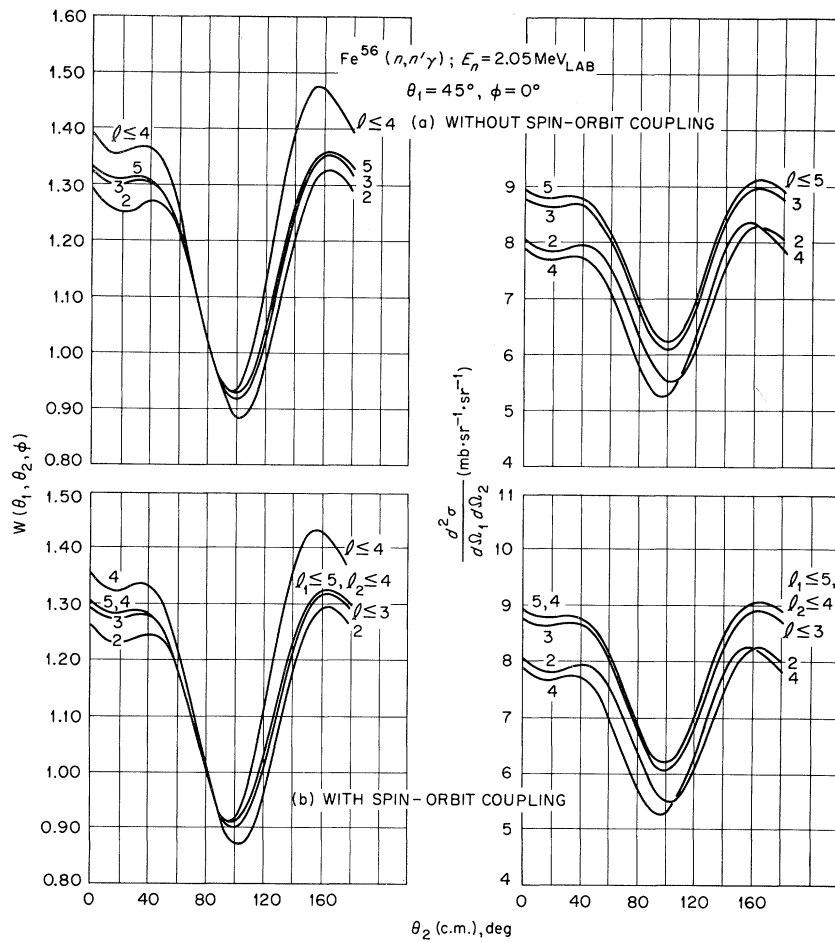


FIG. 40. Comparison of the  $\theta_2$  dependence of the (normalized) CN correlation function and the (absolute) double-differential cross section for various maximum orbital momenta, with and without inclusion of spin-orbit interaction for  $\theta_1 = 45^\circ$  for the  $\text{Fe}^{56}(n, n'\gamma)$  reaction ( $Q = -0.845 \text{ MeV}$ ) at  $2.05 \text{ MeV}_{\text{lab}}$ .

waves. As already pointed out in Sec. 6, plots of the (normalized) correlation function indicated that "odd- $l_{\max}$ " and "even- $l_{\max}$ " curves tend to bunch together; this, however, is no longer the case when plotted as an absolute double-differential cross section. The sequence for curves becomes transposed for the various  $l$  values, the ensuing shift being such that although the relative amplitudes are, of course, unchanged, the minima are less localized in position and the curves are more evenly separated. Since the curves for all  $l$  values at a given  $\theta_1$  are practically identical, it is not possible in the present analysis to deduce empirically which  $l$  values are, in fact, of significance for a given reaction.

Another feature of interest is the azimuthal dependence of the CN correlation function for given  $\theta_1$  and  $\theta_2$ , which is shown in Fig. 42. This  $\varphi$  dependence proves to be rather too weak to appear potentially

fruitful for experimental investigation. For the pairs of angles  $\theta_1$  and  $\theta_2$  shown, the peak-to-valley ratio varies from 1.15 for the pair  $60^\circ, 60^\circ$  to 1.01 for the pair  $30^\circ, 90^\circ$ , the latter being associated with a virtually constant correlation function. Furthermore, exact constancy of the correlation function in terms of  $\varphi$  ensues whenever  $\theta_1, \theta_2 = 0$  or  $\pi$  for all  $\theta_2, \theta_1$ , respectively. This follows from the property of the Legendre hyperpolynomial as expressed by Eq. (A5) of the Appendix:

$$S_{\mu\nu\lambda}(\theta_1, \theta_2, \varphi) = \sum_m A_m P_\nu^m(\cos \theta_1) P_\lambda^m(\cos \theta_2) \cos m\varphi. \quad (140)$$

For  $\theta_1$  or  $\theta_2$  equal to 0 (or  $\pi$ ) the respective associated Legendre function vanishes unless  $m = 0$ ,

$$P_\nu^m(1) = P_\lambda^m(1) = \delta_{m0}, \quad (141)$$

and thereby the  $\varphi$  dependence simultaneously van-

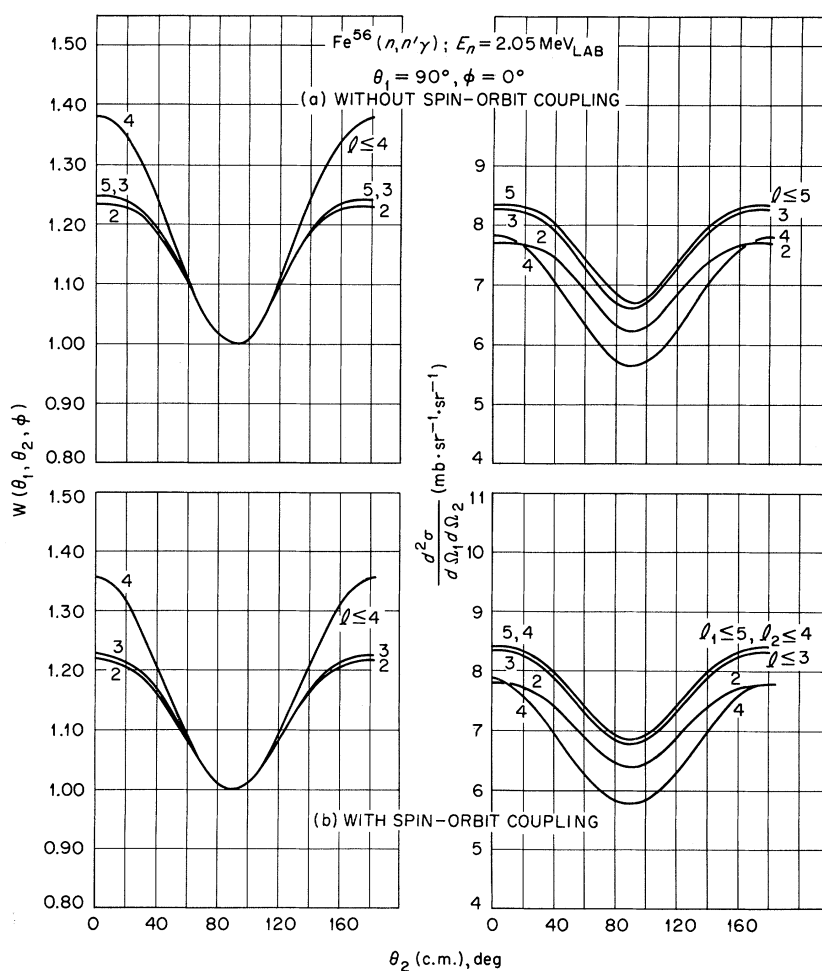


FIG. 41. As Fig. 40 but for  $\theta_1 = 90^\circ$ . The arbitrary normalization of all the left-hand curves to unity at  $\theta_2 = 90^\circ$  influences their sequence for increasing values of  $l_{\max}$ , the orbital momentum cutoff.

ishes. (One notes in passing that the above reasoning indicates the DWDI correlation function also to be independent of  $\varphi$  when  $\theta_2 = 0$  or  $\pi$ .) As a physical requirement, too, this is obvious.

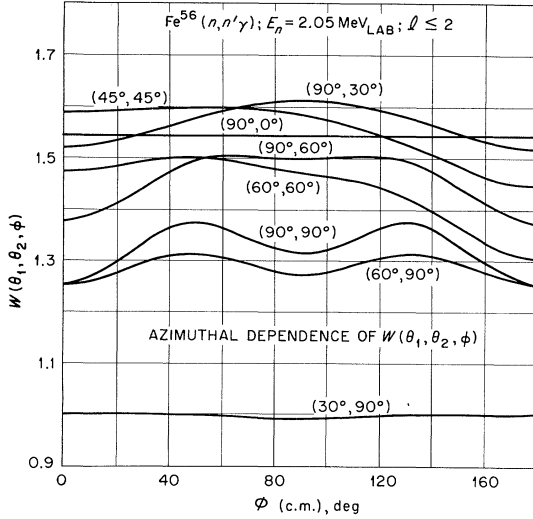


FIG. 42. Illustration of the azimuthal dependence of the CN correlation function for various pairs of values of the emission angles  $(\theta_1, \theta_2)$  for the reaction  $\text{Fe}^{56}(n, n'\gamma)$  at 2.05 MeV using Perey-Buck nonlocal transmission coefficients for  $l \leq 2$ .

Thus,

$$S_{\mu\nu\lambda}(\theta_1, 0, \varphi) = A_0(\mu\nu\lambda)P_\nu(\cos \theta_1) \quad (142)$$

and

$$S_{\mu\nu\lambda}(0, \theta_2, \varphi) = A_0(\mu\nu\lambda)P_\lambda(\cos \theta_2), \quad (143)$$

wherein it should be noted that, through the  $A_0$ , the dependence upon the triad  $(\mu\nu\lambda)$  is retained and the numerical values, therefore, differ from those for a simple angular distribution.

Thus,

$$W(\theta_1, 0, \varphi) = W(\theta_1, \pi, \varphi) \sim P_\nu(\cos \theta_1) \quad (144)$$

and

$$W(0, \theta_2, \varphi) = W(\pi, \theta_2, \varphi) \sim P_\lambda(\cos \theta_2). \quad (145)$$

Additionally, the following symmetries apply:

$$\begin{aligned} W(\theta_1, \theta_2, \varphi) &= W(\theta_1, \pi - \theta_2, \pi - \varphi) \\ &= W(\pi - \theta_1, \theta_2, \pi - \varphi) = W(\pi - \theta_1, \pi - \theta_2, \varphi). \end{aligned} \quad (146)$$

Finally, before going on to analyze experimental results, it is of interest to furnish examples of theoretical angular distributions although the latter fall outside the purview of the present survey. It should be mentioned that the theoretical computations at this

energy have throughout been based on the Perey-Buck optical potential for neutrons. In Fig. 43 are depicted absolute angular distributions of the inelastically scattered neutrons from the  $\text{Fe}^{56}(n, n'\gamma)$  reaction at 2.05 MeV. The CN curves show the effect of incorporating higher partial waves and have been computed by integration of the double-differential cross section as described in Sec. 3B. The DWDI distribution has been computed directly for  $l = 2$  momentum transfer and is not only of higher absolute magnitude than the corresponding curve for the CN mechanism, but also of larger amplitude. It displays strong forward peaking, though, as should perhaps be emphasized, this in itself is not an essential requirement for DWDI distributions in inelastic scattering processes. Extensive analysis of DWDI angular distributions leads to the realization that only as a general trend does forward peaking occur, and then more pronouncedly in the case of elastic nucleon scattering than in inelastic scattering. Satchler *et al.*<sup>47</sup> have drawn attention to exceptions from this tendency, e.g., the DWDI inelastic proton angular distribution for the  $\text{Cr}^{52}(p, p'\gamma)$  reaction at  $E_p = 5.54$  MeV<sub>lab</sub> proves to be U shaped (i.e., with forward and backward peaking) and practically symmetrical about  $\theta_1 = 90^\circ$ .

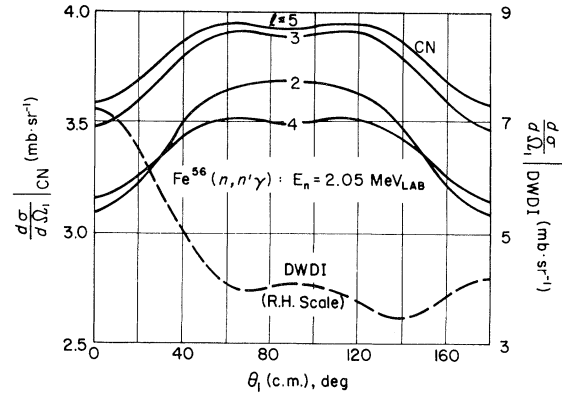


FIG. 43. Illustration for the reaction  $\text{Fe}^{56}(n, n'\gamma)$  at 2.05 MeV, of the change in magnitude of the CN neutron differential cross section with increasing permitted orbital momenta and comparison with that for the DI mechanism (omitting spin-orbit interaction) for  $l = 2$ .

The extensive correlation measurements at  $E_n = 2.05$  MeV<sub>lab</sub> by Niewodniczanski and Steiger, to be examined next, supply data for analysis not only of the  $\theta_2$  dependence at supplementary neutron angles, but also of the  $\theta_1$  dependence at supplementary  $\gamma$  angles, the azimuth  $\varphi$  being zero throughout in consequence of the use of ring geometry. The experimental points in the present analysis represent

the latest results and supercede those published previously; they have been corrected for multiple scattering and normalized by a single norm throughout to yield a least-squares fit to the  $l \leq 2$  curves (using a subsidiary IBM 709 code to accomplish this). In Figs. 44 and 45 are shown results for three

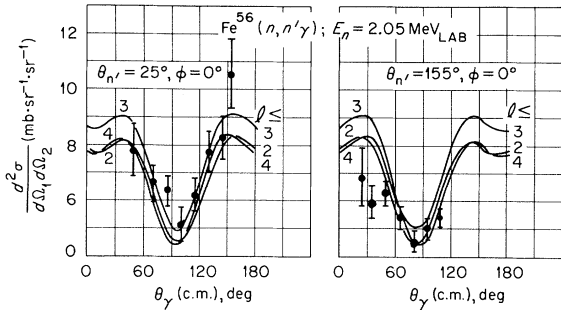


FIG. 44. Theoretical CN fits to the correlation measurements of Niewodniczanski and Steiger (Ref. 57) for inelastic neutron scattering on  $\text{Fe}^{56}$  at 2.05 MeV<sub>lab</sub> for the supplementary angles  $\theta_1 = 25^\circ, 155^\circ$ . The left-hand and right-hand curves are, respectively, mirror images of one another. All the points in Figs. 44–48 have been multiplied by a single norm.

pairs of supplementary angles compared with the predictions of CN theory for momenta  $l \leq 2, 3, 4$ . The agreement, though not perfect, is satisfactory; one feature which stands out, however, is the fact that points for forward scattering angles  $\theta_1$  tend to

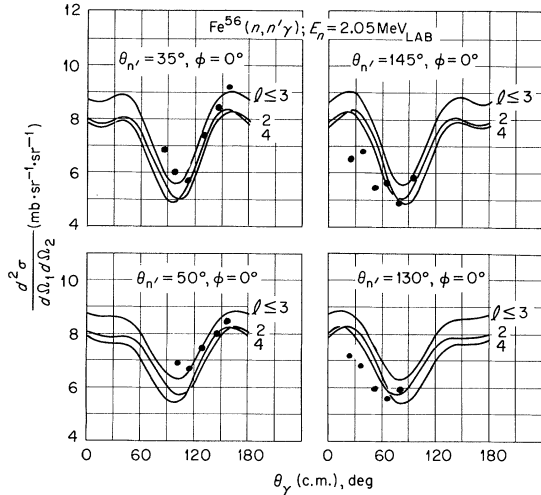


FIG. 45. As Fig. 44, but for the pairs of supplementary angles  $\theta_1 = 35^\circ, 145^\circ$  and  $50^\circ, 130^\circ$ .

lie higher than those for the supplementary backward scattering angles. This effect may be caused by admixture of DWDI (e.g., interference between CN and DWDI) or it may lie in the measurement technique (it would be desirable to have results at  $\theta_2$

$= \frac{1}{2} \pi$  for supplementary angles  $\theta_1$ , as also measurements of the  $n'$  angular distribution). As is apparent from Fig. 46, which not only shows points for a further pair of supplementary scattering angles compared with CN theoretical curves, but also DWDI curves with and without spin-flip for comparison, the results are incompatible with predominance of DWDI mechanism in form (no comparison of magnitudes is possible). The figure indicates the inequality of the double-differential DI cross section for supplementary neutron angles at  $\theta_2 = \frac{1}{2} \pi$  and also shows that, in general, this cross section at forward  $\theta_1$  and backward  $\theta_2$  tends to be higher than that at backward  $\theta_1$  and forward  $\theta_2$ , as is paralleled by the experimental results. The very small magnitude of the DWDI double-differential cross section compared with that for the CN mechanism, remarkable in view of the

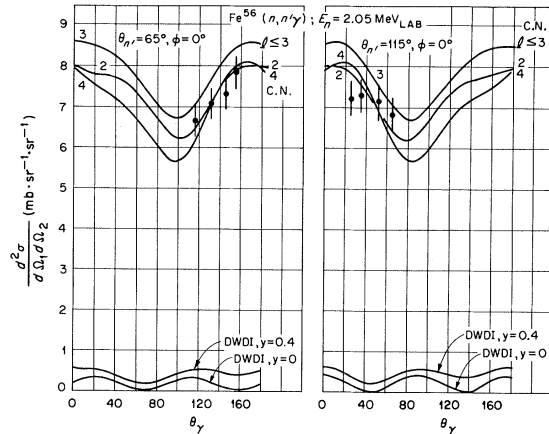


FIG. 46. As Figs. 44 and 45 but for  $\theta_1 = 65^\circ, 115^\circ$ .

comparatively large differential cross section, would tend to rule out any appreciable DI contribution or interference, as one would expect for so low an incident energy. The  $\theta_1$  dependence of the correlation for pairs of supplementary  $\gamma$  angles as shown in Figs. 47 and 48 displays interesting structure, in moderately reasonable agreement with CN theory.

Proton correlation studies on  $\text{Fe}^{56}$  at 4.3 MeV<sub>lab</sub> ( $= 4.22$  MeV<sub>e.m.</sub>) yield equally satisfactory agreement with CN theoretical predictions; the only marked discrepancies occur around  $\theta_2 \approx 0^\circ$  as can be seen from Fig. 49. The  $l \leq 2$  curves therein computed using a Preskitt–Alford potential may be compared with those shown in Ref. 68; the latter, which had been obtained from calculations incorporating mixed- $j$  interference terms, are practically identical.

Figure 50 shows the measure of agreement between CN theory and experiment for the  $p'$ -perpendicular correlation at 4.3 MeV; again, apart from deviations at low  $\theta_2$ , the fit is remarkably good.

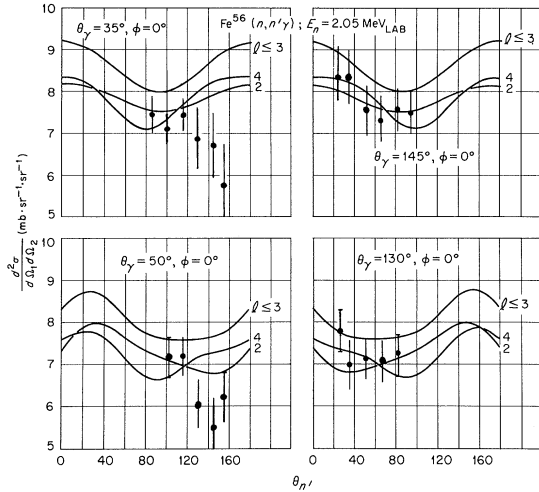


FIG. 47. As Figs. 44–46, but illustrating the  $\theta_1$  dependence of the CN double-differential cross section for the pairs of supplementary angles  $\theta_2 = 35^\circ, 145^\circ$  and  $50^\circ, 130^\circ$  in the reaction  $\text{Fe}^{56}(n, n'\gamma)_{\mathcal{Q} = -0.845 \text{ MeV}}$  at  $2.05 \text{ MeV}_{\text{lab}}$ . Left-hand and right-hand curves are again, respectively, mirror images of each other and all experimental points have been multiplied by but a single norm.

To complement the theoretical  $n'$ -angular distributions shown in Fig. 43, a single example is given here (Fig. 51) to illustrate the agreement between CN theory and experiment for a  $\gamma$ -angular distribution and in particular to show the symmetry of the latter when measurements are taken on both sides

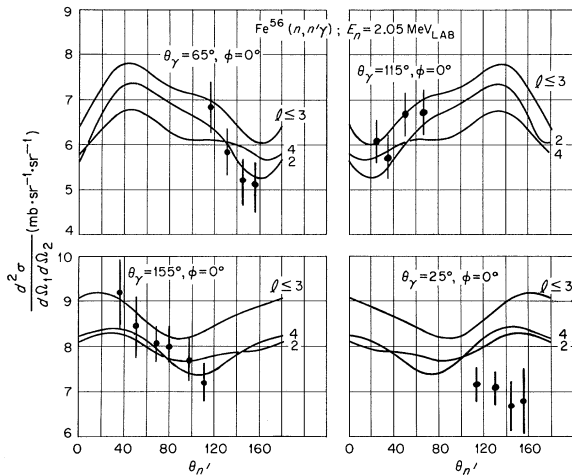


FIG. 48. As Fig. 47 but for  $\theta_2 = 65^\circ, 115^\circ$  and  $155^\circ, 25^\circ$ .

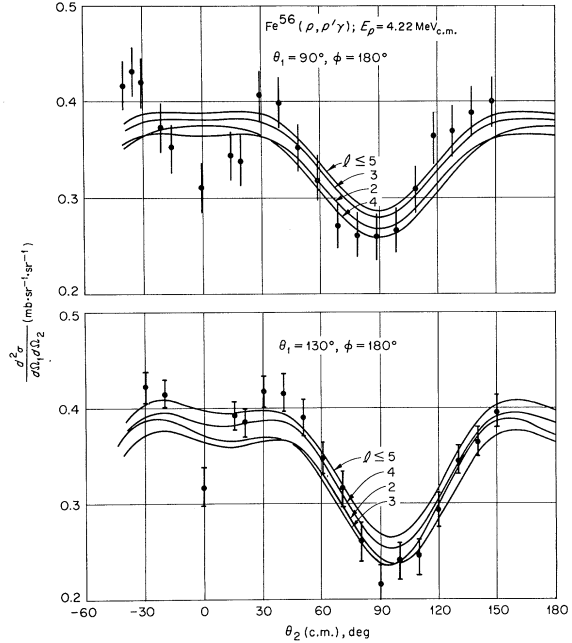


FIG. 49. Theoretical CN fits based upon a Preskitt–Alford optical model to the correlation results at  $\theta_1 = 90^\circ$  and  $130^\circ$  of Gobbi and Pixley (Refs. 67, 68) for inelastic scattering of  $4.3\text{-MeV}_{\text{lab}}$  protons on  $\text{Fe}^{56}$ . The only noteworthy discrepancy occurs in the neighborhood of  $\theta_2 = 0^\circ$ .

of the incident axis. Apart from the characteristic deviation at low  $\theta_2$ , the agreement is excellent.

Correlation results at  $E_p = 5.8 \text{ MeV}_{\text{lab}}$  have been collated in Fig. 52, which shows the data from

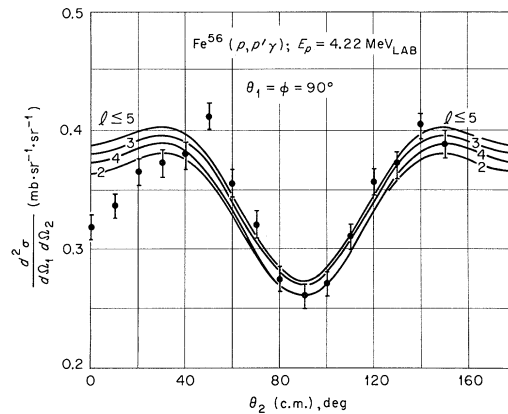


FIG. 50. Comparison of the CN theoretical predictions for the  $p'$ -perpendicular correlation with the measurements of the Zürich group (Ref. 67) for  $\text{Fe}^{56}(p, p'\gamma)_{\mathcal{Q} = -0.845 \text{ MeV}}$  at  $4.3 \text{ MeV}_{\text{lab}}$ .

absolute measurements extended over both scattering half-planes as a test of the predicted CN symmetry

$$W(\theta_1, \theta_2, 0) = W(\theta_1, \theta_2 - \pi, 0) = W(\theta_1, \pi - \theta_2, \pi). \quad (147)$$

The results for the supplementary angles  $\theta_1 = 45^\circ$  and  $135^\circ$  further support the additional symmetry prediction

$$W(\theta_1, \theta_2, 0) = W(\pi - \theta_1, \theta_2, \pi), \quad (148)$$

in that the solid and open data points both display an identical dependence upon  $\theta_2$ . Comparison between

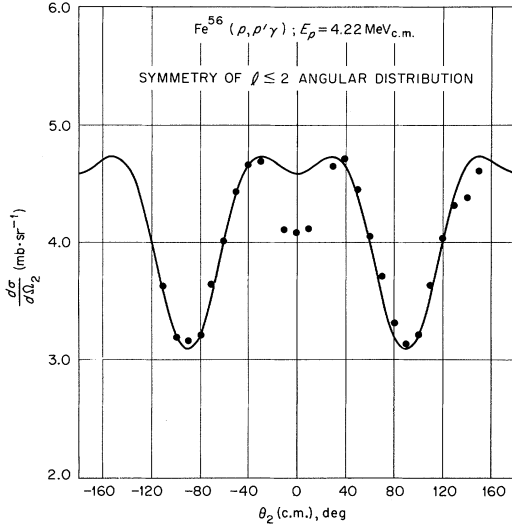


FIG. 51. Theoretical CN fit to the  $\gamma$  distribution measured by the Zürich group (Ref. 67) in both scattering half-planes for the reaction  $\text{Fe}^{56}(p, p'\gamma)$  at 4.3 MeV<sub>lab</sub>. The calculation employed Preskitt-Alford transmission coefficients for orbital momenta up to  $l_{\text{max}} = 2$ ; the experimental points were arbitrarily normalized.

theory and experiment indicates that although the absolute magnitudes are appreciably too small, the experimental results in form have a  $\theta_2$  dependence which is in good accord with that for a CN mechanism. To illustrate this latter contention, the points for  $\theta_1 = 90^\circ$  are shown twice in the lower part of Fig. 52; first as measured and second as arbitrarily renormalized by a factor of 1.86 to coincide with the theoretical curves. These  $\theta_1 = 90^\circ$  results are also depicted in Fig. 53, wherein the solid circles represent the renormalized values. This figure serves principally to indicate that both in form and in absolute magnitude these correlation measurements are altogether at variance with DWDI predictions. It may also be seen that the latter do not display the dip around  $\theta_2 \cong -10^\circ$  which appears to be a characteristic of these measurements. To show the extent of agreement between results at  $\theta_1 = 135^\circ$  and the correlation curves, the measured values have been renormalized by the same factor of 1.86 to tally with the theoretical curves and are shown as solid circles

in Fig. 54. Although the amplitude of the theoretical curves is slightly too small to accord perfectly with the measured points, the over-all agreement, apart from the characteristic dip in the experimental points around  $\theta_2 \cong -10^\circ$ , is very good, so that one is justified in concluding that the CN mechanism is predominant at this energy, even though some admixture of DI is doubtless present and may be responsible for causing experimental values to take

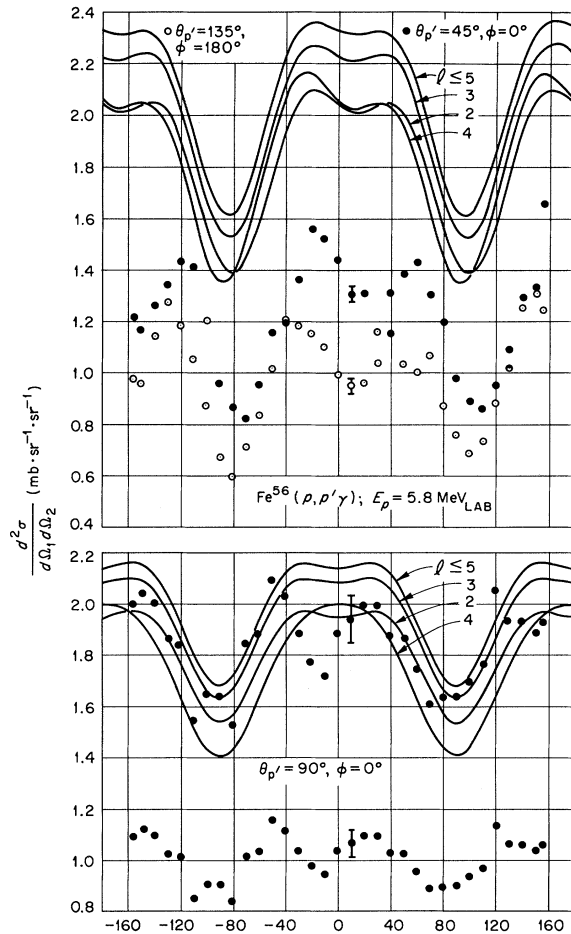


FIG. 52. Comparison for  $\theta_1 = 45^\circ, 90^\circ, 135^\circ$  of measured (Ref. 67) absolute double-differential cross sections with the CN theoretical  $\theta_2$  dependence for the reaction  $\text{Fe}^{56}(p, p'\gamma)$  at 5.8 MeV<sub>lab</sub>. In the upper part, the points for  $\theta_1 = 45^\circ$  (solid circles) and those for  $\theta_1 = 135^\circ$  (open circles) confirm predicted CN symmetries. The agreement in shape, though not in absolute magnitude, of the correlation is illustrated in the lower part, in which original and renormalized points for  $\theta_1 = 90^\circ$  are shown.

on lower values than would be the case with a pure CN process. Some preliminary semiempirical estimates of the DI admixture derived from consideration of the presence of reflection symmetries in CN theory and their absence from DI theory have been

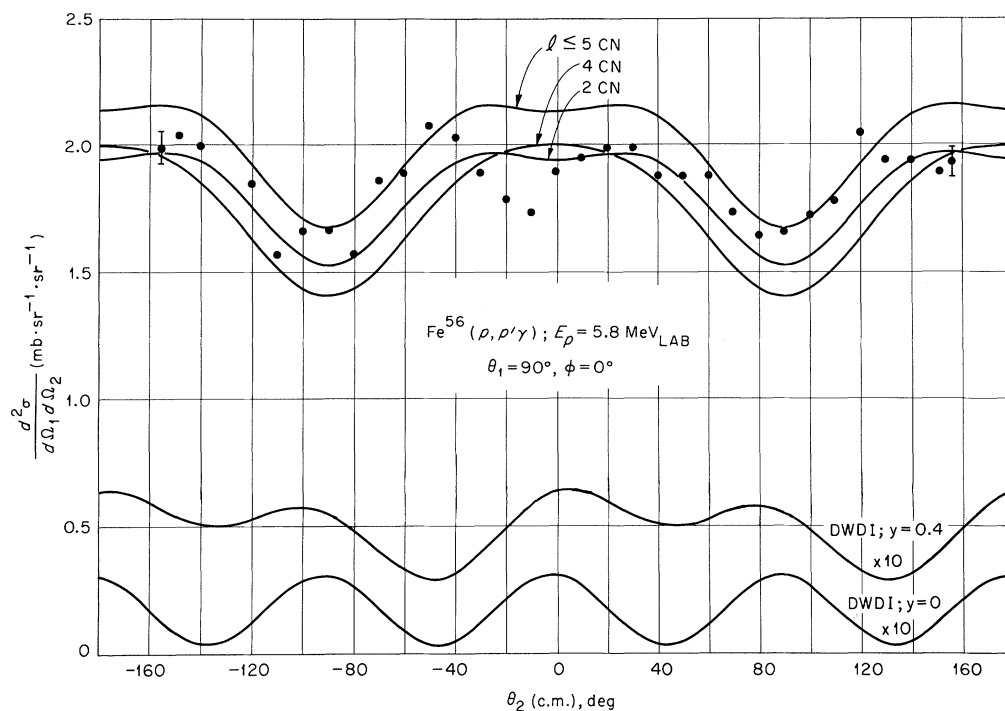


FIG. 53. As in Fig. 52 for  $\theta_1 = 90^\circ$  but with inclusion of the absolute DWI double-differential cross section with and without spin-flip to demonstrate that the experimental result is incompatible with predominance of DI mechanism. The solid circles represent renormalized points (absolute values multiplied by 1.86).

undertaken by the Zürich group. The experimental asymmetry

$$\Delta \left( \frac{d^2\sigma}{d\Omega_1 d\Omega_2} \right) \equiv \frac{d^2\sigma}{d\Omega_1 d\Omega_2} (\theta_1, \theta_2, 0) - \frac{d^2\sigma}{d\Omega_1 d\Omega_2} (\pi - \theta_1, \theta_2, \pi) \quad (149)$$

and analogous expressions which would vanish for zero admixture of DI prove, in fact, to be consistent with the assumption of as much as 30% DI admixture when applied to the ensemble of data at 5.8 MeV for Cr, Fe, Zn, a value appreciably higher than would ensue from the computed respective double-differential cross sections. Details of this approach are to be published later.

A further effect which may play a significant rôle in causing discrepancy between CN theoretical and experimental absolute magnitudes arises from the possibility of populating target nucleus states higher than merely the first excited level with 5.8-MeV incident protons. The present theoretical approach does not take this into account, though calculations are now in progress which aim to take cognizance of population of higher excited levels. The ensuing modification to the correlation function cannot be estimated, since the problem is too complicated to be amenable to hand calculation, but it appears very unlikely that incorporation of higher populated levels

could lead to a diminution in the double-differential cross section. On the other hand, since the incident energy here exceeds the  $(p, n)$  threshold, one should for consistency include neutron decay channels in the  $\tau$  terms of the CN correlation function. Preliminary calculations have shown that incorporation of a single neutron exit channel lowers the double-differential cross section by 20% without greatly affecting the form.

To complement the curves shown in Fig. 50 which illustrate the  $l$  dependence of the  $p'$ -perpendicular correlation at 4.3 MeV<sub>lab</sub> in function of  $\theta_2$ , Fig. 55 shows the dependence for 5.8 MeV<sub>lab</sub> and is depicted in correlation-function form, normalized to unity at  $\theta_2 = 90^\circ$ . It is clear that the fairly weak  $l$  dependence precludes the possibility of establishing the partial-wave composition of incident and scattered beams experimentally from study of perpendicular correlations.

#### G. Ni<sup>58,60</sup>

Target	$Q(\text{MeV})$	$E_p(\text{MeV})_{\text{lab}}$	$\mathcal{N}$	$\theta_1$	Authors
Ni <sup>58</sup>	-1.45	5.8	$p$	$45^\circ, 90^\circ, 135^\circ$	Taketani and Alford <sup>24</sup>
Ni <sup>58</sup>	-1.45	6.9	$p$	$45^\circ, 90^\circ, 135^\circ$	Taketani and Alford <sup>24</sup>
Ni <sup>60</sup>	-1.33	5.8	$p$	$90^\circ, 135^\circ$	Taketani and Alford <sup>24</sup>
Ni <sup>60</sup>	-1.33	6.9	$p$	$50^\circ, 90^\circ, 135^\circ$	Taketani and Alford <sup>24</sup>

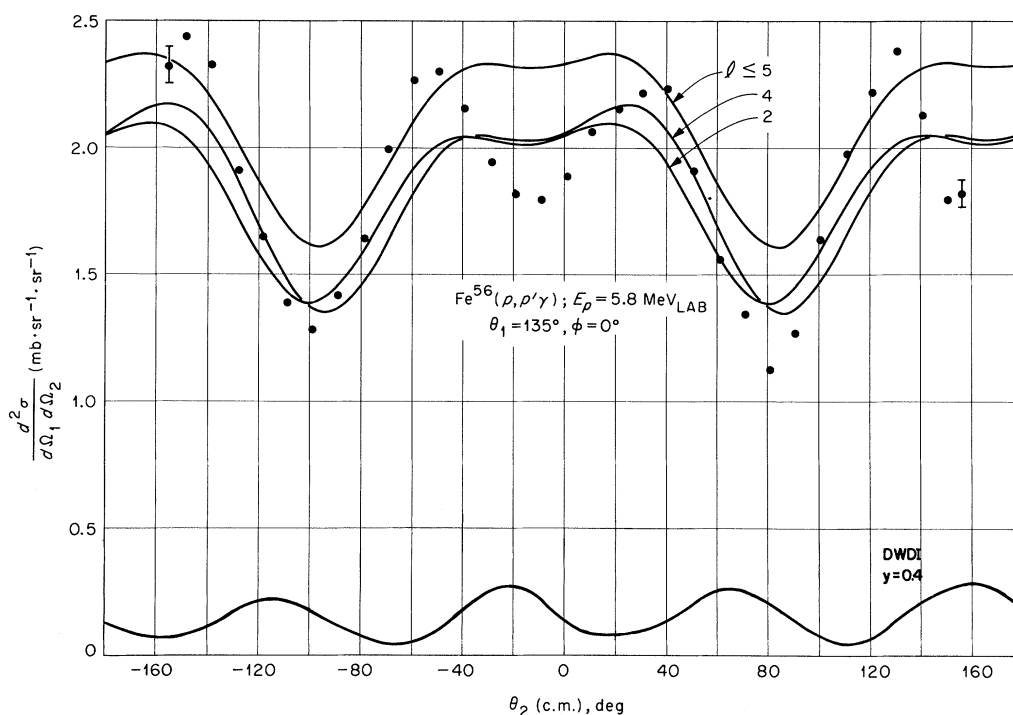


FIG. 54. As in Fig. 52 for  $\theta_1 = 135^\circ$  but with the measured values renormalized by a factor of 1.86 (solid circles) to lie along the CN theoretical curves. Except for characteristic deviation around  $\theta_2 = 0^\circ$ , the fit to the  $\theta_2$ -dependent correlation curve is satisfactory.

The investigations on  $\text{Ni}^{58}$  and  $\text{Ni}^{60}$  by the Rochester group at 5.8  $\text{MeV}_{\text{lab}}$  ( $=5.73 \text{ MeV}_{\text{c.m.}}$ ) and 6.9  $\text{MeV}_{\text{lab}}$  ( $=6.8 \text{ MeV}_{\text{c.m.}}$ ) have, in part, since their original theoretical analysis (which comprised CN calculations including mixed- $j$  interferences and em-

pirical curve fitting with expressions of the DWDI form) already been reanalyzed<sup>14</sup> on the basis of the present CN and DWDI theoretical approach; the results are reproduced in Fig. 56. Figure 56 shows the

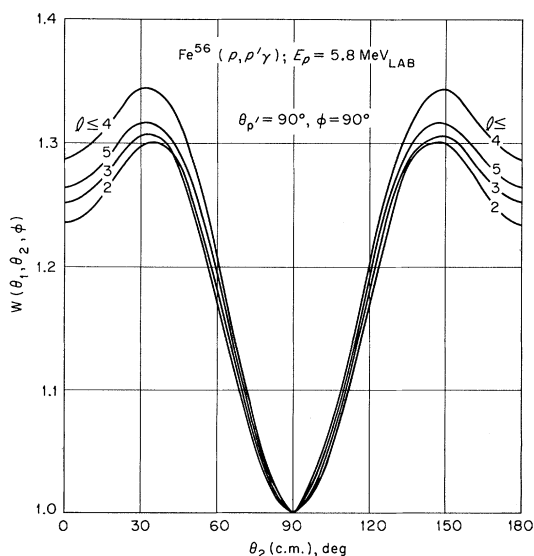


FIG. 55. Theoretical  $\theta_2$  dependence of the (normalized)  $p'$ -perpendicular CN correlation for various maximum orbital momenta for the reaction  $\text{Fe}^{56}(p, p'\gamma)$  at 5.8  $\text{MeV}_{\text{lab}}$ .

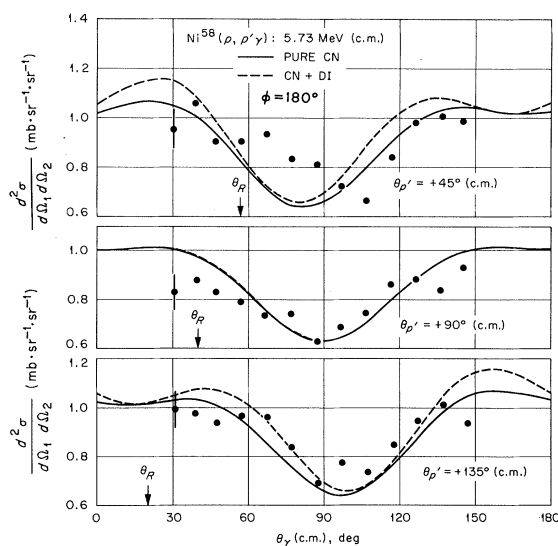


FIG. 56. Effect of direct superposition of the DWDI double-differential cross section (with zero spin-flip) for the reaction  $\text{Ni}^{58}(p, p'\gamma)_{Q=-1.45 \text{ MeV}}$  at 5.73  $\text{MeV}_{\text{c.m.}}$  on that for pure CN mechanism ( $l \leq 2$ ). The points represent normalized experimental results for the  $\varphi = 180^\circ$  plane of Taketani and Alford (Ref. 24).

effect of direct superposition of the DWDI correlation (with zero spin-flip) on the CN correlation for  $l \leq 2$ , calculated using the Preskitt-Alford optical potential, as discussed in Sec. 4. On comparison of Fig. 56 with Fig. 57 it is apparent that almost the same effect as that of incorporating a DWDI contribution can result merely from consideration of higher partial waves in pure CN theory; in either case, the fit is good and the preponderance of the CN mechanism may be considered to be established, particularly when examined in conjunction with angular distribution results<sup>24</sup> at almost the same energy (5.64 MeV<sub>e.m.</sub>) which are in fair accord with CN predictions. The measured  $\theta_1$  dependence of the distribution shows rather too much structure and

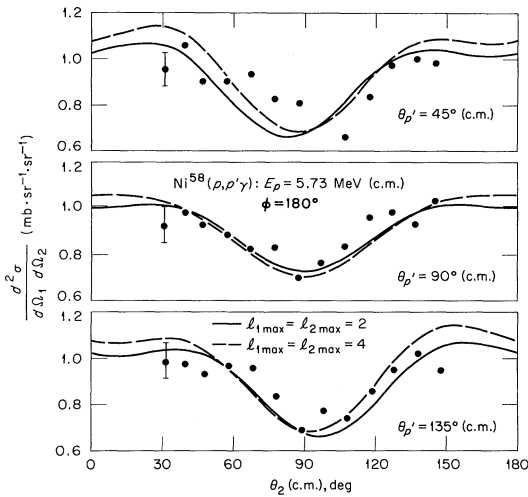


FIG. 57. The same experimental results of the Rochester group as in Fig. 56, contrasted with pure CN correlation curves for  $l_{\max} = 2$  and 4 in the  $\varphi = 180^\circ$  half-plane.

could not quantitatively be fitted with a Preskitt-Alford potential, but the qualitative CN fit, especially when a Perey potential is employed with  $l \leq 5$  is fairly good.

Attention is also drawn to other recent theoretical correlation results for the  $\text{Ni}^{58}(p, p'\gamma)$  reaction at 5.73 MeV<sub>e.m.</sub> which have been depicted graphically in Ref 17. The DWDI correlation surfaces, calculated as illustrative examples using a Perey potential at this energy, have been included in Sec. 6 (Figs. 10, 11, and 12).

At 6.8 MeV<sub>e.m.</sub> the Rochester group observed slight forward peaking in the proton distribution and, attributing this to appreciable influence of DI mechanism, analyzed their correlation results from the standpoint of the DWDI correlation theory.

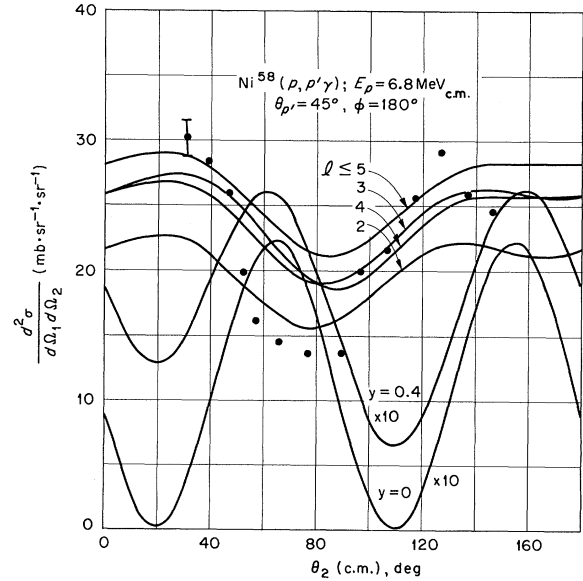


FIG. 58. Comparison of the correlation as measured at  $\theta_1 = 45^\circ$  by the Rochester group (Ref. 24) for  $\text{Ni}^{58}(p, p'\gamma)$  at 6.8 MeV<sub>e.m.</sub> with theoretical pure CN and pure DI curves, the latter with and without spin-flip.

Numerical computations using the Perey optical potential indicate, however, that the CN differential cross section is larger than that for DWDI by a factor ranging from 2.9 at  $\theta_1 = 0^\circ$  to 16.5 at  $\theta_1 = 90^\circ$ , and that the CN double-differential cross section is roughly tenfold that for DWDI as can be seen from Figs. 58, 59, and 60. These figures indicate the measured correlations to be in entire disagreement with absolute DWDI predictions, but to be in fair agreement with CN calculations. For the supplementary angles  $\theta_1 = 45^\circ$  and  $135^\circ$ , the points display the expected CN symmetry (they have throughout been multiplied by the same norm).

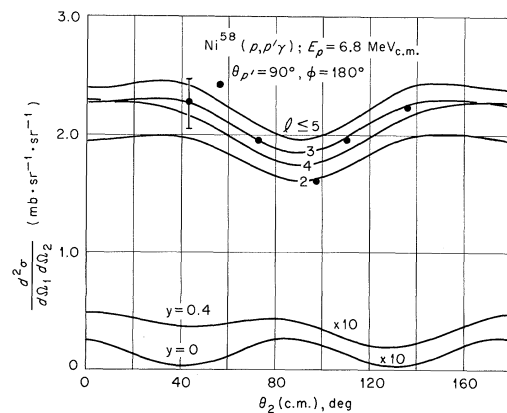


FIG. 59. As Fig. 58 but for  $\theta_1 = 90^\circ$ .

For Ni<sup>60</sup> at 5.73 MeV<sub>c.m.</sub>, results as shown in Fig. 61 are in very close agreement with CN theory, but altogether contrary to absolute DWDI predictions. Although Taketani and Alford had empirically fitted the points with a correlation curve of DI form, they were careful not to exclude the possibility of a predominant CN mechanism, as the present analysis shows, indeed, to be the case. This conclusion is further substantiated by the relative insignificance of the DI differential cross section as compared with that for the CN mechanism. Theoretically the former ranges from a maximum of 1.30 mb sr<sup>-1</sup> at θ<sub>1</sub> = 0° to a minimum of 0.26 mb sr<sup>-1</sup> at θ<sub>1</sub> = 90°, whereas the actual measured cross section fluctuates but little around 5.5 mb sr<sup>-1</sup>. At the higher energy of 6.8 MeV<sub>c.m.</sub> the relative influence of the DI mechanism

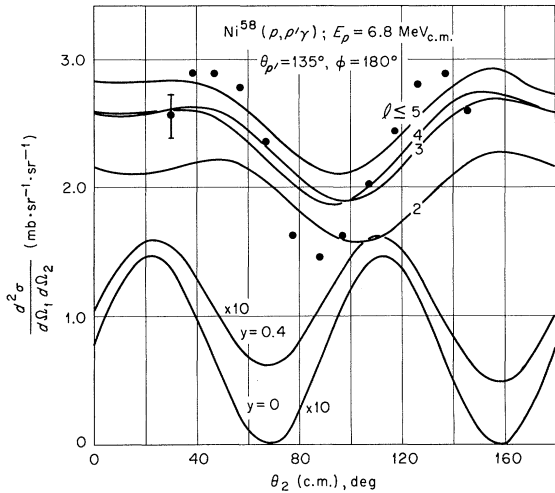


FIG. 60. As Fig. 58 but at the supplementary angle θ<sub>1</sub> = 135°. The CN curves are reflections of those for θ<sub>1</sub> = 45°, unlike those for the DI mechanism.

can no longer be regarded as small, as is evident from Fig. 62, which shows the resultant angular distribution from direct superposition of CN and DI differential cross sections, compared with the experimental values of Taketani and Alford. An unfortunate, but trivial, internal inconsistency underlies the respective theoretical curves in that the CN distribution has been computed for a Perey potential (V = 51 MeV, r<sub>0</sub> = 1.25 F, a = 0.65 F, W' = 11 MeV, r'<sub>0</sub> = 1.25 F, a' = 0.47 F, V<sub>s</sub> = 8 MeV), whereas numerical values for the DI distribution were at hand only for a Satchler potential, whose parameters differ very slightly from the above, the discrepant values being V = 47 MeV, r<sub>0</sub> = 1.35 F (giving approximately the same value for Vr<sup>2</sup>). As the effect upon the DI

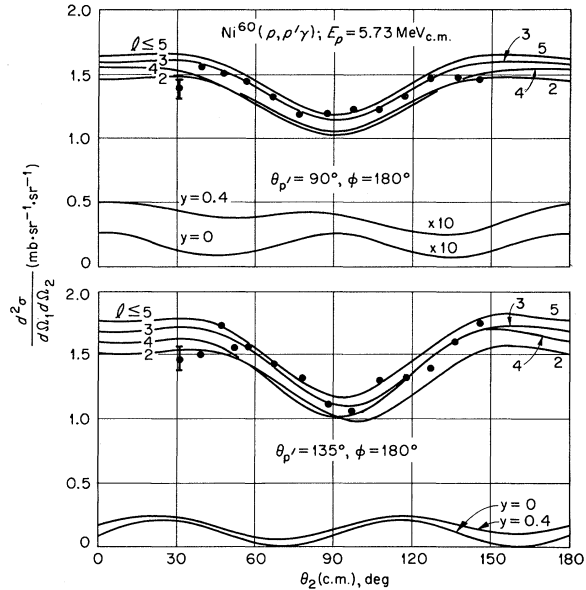


FIG. 61. Analysis of the Rochester group's (Ref. 24) correlation results for Ni<sup>60</sup>(p,p'γ)<sub>Q</sub> = -1.33 MeV at 5.73 MeV<sub>c.m.</sub> for θ<sub>1</sub> = 90° and 135°, showing the CN mechanism to be dominant.

differential cross section cannot be but slight, it was considered unnecessary to recalculate the latter for a Perey potential, which would not appreciably influence the superposed result. In view of the large DI differential cross section it is not surprising that in Figs. 63, 64, and 65 the CN correlation fit becomes less satisfactory, and the DWDI double-differential

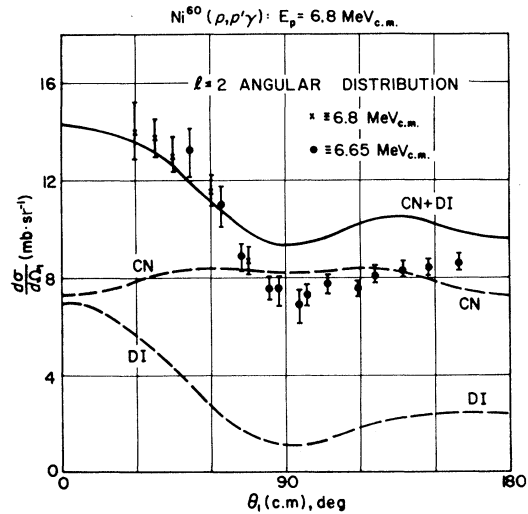


FIG. 62. Direct superposition for the reaction Ni<sup>60</sup>(p,p'γ) at 6.8 MeV<sub>c.m.</sub> of the l ≤ 2 angular distribution for a pure CN mechanism based upon a Perey potential on that for pure DI mechanism (based upon the almost identical Satchler optical potential). The resultant fit to the experimental absolute results of the Rochester group (Ref. 24) is improved.

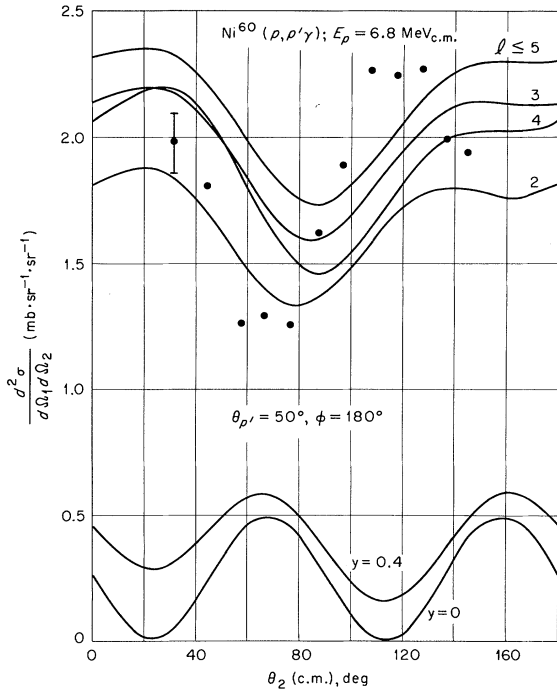


FIG. 63. Analysis of the experimental correlation results of the Rochester group (Ref. 24) for  $\text{Ni}^{60}(p,p'\gamma)$  at 6.8 MeV<sub>c.m.</sub> for  $\theta_1 = 50^\circ$  using a Perey potential ( $V = 51$  MeV,  $r_0 = 1.25$  F,  $a = 0.65$  F,  $W' = 11$  MeV,  $r_0' = 1.25$  F,  $a' = 0.47$  F,  $V_s = 8$  MeV) throughout.

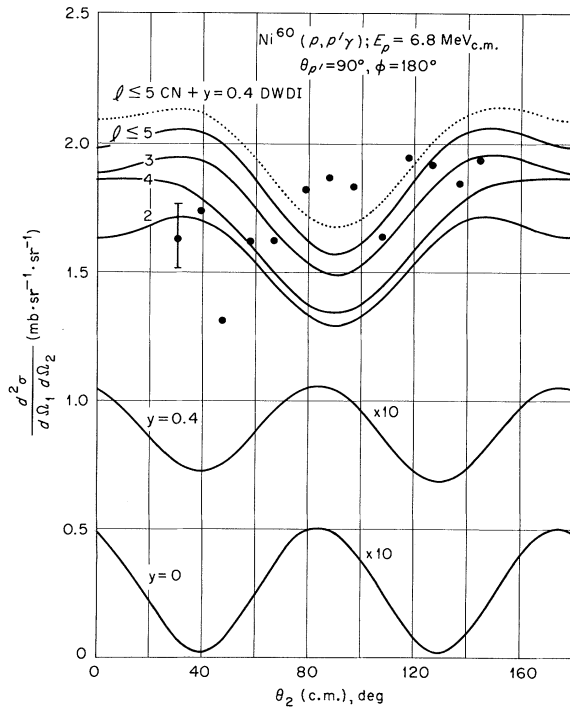


FIG. 64. As Fig. 63 but for  $\theta_1 = 90^\circ$ . Also shown (dotted curve) is the theoretical result of direct superposition of the DWDI double-differential cross section (with spin-flip) on to that for pure CN mechanism.

cross section assumes values which are no longer negligibly small. Nevertheless, the data are still consistent with the contention that the CN mechanism is dominant even at this energy though the actual mechanism involves a mixture of CN and DI processes. It is apparent from inspection of Figs. 63 and 65 that simple superposition of CN and DI double-differential cross sections will not lead to an appreciably better fit to the somewhat scattered points. These points had to be multiplied by mutually different norms in order to lie within the region of theoretical CN curves and, thus, do not reproduce, even roughly, the symmetry which would be expected to apply to CN correlations for the approxi-

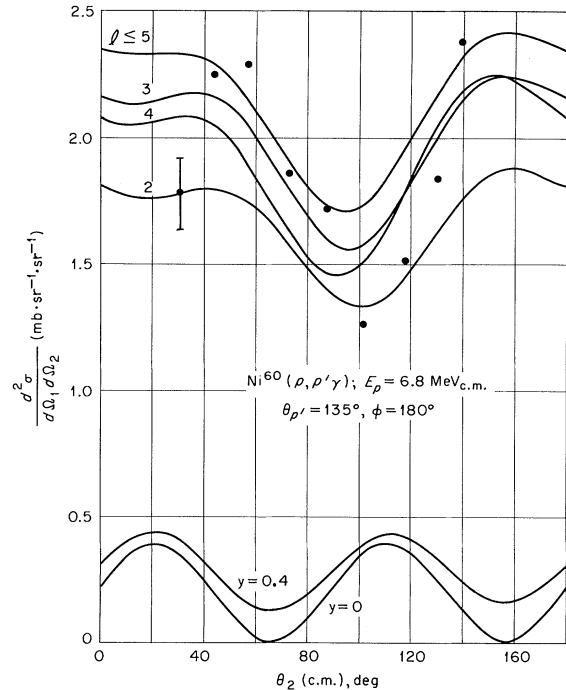


FIG. 65. As Fig. 63 but for  $\theta_1 = 135^\circ$ .

mately supplementary angles  $\theta_1 = 50^\circ$  and  $135^\circ$ . For the proton angle  $\theta_1 = 90^\circ$ , the comparatively small magnitude of the DI correlation precludes the cancellation of structure in the correlation function resulting from composition of a CN correlation having a dip at  $\theta_2 = 90^\circ$  with a DI correlation having a peak in that region. Taketani and Alford's suggestion that an almost isotropic correlation function might thereby result which would furnish a reasonable fit to the almost constant experimental values cannot therefore be realized. By way of example, in Fig. 64 the dotted curve which represents the superposition of the  $y = 0.4$  DWDI double-differential cross section on the  $l \leq 5$  CN curve has been drawn

in and can be seen to have a pronounced dip around  $\theta_2 = 90^\circ$ . Not only is there likely to be interference between CN and DI correlations at this energy, but the assumption inherent in the present CN calculations that no states of the target nucleus higher than the first become excited is unlikely to be fulfilled and, hence, perfect theoretical fits cannot be expected.

### H. Zn<sup>64,66,68</sup>

Target	$Q(\text{MeV})$	$E_p(\text{MeV})_{\text{lab}}$	$\mathfrak{N}$	$\theta_1$	Authors
Zn <sup>64</sup>	-0.99	5.8	<i>p</i>	45°, 90°, 135°	Szostak and Gobbi <sup>69</sup>
Zn <sup>66</sup>	-1.04	5.8	<i>p</i>	45°, 90°, 135°	Szostak and Gobbi <sup>69</sup>
Zn <sup>68</sup>	-1.08	5.8	<i>p</i>	45°, 90°, 135°	Szostak and Gobbi <sup>69</sup>

On account of the desirability of extending correlation investigations to heavier elements, a series of absolute measurements on isotopes of Zn have been taken by the Zürich group with 5.8-MeV protons.

Results for Zn<sup>64</sup>, shown in Fig. 66, are in very good

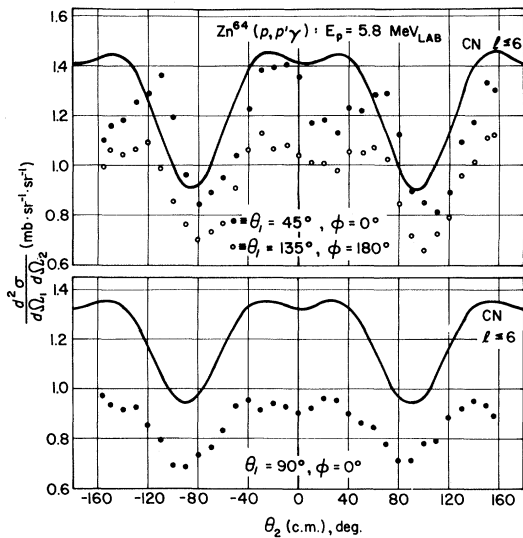


FIG. 66. Comparison of absolutely measured (Ref. 69) double-differential cross sections for  $\theta_1 = 45^\circ, 90^\circ, 135^\circ$  in both scattering half-planes for the Zn<sup>64</sup>(*p,p'*γ) reaction ( $Q = -0.99$  MeV) at 5.8 MeV<sub>lab</sub> with the theoretical CN curves.

qualitative agreement with the predictions of CN theory, albeit of absolute magnitude some 10% lower than the theoretical double-differential cross sections for momenta  $l \leq 2$  (or 20% lower for momenta  $l \leq 6$ ). This behavior is strikingly akin to

<sup>69</sup> R. Szostak and B. Gobbi (private communication).

that for Cr<sup>52</sup> under the same conditions (Fig. 37) for the supplementary angles  $\theta_1 = 45^\circ$  and  $135^\circ$ . The results shown here similarly display the CN symmetry character

$$W(\theta_1, \theta_2, 0) = W(\theta_1, \pi - \theta_2, \pi) = W(\pi - \theta_1, \theta_2, \pi) \quad (150)$$

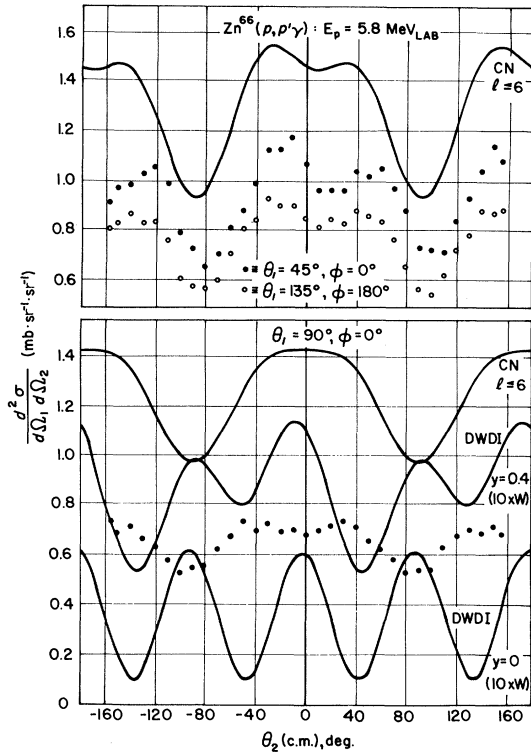


FIG. 67. As Fig. 66 but for the target nucleus Zn<sup>66</sup>.

and do not display any marked discrepancy from theory around  $\theta_2 = 0^\circ$ . The Zn<sup>64</sup> results are also analogous to those for Cr<sup>52</sup> in that values for  $\theta_1 = 135^\circ$  are consistently lower than those for the forward scattering angle of  $\theta_1 = 45^\circ$ , though one cannot attach significance to this effect in view of the relatively large absolute experimental error of about  $\pm 20\%$ . The present results for  $\theta_1 = 90^\circ$  differ from the corresponding values for Cr<sup>52</sup> in their absolute magnitude, which is approximately the same as that for  $\theta_1 = 45^\circ$  and  $135^\circ$  (the points shown in Fig. 66 have *not* been normalized).

The fact that the quantitative agreement is not markedly different for any of the three scattering angles in the case of Zn<sup>64</sup> and Zn<sup>66</sup> (see Fig. 67) renders the present unpublished results particularly interesting. The measured values for Zn<sup>66</sup> shown in Fig. 67, are three-quarters of the magnitude of the theoretical double-differential cross section through-

out, but are qualitatively in excellent agreement with CN theory. It is clear that the rather stringent requirement of *quantitative* agreement between absolute magnitude has not yet been met by correlation studies, even for fairly heavy nuclei with high level densities in the compound nuclei, but *qualitative* agreement with CN theory, even when such conditions as inelastic decay to only the first excited level of the target nucleus are unlikely to be satisfied, is remarkably good. The degree of fitting is obviously not fortuitous, in which connection it may be mentioned that in order to avoid influencing the measurements of the Zürich group, the matching of the theoretical curves to experimental results has been undertaken only upon completion of the latter. Until definitive experimental values had been accumulated, the theoretical quantitative predictions have been withheld, the union of theory with experiment being deferred to the conclusion of the investigation.

One is, thus, in a position to survey the absolute measurements for protons incident at 5.8 MeV on the nuclei  $\text{Cr}^{52}$ ,  $\text{Fe}^{56}$ ,  $\text{Zn}^{64}$ ,  $\text{Zn}^{66}$ , arriving at the following conclusions:

- (i) For all nuclei, measurements at the scattering angles  $\theta_1 = 45^\circ, 90^\circ, 135^\circ$  are in very good qualitative agreement with CN theory and display the expected CN symmetries.
- (ii) For  $\text{Cr}^{52}$ , the absolute magnitude tallies fairly well with theory for  $\theta_1 = 45^\circ$  and  $135^\circ$ , but is lower by a factor of 2.2 for  $\theta_1 = 90^\circ$ .
- (iii) For  $\text{Fe}^{56}$ , discrepancy in the absolute magnitudes for  $\theta_1 = 90^\circ$  and  $135^\circ$  exists, the measured values being about one-half of the theoretical throughout.
- (iv) For  $\text{Zn}^{64}$ , magnitudes for all three scattering angles  $\theta_1 = 45^\circ, 90^\circ, 135^\circ$  are consistently four-fifths of the predicted values.
- (v) For  $\text{Zn}^{66}$ , magnitudes for all three scattering angles  $\theta_1 = 45^\circ, 90^\circ, 135^\circ$  are consistently three-quarters of the predicted values (they are about 20% lower than corresponding experimental points for  $\text{Zn}^{64}$ ).

Three factors may combine to vitiate quantitative agreement: underestimation of the experimental error, influence of DI admixture upon the pure CN theoretical predictions, and the rather strong energy dependence of the CN double-differential cross section, as illustrated for  $\text{Zn}^{66}$  in Fig. 68. Though for different energies the shape of the correlation remains practically unaltered, there is a progressively rapid increase in the absolute magnitude of the cross section with increasing incident proton energy, so that even a small discrepancy between the experi-

mental and theoretical values of the energy could lead to an appreciable difference in the absolute magnitude of correlation results. The retention of shape but change in magnitude of the correlation upon changing the incident energy prompts the comment that the *correlation surface* representation as employed at present has the drawback of suppressing the energy dependence by employing arbitrary normalization to unity at the center for clarity of structural comparison with other surfaces. This point will be discussed in more detail in the next section.

A portent of the striking difference observed in the experimental correlation behavior for 5.8-MeV protons on the above Zn isotopes and that for the heavier isotope  $\text{Zn}^{68}$  at the same energy is provided

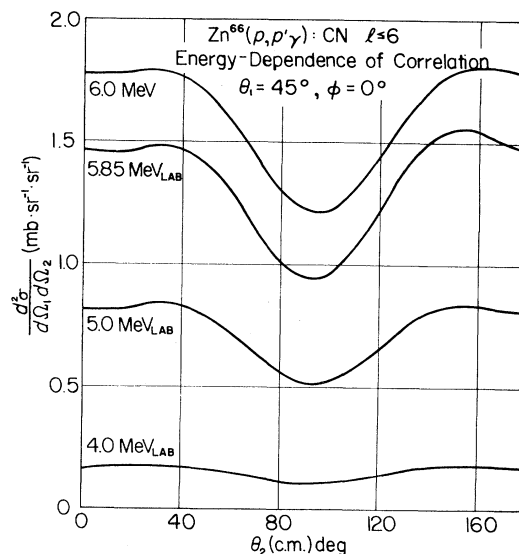


FIG. 68. Illustration of the energy dependence of the CN double-differential cross section ( $l \leq 6$ ) for the  $\text{Zn}^{66}(p,p'\gamma)$  reaction ( $Q = -1.04$  MeV) at 5.8 MeV for  $\theta_1 = 45^\circ$ .

by the realization that, for the latter, both the Coulomb barrier and the  $(p,n)$  threshold fall appreciably below the incident energy (see Table III in the following section). Whereas for the nuclei  $\text{Zn}^{64,66}$  the scattering mechanism clearly proceeds predominantly by way of CN formation, measurements by Szostak and Gobbi, which because of their preliminary nature have not been illustrated here, indicate DI to be the dominant mechanism for  $\text{Zn}^{68}$ . The low  $(p,n)$  threshold points to the likelihood that in the presence of competing CN decay modes, the inelastic scattering process via a CN would considerably be inhibited, with the result that the DI process could gain the ascendancy. The results thereby furnish a most interesting instance of an apparent switch in mechanism among a family of

isotopes having otherwise very similar nuclear properties (e.g., deformation, etc.) at the same comparatively low energy associated with the presence of alternative reaction modes of which the present CN correlation theory does not take cognizance (it is limited to two exit channels, the elastic and the inelastic channel to the first level only). Explicit quantitative calculations taking possible neutron exit channels into consideration are precluded by the number of such channels which go to levels of unknown spin and parity in the residual nucleus Ga<sup>68</sup>. The noteworthy feature in the present results is not only their distinctive DI angular dependence but their small absolute magnitude; all three sets of results are of roughly sevenfold smaller magnitude than the corresponding values for Zn<sup>64,66</sup>. Such a diminution in magnitude is incommensurate with theoretical calculations; the CN double-differential cross section for Zn<sup>68</sup> is very similar to that for Zn<sup>64,66</sup> and is about 1.2 mb sr<sup>-2</sup>, whereas the DWDI cross section, both for  $y = 0$  and  $y = 0.4$ , has reasonably large amplitude around 0.8 and 0.5 mb sr<sup>-2</sup> for  $\theta_1 = 45^\circ$  and  $135^\circ$ , respectively, and smaller amplitude around 0.15 mb sr<sup>-2</sup> for  $\theta_1 = 90^\circ$ . In no instance do the minima in the computed DI correlations agree with those in the experimental results. The minima of the latter coincide with the classical recoil angle quite closely in the case of the  $\theta_1 = 45^\circ$  and  $135^\circ$  results, but differ markedly for the  $\theta_1 = 90^\circ$  results. The mean experimental magnitudes lie around one-quarter of the theoretical DWDI ( $y = 0.4$ ) values for the former two scattering angles and around one-half for the  $\theta_1 = 90^\circ$  case. Detailed theoretical analysis of this striking behavior will be deferred pending ratification of the experimental findings.

### 8. CONCLUDING REMARKS

The systematic improvement in agreement between CN theory and experiment with increasing mass number  $A$  of the target nucleus is directly related to the progressively improved justification for the statistical assumption in consequence of the increase in the CN level density. Even more fundamental a requirement than the random-phase hypothesis is the "availability" in practice of all the levels in the CN which would theoretically fulfill the various selection rules and which, thus, figure in the theoretical calculations. To obtain some quantitative impression of the extent to which this is likely, the mean separation of levels having zero spin was evaluated from Lang-LeCouteur theory<sup>70</sup> for all

<sup>70</sup> J. M. B. Lang and K. J. LeCouteur, Proc. Phys. Soc. (London) **A67**, 586 (1954).

compound nuclei which are encompassed by the present correlation analysis (at such excitation energies as would correspond with 3-MeV neutron or 5-MeV proton bombardment, e.g., with hypothetical medium incident energies). The above treatment predicts the CN temperature at an excitation energy  $E^*$  to be

$$T = (4/A)[1 + (1 + \frac{1}{2}AE^*)]^{1/2} \text{ MeV} \quad (151)$$

and the spin-0 level spacing, assuming surface oscillations, to be

$$D_0 = 0.0184804 A^2 (E^* + T)^2 \times \exp[-2(AE^*/11)^{1/2} - 0.09375(11E^*)^{3/2}]. \quad (152)$$

The spacing of levels having spin  $J$  is then given by the relation

$$D_J = D_0 \left\{ \frac{(8\pi)^{3/2} \sigma^3}{2J+1} \exp\left[\frac{J(J+1)}{2\sigma^2}\right] \right\}, \quad (153)$$

with the spin cutoff parameter of magnitude  $\sigma \approx 3$ .

The resulting spin-0 level spacings as listed in Table III can then be compared with typical values of the experimental energy spread in an incident nucleon beam, viz., roughly 100 keV for a neutron beam and 50 keV for a proton beam, to arrive at quantitative confirmation of the fact that only for nuclei with  $A \gtrsim 40$  is there sufficient likelihood of the CN, in fact, having those levels which are theoretically assumed to become populated. Table III also lists Coulomb barrier heights and threshold energies (calculated from theoretical  $Q$  values<sup>71</sup>) since these play a rôle in the operative scattering mechanism; a point frequently mentioned in the past and strikingly borne out by results for 5.8-MeV protons incident upon the isotopes Zn<sup>64,66,68</sup>. It would be complicated, though straightforward, to extend CN theory to consideration of competing exit channels (a preliminary calculation to this end has been mentioned in Sec. 7F) and population of states higher than the first level in the target nucleus (wherein the  $0+ \rightarrow 2+$  spin sequence can readily be generalized to arbitrary spins). However, there are as yet no indications as to how the principal point of weakness inherent in CN theory, the statistical assumption of random phase, may be sidetracked. Though justified by expediency, its physical validity, particularly for light compound nuclei at low excitation, is questionable in spite of its partial vindication by the Porter-Thomas<sup>72</sup> and Blumberg-Porter<sup>73</sup> statistical approach

<sup>71</sup> V. J. Ashby and H. C. Catron, UCRL Report UCRL-5419, 1959 (unpublished).

<sup>72</sup> C. E. Porter and R. G. Thomas, Phys. Rev. **104**, 483 (1956).

<sup>73</sup> S. Blumberg and C. E. Porter, Phys. Rev. **110**, 786 (1958).

TABLE III. Mean level spacing in CN formed from 3-MeV neutrons or 5-MeV protons, calculated from Lang-LeCouteur theory, together with the Coulomb barrier height and respective  $(n,p)$  or  $(p,n)$  threshold.

Target	$\mathfrak{N}$	CN	Binding energy (MeV)	Excitation energy (MeV)	CN Temp (MeV)	Mean spacing $D_0(A,E^*)$ (keV)	Coulomb barrier (MeV)	$(n,p)$ or $(p,n)$ threshold (MeV)
Mg <sup>24</sup>	<i>n</i>	Mg <sup>25</sup>	7.331	10.33	1.984	12.0	...	4.93
Mg <sup>24</sup>	<i>p</i>	Al <sup>25</sup>	2.287	7.29	1.696	47.6	2.93	15.46
Si <sup>28</sup>	<i>p</i>	P <sup>29</sup>	2.74	7.74	1.605	26.4	3.33	15.11
S <sup>32</sup>	<i>p</i>	Cl <sup>33</sup>	2.29	7.29	1.922	26.0	3.68	14.39
Ti <sup>48</sup>	<i>p</i>	V <sup>49</sup>	6.752	11.75	1.469	0.37	4.55	4.90
Cr <sup>52</sup>	<i>p</i>	Mn <sup>53</sup>	6.563	11.56	1.399	0.27	4.87	5.62
Fe <sup>56</sup>	<i>n</i>	Fe <sup>57</sup>	7.643	10.64	1.294	0.33	...	2.98
Fe <sup>56</sup>	<i>p</i>	Co <sup>57</sup>	6.29	11.29	1.331	0.21	5.17	5.50
Ni <sup>58</sup>	<i>p</i>	Cu <sup>59</sup>	3.42	8.42	1.139	1.26	5.51	2.44
Ni <sup>60</sup>	<i>p</i>	Cu <sup>61</sup>	4.809	9.81	1.202	0.39	5.47	7.17
Zn <sup>64</sup>	<i>p</i>	Ga <sup>65</sup>	3.96	8.96	1.114	0.51	5.76	8.13
Zn <sup>66</sup>	<i>p</i>	Ga <sup>67</sup>	5.28	10.28	1.169	0.16	5.71	6.04
Zn <sup>68</sup>	<i>p</i>	Ga <sup>69</sup>	6.528	11.53	1.216	0.05	5.67	3.75

to the CN model. A very cogent resumé of the theory and evidence underlying the randomness hypothesis has been given by Feshbach<sup>74</sup> and recent aspects have been treated by Dyson.<sup>75</sup> The independence of CN decay from the mode of formation is itself fundamentally connected with the random-phase hypothesis. As outlined by Satchler,<sup>76</sup> the crucial requirement of the factorization of a reaction (absorption) cross section into the product of a CN formation cross section with a branching ratio for particle emission in the appropriate exit channel is automatically met by the Breit-Wigner single-level formula for isolated resonances (level width  $\Gamma \ll$  average level spacing  $D$ , as is the case at low excitation), but breaks down at higher excitation as level overlapping begins to occur ( $\Gamma \approx D$ ) since the phases of the two or more quantum states populated at a given energy will depend upon the mode of formation. Thereafter, as overlapping becomes more pronounced, the Breit-Wigner many-level resonance formula can be used and nondependence of decay upon formation again thereby achieved, but with increasing excitation energy this becomes increasingly unwieldy with the result that only upon entering the region where very many levels are populated, e.g., the continuum region, can a suitable formalism be evolved on assuming that so many states are involved that, even though their relative phases depend upon the manner of formation, they may be treated as random for the decay process (by averaging over a small energy region). In this formalism,<sup>21</sup> upon assuming the

reduced widths (i.e., wave amplitudes at the various decay channels) to be uncorrelated in sign, the above random-phase approximation permits reduction of the  $S$  matrix to a form which resembles the many-level resonance formula and, thus, again permits "independence factorization." Complete independence of the cross section obtains only when one averages over residual nuclear states in a small energy region ( $\Delta E \ll \Gamma$ ), making two inherent assumptions in effecting the requisite summation over channel spins and final nuclear spins,

- (i) that the spin dependence of the level density display a  $(2J + 1)$  form;
- (ii) that the transmission coefficients be spin-independent (viz.,  $T_i$  and not  $T_i^{(\pm)}$ ).

At very high CN excitation, when  $\Gamma \gg D$ , it would be unreasonable to expect a statistical CN formalism to be applicable, since the lifetime of the intermediate state would be too short in relation to the relaxation time to permit attainment of statistical equilibrium. Indications that this may indeed be the case have been furnished by investigations of Ericson fluctuations<sup>77-81</sup> in cross section with energy, from which one might infer a lifetime of about  $10^{-19}$  sec for a nucleus of medium mass number at an excitation energy of 18 MeV. It remains to be seen whether nuclear lifetime measurement in function of excitation energy may prove directly feasible in the near future; two suggestions to this effect have recently been made, viz., the study of interference effects in

<sup>74</sup> H. Feshbach, in *Nuclear Spectroscopy*, edited by F. Ajzenberg-Selove (Academic Press Inc., New York, 1960), Part B, p. 625.

<sup>75</sup> F. J. Dyson, *J. Math. Phys.* **3**, 140, 157, 166 (1962).

<sup>76</sup> G. R. Satchler, Oak Ridge Report ORNL-2606, 1958 (unpublished); Proceedings of the Gatlinburg Conference (1958).

<sup>77</sup> T. Ericson, *Advan. Phys.* **9**, 425 (1960).

<sup>78</sup> F. E. Durham, M. L. Halbert, C. D. Moak, and A. Zucker, *Phys. Rev. Letters* (to be published).

<sup>79</sup> L. Colli, U. Facchini, T. Iori, G. M. Marazzan, M. Milazzo, and F. Tonolini, *Phys. Letters* **1**, 120 (1962).

<sup>80</sup> U. Facchini, E. Saetta Menichella, and F. Tonolini, *Phys. Letters* **1**, 209 (1962).

<sup>81</sup> T. Ericson, *Phys. Rev. Letters* **5**, 430 (1960).

the bremsstrahlung produced by charged particles entering and leaving nuclei in a target<sup>82</sup> and the estimation of very short lifetimes ( $\approx 10^{-20}$  sec) for a residual nucleus from observation of the angular correlations between particles emergent from a nuclear reaction.<sup>83</sup>

The application of the random-phase hypothesis to evaluation of differential cross sections cuts out interference between terms of different parity and, hence, produces symmetry of the angular distribution about  $90^\circ$ . Asymmetry in the distributions of the particles from decay of the CN can, thus, be ascribed to

- (1) nonrandomicity of phase in the CN states;
- (2) influence of levels in the residual nucleus which lie outside the energy range over which one averages.

If this averaging over residual nuclear states to obtain the differential cross section invokes assumptions (i) and (ii), the random-phase hypothesis leads not merely to symmetry but, indeed, to isotropy of the angular distribution. But this latter presupposes a simple  $(2J + 1)$  form for the spin dependence of the levels in the residual nucleus which appears<sup>77,84</sup> to be untenable. Mounting evidence, in fact, suggests a relationship of the form (153) which leads to nonisotropic but symmetrical angular distributions. It should again, however, be emphasized firstly that, particularly in the case of inelastic nucleon scattering, approximate symmetry of the nucleon distribution about  $90^\circ$  is not a prerogative of the CN mechanism; secondly, that symmetry of the  $\gamma$ -radiation distribution is to be expected generally and can shed no light upon the reaction mechanism; and thirdly that the random-phase approximation as applied to CN correlation theory does *not* lead to exact symmetry about  $\theta_1 = 90^\circ$  or  $\theta_2 = 90^\circ$  of the correlation function except in the special cases  $\theta_1, \theta_2 = 0, \frac{1}{2}\pi, \pi$ .

The symmetries of angular correlation for inelastic nucleon scattering have been examined by Sheldon<sup>17</sup> and illustrated by correlation surfaces. Though the latter are in consequence of the arbitrary normalization employed, fairly insensitive to variations in incident energy, the (unnormalized) double-differentiation cross section can, as was shown in Sec. 7G, be strongly energy-dependent. Though this cross section is not markedly dependent upon the number of higher partial waves incorporated in the calculation,

it is in magnitude, if not in form, influenced by the optical potential chosen to describe the scattering. As an example to illustrate this point, theoretical CN and DWDI double-differential cross sections for the reaction  $\text{Ni}^{58}(p, p'\gamma)$  at 5.73 MeV<sub>c.m.</sub> are shown in Fig. 69 for  $\theta_1 = 40^\circ$  ( $\varphi = 0^\circ$ ) to contrast the absolute

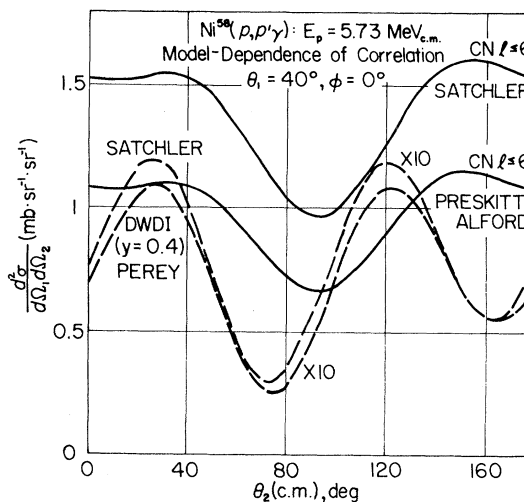


Fig. 69. Illustration of the influence upon the respective double-differential cross sections for the  $\text{Ni}^{58}(p, p'\gamma)_{Q = -1.45}$  MeV reaction at 5.73 MeV for  $\theta_1 = 40^\circ$  of selecting different optical potentials for the correlation analysis.

results for different potentials. The two CN curves, both for  $l \leq 6$ , the upper computed using a modified Satchler potential having parameters  $V = 44$  MeV,  $W = 0$  MeV,  $r_0 = 1.35$  F,  $a = 0.65$  F,  $W' = 11$  MeV,  $r'_0 = 1.25$  F,  $a' = 0.47$  F, and the lower computed from a Preskitt-Alford potential (see Sec. 5A) differ by a factor 1.4; the two DWDI curves with spin-flip ( $y = 0.4$ ), both for  $l = 2$  and enlarged tenfold, differ less markedly but nevertheless appreciably in spite of the parameter similarity (the Perey potential differed from Satchler's in having  $V = 55$  MeV,  $r_0 = 1.25$  F, and  $W' = 10.5$  MeV). Again, this potential dependence is masked in correlation surfaces by the normalization procedure.

It is clear that future experimental investigations of correlation should aim at securing accurate absolute results for the double-differential cross section over a wide range of angles to test symmetry characteristics in addition to providing data for stringent comparison with theory. In particular, further studies are desirable for neutron and proton scattering at low energies from nuclei around  $A = 40$ . The only such work to date was reported in a recent publication by Wakatsuki *et al.*,<sup>85</sup> for 5.6-MeV protons incident upon

<sup>82</sup> R. M. Eisberg, D. R. Yennie, and D. H. Wilkinson, Nucl. Phys. 18, 338 (1960); H. Feshbach and D. R. Yennie, *ibid.* 37, 150 (1962).

<sup>83</sup> R. Fox, Phys. Rev. 125, 311 (1962).

<sup>84</sup> T. Ericson and V. Strutinski, Nucl. Phys. 8, 284 (1958); 9, 689 (1959).

<sup>85</sup> T. Wakatsuki, Y. Hirao, and I. Miura, Nucl. Phys. 39, 335 (1962).

$A^{40}$  in which coincidences were measured between protons going to the *second* excited level of  $A^{40}$  and  $\gamma$  radiation decaying from the second to the first level. The observed correlation in the scattering plane was isotropic in  $\theta_2$  which, together with the results of  $\gamma - \gamma$  correlation measurements, is commensurate with a  $0+$  assignment to the second state of  $A^{40}$ , i.e., to a  $0 \rightarrow 2 \rightarrow 0$  spin sequence. In this connection, one might stress the desirability of extending correlation studies to absolute measurement of correlation between nucleon and  $\gamma$  radiation associated with the nucleon exit channel populating the first level and that for channels inducing population of the second or higher excited states of the target nucleus. For a nucleus such as  $A^{40}$ , the spin sequence  $0+/2+/0+$  results in the CN correlation associated with population of the *second* level being dependent only upon  $\theta_1$ , and not upon  $\theta_2$  (this latter isotropy ensues from the fact that for such a transition scheme,  $\mu = \nu$  and  $\lambda = 0$ ; alternative conditions leading to correlation isotropy have been collated in Ref. 17). Explicitly, on going from a  $0+$  ground state to CN states of spin and parity  $J_1, \pi_1$ , followed by nucleon decay to a  $0+$  state and  $\gamma$ -decay to a  $2+$  level, the double-differential cross section (essentially a *distribution*) can be calculated from Eqs. (54) and (56) to be simply

$$\frac{d^2\sigma}{d\Omega_1 d\Omega_2} = \frac{1}{4\pi} \frac{d\sigma}{d\Omega_1} = \frac{\lambda^2}{32\pi} \sum_{\mu, J_1} [\hat{\mu}(\hat{J}_1)^4] \times [\langle \mu 0 | J_1 J_1 \frac{1}{2} - \frac{1}{2} \rangle]^2 \cdot \tau \cdot P_\mu(\cos \theta_1) \quad (154)$$

and this, in turn, for orbital momenta restricted to  $l \leq 2$  and spin-independent transmission coefficients  $T_l$ , can be reduced to

$$\begin{aligned} \frac{d^2\sigma}{d\Omega_1 d\Omega_2} &= \frac{\lambda^2}{16\pi} \{x^4[11.25 \tau^{(6)}] + x^2[3 \tau^{(7)} - 1.5 \tau^{(8)}] \\ &\quad + [\tau^{(6)} + 2 \tau^{(7)} + 3.25 \tau^{(8)}]\} \quad (155) \\ &= [1/E_1^{(\text{MeV})}] \{x^4[46.4177 \tau^{(6)}] + x^2[12.3781 \tau^{(7)} \\ &\quad - 6.1890 \tau^{(8)}] + [4.1260 \tau^{(6)} + 8.2520 \tau^{(7)} \\ &\quad + 13.4096 \tau^{(8)}]\} \text{ mb sr}^{-2}, \quad (156) \end{aligned}$$

with  $x \equiv \cos \theta_1$  and

$$\begin{aligned} \tau^{(6)} &\equiv \frac{T_0(E_1) \cdot T_0(E_2')}{T_0(E_1) + T_0(E_2')} ; \quad \tau^{(7)} \equiv \frac{T_1(E_1) \cdot T_1(E_2')}{T_1(E_1) + T_1(E_2')} ; \\ \tau^{(8)} &\equiv \frac{T_2(E_1) \cdot T_2(E_2')}{T_2(E_1) + T_2(E_2')} . \quad (157) \end{aligned}$$

In Eq. (157), the energy  $E_2$  is that of the nucleon inelastically scattered to the *second* level ( $0+$ ) and, hence, has been labeled with a prime to distinguish

it from that in Eq. (63). Other nuclei than  $A^{40}$  which also possess the  $0+/2+/0+$  spin sequence would appear to be more advantageous for such measurements, in particular  $S^{32}$  or  $Ge^{70}$ , which it is hoped to investigate in the near future.

For studies upon the heavier nuclei ( $A \geq 70$ ), the use of neutrons rather than protons would appear preferable, since not only would the latter be required to penetrate a very considerable Coulomb barrier but, in addition, the Coulomb excitation cross section would also assume non-negligible magnitudes. Since Sr or Mo targets would seem to be likely choices for extension of present investigations, they have been included in Table IV, which compares the

TABLE IV. Comparison of computed total cross sections for Coulomb excitation with those for DI or CN inelastic proton scattering.

Target	Incident energy (MeV)	$\sigma_{\text{CE}}$ (mb)	$\sigma_{\text{DI}}$ (mb)	$\sigma_{\text{CN}}$ (mb)
Ni <sup>58</sup>	4.5	0.409	...	...
Ni <sup>58</sup>	5.8	0.836	5.9	120
Ni <sup>58</sup>	6.9	0.971	13.9	193
Zn <sup>66</sup>	4.8	0.154	0.08	67
Sr <sup>88</sup>	6.0	0.160	...	33
Mo <sup>96</sup>	6.0	0.747	...	36

total cross sections for Coulomb excitation (calculated using the ORNL code "SALLY") with those for pure CN and DI mechanism in inelastic proton scattering to the first excited level for fairly low incident energies. Measurements upon families of isotopes for a given target element such as Mo at a given energy might be expected to substantiate the mechanism switch displayed by the Zn isotopes.

On insertion of appropriate transmission coefficients, the CN correlation theory described here for inelastic scattering processes would apply as it stands also to  $(n, p\gamma)$  and  $(p, n\gamma)$  reactions, for which confirmatory correlation measurements would urgently be desirable. Cohen<sup>86</sup> has made the interesting observation that at energies where the DI mechanism might be expected to prevail, significant differences arise between commensurate  $(p, p')$  and  $(p, n)$  reaction cross sections, e.g., the former are an order of magnitude larger than the latter and display an altogether different dependence upon the incident energy and target mass number, which he considered compatible with the Blair diffraction scattering model but not with the nucleon-nucleon collision model. Angular correlation studies might well shed further light upon this effect.

<sup>86</sup> B. L. Cohen, Phys. Rev. 116, 426 (1959).

The absence of interferences in the statistical model with the random-phase hypothesis precludes polarization of scattered particles when the CN mechanism alone operates, for which reason low-energy polarization studies<sup>87</sup> in conjunction with correlation measurements could provide very valuable information.

Perpendicular-correlation studies also offer a sensitive means of establishing reaction mechanism, and are not only of value in their own right but can yield data for determination of ratios of anisotropy parameters in the successive emission of particles from a compound system (see the note of Halpern<sup>88</sup> and the recent review article on compound nuclear reactions by Bodansky<sup>89</sup>).

A basis for future experimental and theoretical work is the study of correlations when, upon inelastic scattering, levels of the target nucleus higher than the first excited state become populated under conditions when the CN mechanism prevails. For comparison of CN and DI predictions, it would be desirable to determine CN tensor parameters explicitly, coding for which is now under way; alternatively, the reformulation of DI theory to yield an explicit analytical  $\theta_1$  dependence for the correlation might also be undertaken. Indeed, combination of CN with DI scattering theory on the basis of dispersion relations, e.g., Feshbach's "Unified Reaction Theory,"<sup>90</sup> appears to offer considerable promise for the near future. Apart from the approach of Rodberg,<sup>91</sup> the only such attempt based on dispersion formalism has been undertaken by Sano *et al.*<sup>43</sup> and discussed by Austern,<sup>42</sup> but the treatment has, of necessity, been confined to a synthesis of a DI process coupled to an isolated CN resonance, whereas it is for the intermediate region of many CN resonances and their progressive fusion into a continuum that the most pronounced theoretical developments are to be awaited.

## 9. APPENDIX: LEGENDRE HYPERPOLYNOMIALS

When a nuclear reaction proceeds by way of formation of a compound nucleus, the reaction products are, in general, not emitted isotropically. The angular distribution can be expressed in terms of a sum of Legendre polynomials  $P_\lambda(\cos \theta)$ . Since the angular dependence of the *correlation* function is essentially

<sup>87</sup> L. J. B. Goldfarb and D. A. Bromley, Nucl. Phys. **39** 408 (1962).

<sup>88</sup> I. Halpern, Bull. Am. Phys. Soc. **5**, 510 (1960).

<sup>89</sup> D. Bodansky, Ann. Rev. Nucl. Sci. **12**, 79 (1962).

<sup>90</sup> H. Feshbach, Ann. Phys. **5**, 357 (1958); **19**, 287 (1962).

<sup>91</sup> L. Rodberg, Phys. Rev. **124**, 210 (1961).

contained in terms involving products of two spherical harmonics, i.e., *two* Legendre functions basically, Rose<sup>29</sup> has designated such terms "Legendre hyperpolynomials." An alternative designation<sup>92</sup> is "bipolar harmonics." The properties and numerical evaluation of these entities form the subject of this Appendix. (See also Ref. 29.)

Explicitly, for the inelastic scattering processes considered in the present analysis, the Legendre hyperpolynomial has the form

$$S_{\mu\nu\lambda}(\mathbf{k}_0, \mathbf{k}_1, \mathbf{k}_2) = (4\pi)^{\frac{3}{2}}(2\lambda + 1)^{-\frac{1}{2}} \times \sum_{m_1, m_2} \langle \lambda m_2 | \mu\nu m_1, m_2 - m_1 \rangle Y_\mu^{m_1*}(\mathbf{k}_0) \times Y_\nu^{m_2 - m_1*}(\mathbf{k}_1) Y_\lambda^{m_2}(\mathbf{k}_2), \quad (\text{A1})$$

when expressed in terms of the incident and emergent nucleon propagation vectors  $\mathbf{k}_0$ ,  $\mathbf{k}_1$  and the  $\gamma$  radiation vector  $\mathbf{k}_2$ . It is more convenient to express this directly in terms of angles referred to the incident direction  $\mathbf{k}_0$ ; in this form the Legendre hyperpolynomial reduces to

$$S_{\mu\nu\lambda}(\theta_1, \theta_2, \varphi) = 4\pi(\hat{\mu}, \hat{\lambda}) \sum_m (-)^m \langle \lambda m | \mu\nu 0 m \rangle \times Y_\nu^{-m}(\theta_1, 0) Y_\lambda^m(\theta_2, \varphi), \quad (\text{A2})$$

which displays the bipolar harmonic dependence.

The  $Y_\nu^{-m}$  and  $Y_\lambda^m$  are Condon-Shortley spherical harmonics and it may be noted in passing that the  $S_{\mu\nu\lambda}$  are identical with those of Satchler,<sup>11</sup> as also with the  $\Theta_{\nu_0\nu_1\nu_2}$  of Rose<sup>28</sup> and the  $\Theta_{\text{abc}}$  of Seward.<sup>23</sup> They are related to the  $\Lambda$  function of Biedenharn and Rose,<sup>1</sup>

$$S_{\mu\nu\lambda} \equiv (4\pi)^{\frac{3}{2}}(2\lambda + 1)^{-\frac{1}{2}} \Lambda \quad (\text{A3})$$

and to the  $S(\mu\nu\lambda)$  - functions,

$$S_{\mu\nu\lambda} \equiv \hat{\mu} \cdot \hat{\nu} \langle \lambda 0 | \mu\nu 0 0 \rangle S(\mu\nu\lambda). \quad (\text{A4})$$

For evaluation of the  $S_{\mu\nu\lambda}$ , Eq. (A2) can be expressed in terms of associated Legendre functions,

$$S_{\mu\nu\lambda}(\theta_1, \theta_2, \varphi) = \sum_m A_m P_\nu^m(\cos \theta_1) P_\lambda^m(\cos \theta_2) \cos m\varphi, \quad (\text{A5})$$

where the summation runs over all negative and positive integer values of  $m$  up to the lesser of the values  $(\nu, \lambda)$ . The expansion coefficient is

$$A_m \equiv \hat{\mu} \cdot \hat{\nu} \left[ \frac{(\nu - m)!(\lambda - m)!}{(\nu + m)!(\lambda + m)!} \right]^{\frac{1}{2}} \langle \lambda m | \mu\nu 0 m \rangle, \quad (\text{A6})$$

and since it has the symmetry property

$$A_m(\mu\nu\lambda) = A_{-m}(\mu\nu\lambda), \quad (\text{A7})$$

<sup>92</sup> D. Brink and G. R. Satchler, *Angular Momentum* (Oxford University Press, Oxford, 1962).

Eq. (A5) can be written

$$S_{\mu\nu\lambda}(\theta_1, \theta_2, \varphi) = A_0(\mu\nu\lambda)P_\nu(\cos \theta_1)P_\lambda(\cos \theta_2) + 2 \sum_{m \geq 1} A_m(\mu\nu\lambda)P_\nu^m(\cos \theta_1)P_\lambda^m(\cos \theta_2) \cos m\varphi. \quad (\text{A8})$$

This expression has previously been given in a report<sup>28</sup> by Rose, together with a useful recursion relation for the  $A_m$ ,

$$A_{m-1} + [\mu(\mu + 1) - \nu(\nu + 1) - \lambda(\lambda + 1) + 2m^2]A_m + [(\nu - m)(\nu + m + 1)(\lambda - m)(\lambda + m + 1)]A_{m+1} = 0, \quad (\text{A9})$$

which follows from a recursion relation for the magnetic quantum numbers of Clebsch-Gordan coefficients,<sup>33</sup>

$$\begin{aligned} &[\mu(\mu + 1) - \nu(\nu + 1) - \lambda(\lambda + 1) + 2m^2] \\ &\quad \times \langle \lambda m | \mu\nu 0 m \rangle + [\lambda(\lambda + 1) - m(m + 1)]^{\frac{1}{2}} \\ &\quad \times [\nu(\nu + 1) - m(m + 1)]^{\frac{1}{2}} \langle \lambda, m + 1 | \mu\nu 0, m + 1 \rangle \\ &+ [\lambda(\lambda + 1) - m(m - 1)]^{\frac{1}{2}} [\nu(\nu + 1) - m(m - 1)]^{\frac{1}{2}} \\ &\quad \times \langle \lambda, m - 1 | \mu\nu 0, m - 1 \rangle = 0. \quad (\text{A10}) \end{aligned}$$

The report neglected to point out, however, that Eq. (A9) is inapplicable when  $m = 0$ ; in this case the relation giving  $A_1$  from a known value of  $A_0$  is

$$\begin{aligned} &[2\nu\lambda(\nu + 1)(\lambda + 1)]A_1 \\ &+ [\mu(\mu + 1) - \nu(\nu + 1) - \lambda(\lambda + 1)]A_0 = 0. \quad (\text{A11}) \end{aligned}$$

Hence, for a given combination  $(\mu\nu\lambda)$  it suffices to compute  $A_0$  from the expression

$$\begin{aligned} A_0(\mu\nu\lambda) &= (-)^{\frac{1}{2}(\mu+\nu+\lambda)} \\ &\times \left[ \frac{\hat{\mu}^2 \cdot \hat{\nu}^2 \cdot \hat{\lambda}^2 (-\mu + \nu + \lambda)! (\mu - \nu + \lambda)! (\mu + \nu - \lambda)!}{(\mu + \nu + \lambda + 1)!} \right]^{\frac{1}{2}} \\ &\times \frac{[\frac{1}{2}(\mu + \nu + \lambda)]!}{[\frac{1}{2}(-\mu + \nu + \lambda)]! [\frac{1}{2}(\mu - \nu + \lambda)]! [\frac{1}{2}(\mu + \nu - \lambda)]!} \quad (\text{A12}) \end{aligned}$$

and then to derive the other  $A_m$  from Eqs. (A12) and (A9). In this connection a further useful symmetry property of the  $A_m$  is

$$A_m(\mu\nu\lambda) = A_m(\mu\lambda\nu). \quad (\text{A13})$$

TABLE V. Numerical values of the coefficients  $A_m(\mu\nu\lambda)$  from which the Legendre Hyperpolynomials  $S_{\mu\nu\lambda}(\theta_1, \theta_2, \varphi)$  for  $\mu, \nu \leq 18$  and  $\lambda \leq 4$  can be calculated. Figures in raised brackets denote powers of 10.

$\mu$	$\nu$	$\lambda$	$A_0$	$A_1$	$A_2$	$A_3$	$A_4$
0	0	0	1.000000				
2	2	0	2.236068				
4	4	0	3.000000				
6	6	0	3.605551				
8	8	0	4.123106				
10	10	0	4.582577				
12	12	0	5.000000				
14	14	0	5.385165				
16	16	0	5.744561				
18	18	0	6.082761				
0	2	2	2.236068	3.726780 <sup>(-1)</sup>	9.316949 <sup>(-2)</sup>		
2	0	2	2.236068				
2	2	2	-2.672612	-2.227177 <sup>(-1)</sup>	1.113589 <sup>(-1)</sup>		
2	4	2	3.585686	2.988072 <sup>(-1)</sup>	2.490060 <sup>(-2)</sup>		
4	2	2	3.585686	-3.984095 <sup>(-1)</sup>	2.490060 <sup>(-2)</sup>		
4	4	2	-3.418817	-8.547042 <sup>(-2)</sup>	4.273521 <sup>(-2)</sup>		
4	6	2	4.522669	2.512594 <sup>(-1)</sup>	1.256297 <sup>(-2)</sup>		
6	4	2	4.522669	-3.015113 <sup>(-1)</sup>	1.256297 <sup>(-2)</sup>		
6	6	2	-4.067609	-4.842391 <sup>(-2)</sup>	2.421196 <sup>(-2)</sup>		
6	8	2	5.291501	2.204792 <sup>(-1)</sup>	7.874258 <sup>(-3)</sup>		
8	6	2	5.291501	-2.519763 <sup>(-1)</sup>	7.874258 <sup>(-3)</sup>		
8	8	2	-4.633968	-3.218034 <sup>(-2)</sup>	1.609017 <sup>(-2)</sup>		
8	10	2	5.960396	1.986799 <sup>(-1)</sup>	5.518885 <sup>(-3)</sup>		
10	8	2	5.960396	-2.207554 <sup>(-1)</sup>	5.518885 <sup>(-3)</sup>		
10	10	2	-5.141029	-2.336831 <sup>(-2)</sup>	1.168416 <sup>(-2)</sup>		
10	12	2	6.560753	1.822431 <sup>(-1)</sup>	4.141889 <sup>(-3)</sup>		
12	10	2	6.560753	-1.988107 <sup>(-1)</sup>	4.141889 <sup>(-3)</sup>		
12	12	2	-5.603649	-1.796041 <sup>(-2)</sup>	8.980207 <sup>(-3)</sup>		
12	14	2	7.110236	1.692913 <sup>(-1)</sup>	3.255603 <sup>(-3)</sup>		
14	12	2	7.110236	-1.823138 <sup>(-1)</sup>	3.255603 <sup>(-3)</sup>		
14	14	2	-6.031566	-1.436087 <sup>(-2)</sup>	7.180435 <sup>(-3)</sup>		
14	16	2	7.619997	1.587499 <sup>(-1)</sup>	2.645832 <sup>(-3)</sup>		
16	14	2	7.619997	-1.693333 <sup>(-1)</sup>	2.645832 <sup>(-3)</sup>		
16	16	2	-6.431460	-1.182254 <sup>(-2)</sup>	5.911268 <sup>(-3)</sup>		
16	18	2	8.097615	1.499558 <sup>(-1)</sup>	2.205233 <sup>(-3)</sup>		
18	16	2	8.097615	-1.587767 <sup>(-1)</sup>	2.205233 <sup>(-3)</sup>		
18	18	2	-6.808183	-9.953484 <sup>(-3)</sup>	4.976742 <sup>(-3)</sup>		

TABLE V. (Continued)

$\mu$	$\nu$	$\lambda$	$A_0$	$A_1$	$A_2$	$A_3$	$A_4$
0	4	4	3.000000	1.500000 <sup>(-1)</sup>	8.333333 <sup>(-3)</sup>	5.952381 <sup>(-4)</sup>	7.440475 <sup>(-5)</sup>
2	2	4	3.585686	2.988072 <sup>(-1)</sup>	2.490060 <sup>(-2)</sup>		
2	2	4	-3.418817	-1.452997 <sup>(-1)</sup>	-3.798685 <sup>(-3)</sup>	2.374178 <sup>(-4)</sup>	1.187089 <sup>(-4)</sup>
2	6	4	4.522669	1.507556 <sup>(-1)</sup>	5.025188 <sup>(-3)</sup>	1.794710 <sup>(-4)</sup>	7.477955 <sup>(-6)</sup>
4	0	4	3.000000				
4	2	4	-3.418817	-8.547042 <sup>(-2)</sup>	4.273521 <sup>(-2)</sup>		
4	4	4	3.620620	9.051549 <sup>(-2)</sup>	-6.146114 <sup>(-3)</sup>	-8.381064 <sup>(-4)</sup>	6.984220 <sup>(-5)</sup>
4	6	4	-4.045198	-1.011300 <sup>(-1)</sup>	0.000000	2.006547 <sup>(-4)</sup>	2.006547 <sup>(-5)</sup>
4	8	4	5.553301	1.388325 <sup>(-1)</sup>	3.305536 <sup>(-3)</sup>	7.870325 <sup>(-5)</sup>	1.967581 <sup>(-6)</sup>
6	2	4	4.522669	-3.015113 <sup>(-1)</sup>	1.256297 <sup>(-2)</sup>		
6	4	4	-4.045198	1.011300 <sup>(-2)</sup>	1.236033 <sup>(-2)</sup>	-6.822259 <sup>(-4)</sup>	2.006546 <sup>(-5)</sup>
6	6	4	4.185537	4.982782 <sup>(-2)</sup>	-4.567550 <sup>(-3)</sup>	-2.076159 <sup>(-4)</sup>	1.730133 <sup>(-5)</sup>
6	8	4	-4.658685	-8.087994 <sup>(-2)</sup>	6.162282 <sup>(-4)</sup>	1.155428 <sup>(-4)</sup>	6.419043 <sup>(-6)</sup>
6	10	4	6.399979	1.279996 <sup>(-1)</sup>	2.370362 <sup>(-3)</sup>	4.232790 <sup>(-5)</sup>	7.558549 <sup>(-7)</sup>
8	4	4	5.553301	-2.221321 <sup>(-1)</sup>	6.170334 <sup>(-3)</sup>	-1.259251 <sup>(-4)</sup>	1.967512 <sup>(-6)</sup>
8	6	4	-4.658685	2.773027 <sup>(-2)</sup>	6.008224 <sup>(-3)</sup>	-2.695998 <sup>(-4)</sup>	6.419043 <sup>(-6)</sup>
8	8	4	4.722241	3.279334 <sup>(-2)</sup>	-3.279334 <sup>(-3)</sup>	-7.807939 <sup>(-5)</sup>	6.506616 <sup>(-6)</sup>
8	10	4	-5.213957	-6.872943 <sup>(-2)</sup>	7.022164 <sup>(-4)</sup>	7.131885 <sup>(-5)</sup>	2.743033 <sup>(-6)</sup>
8	12	4	7.139502	1.189917 <sup>(-1)</sup>	1.802904 <sup>(-3)</sup>	2.575577 <sup>(-5)</sup>	3.577190 <sup>(-7)</sup>
10	6	4	6.399979	-1.828565 <sup>(-1)</sup>	3.809511 <sup>(-3)</sup>	-6.046841 <sup>(-5)</sup>	7.558489 <sup>(-7)</sup>
10	8	4	-5.213956	3.258722 <sup>(-2)</sup>	3.620802 <sup>(-3)</sup>	-1.371516 <sup>(-4)</sup>	2.743032 <sup>(-6)</sup>
10	10	4	5.215491	2.370678 <sup>(-2)</sup>	-2.463359 <sup>(-3)</sup>	-3.658453 <sup>(-5)</sup>	3.048711 <sup>(-6)</sup>
10	12	4	-5.720416	-6.050439 <sup>(-2)</sup>	6.667151 <sup>(-4)</sup>	4.722565 <sup>(-5)</sup>	1.388990 <sup>(-6)</sup>
10	14	4	7.805788	1.115113 <sup>(-1)</sup>	1.429632 <sup>(-3)</sup>	1.701942 <sup>(-5)</sup>	1.934024 <sup>(-7)</sup>
12	8	4	7.139502	-1.586556 <sup>(-1)</sup>	2.644260 <sup>(-3)</sup>	-3.434103 <sup>(-5)</sup>	3.577182 <sup>(-7)</sup>
12	10	4	-5.720416	3.380246 <sup>(-2)</sup>	2.455734 <sup>(-3)</sup>	-8.056141 <sup>(-5)</sup>	1.388990 <sup>(-6)</sup>
12	12	4	5.670887	1.817592 <sup>(-2)</sup>	-1.927749 <sup>(-3)</sup>	-1.967091 <sup>(-5)</sup>	1.639242 <sup>(-6)</sup>
12	14	4	-6.187802	-5.451159 <sup>(-2)</sup>	6.044251 <sup>(-4)</sup>	3.305450 <sup>(-5)</sup>	7.870118 <sup>(-7)</sup>
12	16	4	8.417625	1.052203 <sup>(-1)</sup>	1.169114 <sup>(-3)</sup>	1.192974 <sup>(-5)</sup>	1.147090 <sup>(-7)</sup>
14	10	4	7.805788	-1.419234 <sup>(-1)</sup>	1.971159 <sup>(-3)</sup>	-2.166108 <sup>(-5)</sup>	1.934018 <sup>(-7)</sup>
14	12	4	-6.187802	3.371559 <sup>(-2)</sup>	1.794387 <sup>(-3)</sup>	-5.194278 <sup>(-5)</sup>	7.870118 <sup>(-7)</sup>
14	14	4	6.094829	1.451150 <sup>(-2)</sup>	-1.558126 <sup>(-3)</sup>	-1.162780 <sup>(-5)</sup>	9.689836 <sup>(-7)</sup>
14	16	4	-6.623507	-4.991982 <sup>(-2)</sup>	5.411362 <sup>(-4)</sup>	2.415787 <sup>(-5)</sup>	4.831573 <sup>(-7)</sup>
14	18	4	8.986789	9.985320 <sup>(-2)</sup>	9.789530 <sup>(-4)</sup>	8.740650 <sup>(-6)</sup>	7.283870 <sup>(-8)</sup>
16	12	4	8.417625	-1.295019 <sup>(-1)</sup>	1.541689 <sup>(-3)</sup>	-1.468275 <sup>(-5)</sup>	1.147087 <sup>(-7)</sup>
16	14	4	-6.623511	3.311756 <sup>(-2)</sup>	1.379898 <sup>(-3)</sup>	-3.575366 <sup>(-5)</sup>	4.831576 <sup>(-7)</sup>
16	16	4	6.492637	1.193500 <sup>(-2)</sup>	-1.291730 <sup>(-3)</sup>	-7.367281 <sup>(-5)</sup>	6.139401 <sup>(-7)</sup>
16	18	4	-7.032988	-4.626966 <sup>(-2)</sup>	4.838657 <sup>(-4)</sup>	1.827097 <sup>(-5)</sup>	3.150167 <sup>(-7)</sup>
18	14	4	8.986794	-1.198239 <sup>(-1)</sup>	1.248166 <sup>(-3)</sup>	-1.048879 <sup>(-5)</sup>	7.283871 <sup>(-8)</sup>
18	16	4	-7.032984	3.232070 <sup>(-2)</sup>	1.101298 <sup>(-3)</sup>	-2.583136 <sup>(-5)</sup>	3.150166 <sup>(-7)</sup>
18	18	4	6.868323 <sup>(-1)</sup>	1.004147 <sup>(-3)</sup>	-6.880223 <sup>(-5)</sup>	-3.889812 <sup>(-7)</sup>	2.576677 <sup>(-8)</sup>

This circumstance induces a symmetry relation in the  $S_{\mu\nu\lambda}$ ,

$$S_{\mu\nu\lambda}(\theta_1, \theta_2, \varphi) = S_{\mu\lambda\nu}(\theta_2, \theta_1, \varphi). \quad (\text{A14})$$

The recursion relations appropriate to change in one of the parameters  $(\mu\nu\lambda)$  prove to be inconveniently cumbersome and have not therefore been reproduced. This arises from the fact that the starting relations for Clebsch-Gordan coefficients are themselves fairly involved and that, furthermore, the parameters  $(\mu\nu\lambda)$  change in steps of 2 rather than in integer steps.

The extension of angular correlation calculations to include orbital momenta higher than  $l = 2$  has in the past been restricted by their relative complexity and, in particular, by the difficulty of calculating the Legendre hyperpolynomials  $S_{\mu\nu\lambda}$ . These have now been computed numerically but since they are functions of  $(\theta_1, \theta_2, \varphi)$  as well as of  $(\mu\nu\lambda)$ , their values are too numerous to be tabulated here. They can, how-

ever, be evaluated directly if the numerical values of the coefficients  $A_m(\mu\nu\lambda)$  are known: these quantities have been listed in Table V for  $\mu, \nu = 0$  to 18 i.e.,  $l \leq 9$  and  $\lambda = 0, 2, 4$ . This augments Rose's table<sup>28</sup> of  $A_m(\mu\nu\lambda)$  for  $l \leq 2$  and corrects an erroneous value of  $A_4(444)$  in that compilation. The values of  $A_m$  were computed directly from Eq. (A6) and as a countercheck by the recursion relations (A12) and (A9); the only disagreement occurred in the final decimal place and then only in isolated instances.

For a zero value of one or more of the parameters  $(\mu\nu\lambda)$ , the  $S_{\mu\nu\lambda}(\theta_1, \theta_2, \varphi)$  take on simple forms,

$$S_{000} = 1 \quad (\text{A15})$$

$$S_{\mu\nu 0} = \delta_{\mu\nu} \cdot \hat{\nu} P_\nu(\cos \theta_1) \quad (\text{A16})$$

$$S_{\mu 0 \lambda} = \delta_{\mu\lambda} \cdot \hat{\mu} P_\mu(\cos \theta_2) \quad (\text{A17})$$

$$S_{0\nu\lambda} = \delta_{\mu\lambda} \hat{\lambda} P_\lambda(\cos \xi), \quad (\text{A18})$$

where the angle  $\xi$  between the outgoing radiations,

is given by

$$\omega \equiv \cos \xi = \cos \theta_1 \cos \theta_2 + \sin \theta_1 \sin \theta_2 \cos \varphi. \quad (\text{A19})$$

The set of  $S_{\mu\nu\lambda}$  are complete and orthogonal; it can be shown from Eq. (A8) that

$$\int S_{\mu\nu\lambda} S_{\mu'\nu'\lambda'} d\Omega = 8\pi \delta_{\mu\mu'} \delta_{\nu\nu'} \delta_{\lambda\lambda'}, \quad (\text{A20})$$

where  $d\Omega = \sin \theta_1 \sin \theta_2 d\theta_1 d\theta_2 d\varphi$ .

Rose<sup>28</sup> has shown, furthermore, that

$$\begin{aligned} \int S_{\mu\nu\lambda} S_{\mu'\nu'\lambda'} S_{\mu''\nu''\lambda''} d\Omega &= (-)^{\mu''+\nu''+\lambda''} \times 8\pi \hat{\mu}\hat{\nu}\hat{\lambda}'\hat{\lambda}'' \\ &\times \langle \mu''0 | \mu\mu'00 \rangle \langle \nu''0 | \nu\nu'00 \rangle \langle \lambda''0 | \lambda\lambda'00 \rangle \\ &\times X(\mu\nu\lambda; \mu'\nu'\lambda'; \mu''\nu''\lambda''), \end{aligned} \quad (\text{A21})$$

and that the  $S_{\mu\nu\lambda}$  are invariant under rotation.

The explicit forms for the  $S_{\mu\nu\lambda}(\theta_1, \theta_2, \varphi)$  associated with orbital angular momenta  $l \leq 2$  are given below for arbitrary  $(\theta_1, \theta_2, \varphi)$ , with the notation  $x \equiv \cos \theta_1$ ,  $y \equiv \cos \theta_2$ ,  $z \equiv xy [(1-x^2)(1-y^2)]^{\frac{1}{2}}$ :

$$\begin{aligned} S_{222} &= [-8.017837 x^2 y^2 + 4.008919(x^2 + y^2) \\ &\quad - 2.672612] - [4.008919 z] \cos \varphi \\ &\quad + [4.008919(x^2 y^2 - x^2 - y^2 + 1)] \cos^2 \varphi; \end{aligned} \quad (\text{A22})$$

$$\begin{aligned} S_{224} &= [15.687374 x^2 y^4 - 11.205266 x^2 y^2 + 0.896421 x^2 \\ &\quad - 2.241055 y^2 + 0.448211] + [31.374751 y^2 z \\ &\quad - 13.446322 z] \cos \varphi + [15.687378 x^2 y^4 \\ &\quad - 15.687378 y^4 - 17.928432 x^2 y^2 \\ &\quad + 2.241054 x^2 + 17.928432 y^2 \\ &\quad - 2.241054] \cos^2 \varphi; \end{aligned} \quad (\text{A23})$$

$$\begin{aligned} S_{242} &= [15.687374 x^4 y^2 - 11.205266 x^2 y^2 - 2.241055 x^2 \\ &\quad + 0.896421 y^2 + 0.448211] + [31.374751 x^2 z \\ &\quad - 13.446322 z] \cos \varphi + [15.687378 x^4 y^2 \\ &\quad - 15.687378 x^4 - 17.928432 x^2 y^2 \\ &\quad + 17.928432 x^2 + 2.241054 y^2 - 2.241054] \\ &\quad \times \cos^2 \varphi; \end{aligned} \quad (\text{A24})$$

$$\begin{aligned} S_{244} &= [-41.880466 x^4 y^4 + 26.923113(x^4 y^2 + x^2 y^4) \\ &\quad - 10.256328 x^2 y^2 - 3.846220(x^2 + y^2) \\ &\quad + 2.564137] + [-104.701417 x^2 y^2 z \\ &\quad + 53.846512(x^2 + y^2)z - 32.051553 z] \cos \varphi \\ &\quad + [-62.821001 x^4 y^4 + 89.744381(x^4 y^2 + x^2 y^4) \\ &\quad - 26.923381(x^4 + y^4) - 138.462913 x^2 y^2 \end{aligned}$$

$$\begin{aligned} &+ 48.718530(x^2 + y^2) - 21.795149] \cos^2 \varphi \\ &+ [20.940444(x^2 y^2 z - x^2 z - y^2 z + z)] \cos^3 \varphi \\ &+ [20.940444 x^4 y^4 - 41.880888(x^4 y^2 + x^2 y^4) \\ &+ 20.940444(x^4 + y^4) + 83.761778 x^2 y^2 \\ &- 41.880888(x^2 + y^2) + 20.940444] \cos^4 \varphi; \end{aligned} \quad (\text{A25})$$

$$\begin{aligned} S_{422} &= [7.619582 x^2 y^2 - 2.241054(x^2 + y^2) \\ &\quad + 0.448211] + [-7.171372 z] \cos \varphi \\ &\quad + [0.896422(x^2 y^2 - x^2 - y^2 + 1)] \cos^2 \varphi; \end{aligned} \quad (\text{A26})$$

$$\begin{aligned} S_{442} &= [-35.897583 x^4 y^2 + 20.940257 x^4 \\ &\quad + 34.615526 x^2 y^2 - 21.794962 x^2 \\ &\quad - 3.846170 y^2 + 2.564113] + [-8.974395 x^2 z \\ &\quad + 3.846169 z] \cos \varphi + [26.923189 x^4 y^2 \\ &\quad - 26.923189 x^4 - 30.769358 x^2 y^2 \\ &\quad + 30.769358 x^2 + 3.846170 y^2 - 3.846170] \\ &\quad \times \cos^2 \varphi; \end{aligned} \quad (\text{A27})$$

$$\begin{aligned} S_{424} &= [-35.897583 x^2 y^4 + 20.940257 y^4 \\ &\quad + 34.615526 x^2 y^2 - 3.846170 x^2 \\ &\quad - 21.794962 y^2 + 2.564113] + [-8.974395 y^2 z \\ &\quad + 3.846169 z] \cos \varphi + [26.923189 x^2 y^4 \\ &\quad - 26.923189 y^4 - 30.769358 x^2 y^2 \\ &\quad + 3.846170 x^2 + 30.769358 y^2 - 3.846170] \\ &\quad \times \cos^2 \varphi; \end{aligned} \quad (\text{A28})$$

$$\begin{aligned} S_{444} &= [104.721380 x^4 y^4 - 101.201324(x^4 y^2 + x^2 y^4) \\ &\quad + 12.320158(x^4 + y^4) + 101.327027 x^2 y^2 \\ &\quad - 13.703028(x^2 + y^2) + 2.740603] \\ &\quad + [110.881726 x^2 y^2 z - 79.201298(x^2 + y^2)z \\ &\quad + 65.623971 z] \cos \varphi + [-80.080992 x^4 y^4 \\ &\quad + 102.081244(x^4 y^2 + x^2 y^4) - 22.000252 \\ &\quad \times (x^4 + y^4) - 137.784499 x^2 y^2 \\ &\quad + 35.703256(x^2 + y^2) - 13.703004] \cos^2 \varphi \\ &\quad + [73.921302(-x^2 y^2 z + x^2 z + y^2 z - z)] \cos^3 \varphi \\ &\quad + [12.320129 x^4 y^4 - 24.640258(x^4 y^2 + x^2 y^4) \\ &\quad + 12.320129(x^4 + y^4) + 49.280515 x^2 y^2 \\ &\quad - 24.640258(x^2 + y^2) + 12.320129] \cos^4 \varphi. \end{aligned} \quad (\text{A29})$$

## ACKNOWLEDGMENTS

The bulk of this work was undertaken during 6 months' leave of absence from the E.T.H. as a guest at the Oak Ridge National Laboratory, for which reason sincere thanks are extended to innumerable colleagues at both institutions. At the E.T.H. thanks are due principally to Professor P. Marmier and to the members of the Zürich group who generously permitted inclusion of their results prior to publication, B. Gobbi, T. Niewodniczanski, R. E. Pixley, M. P. Steiger, and R. Szostak; whereas at ORNL thanks are due principally to G. R. Satchler, D. E. Arnurius, R. H. Bassel, B. Buck, K. Denning, R.

Drisko and F. Perey. Among the outstanding facilities at ORNL which were greatly appreciated, special mention must be made of the assistance in coding and computation on an IBM 7090 computer, and also of the preparation and photography of the many figures whose excellence is eloquent testimony to the Graphic Arts Department. Apart from the theoretical support of ORNL and the experimental support of ETH, the author finally wishes to acknowledge his gratitude for the realization of this project through financial support from the Swiss National Science Foundation and the patient support of his wife.

# Spherical Nuclei with Simple Residual Forces\*

LEONARD S. KISSLINGER

*Western Reserve University, Cleveland, Ohio*

AND

RAYMOND A. SORENSEN

*Carnegie Institute of Technology, Pittsburgh,  
Pennsylvania*

## CONTENTS

I. Introduction . . . . .	853	1. Quasi-particle and collective contributions . . . . .	892
II. Description of Hamiltonian and wave functions . . . . .	855	2. Contributions from configurations admixed by a $\delta$ -function force . . . . .	893
A. The Hamiltonians . . . . .	855	B. Electric quadrupole moment of one-phonon state . . . . .	895
B. The pairing solutions . . . . .	855	VII. Electromagnetic transitions . . . . .	897
C. The long-range force . . . . .	857	A. Odd-mass isotopes . . . . .	897
1. Even-even nuclei, QRPA approximation . . . . .	857	B. Even-even isotopes . . . . .	900
2. Even-even nuclei, the adiabatic limit . . . . .	860	1. The one-phonon-to-ground-state transition . . . . .	900
3. Odd-mass nuclei . . . . .	861	2. The crossover $2^+$ -two-phonon-to-ground-state transition . . . . .	901
III. Energy-level systematics . . . . .	862	3. The MI admixture in the two-phonon $2^+$ to one-phonon transition . . . . .	903
A. The parameters and description of method of calculation . . . . .	862	4. Transitions in two-quasi-particle states . . . . .	903
1. The interaction strength parameters . . . . .	862	VIII. Beta decay . . . . .	903
2. The single-particle parameters . . . . .	863	A. Beta-decay matrix elements—odd mass . . . . .	904
B. Energy levels of even-even nuclei . . . . .	864	B. Beta-decay matrix elements—even mass . . . . .	905
C. Energy levels of odd-mass nuclei . . . . .	867	IX. Conclusions . . . . .	907
1. The region $50 \leq Z \leq 82$ ; $82 \leq N \leq 126$ . . . . .	867	Appendix I . . . . .	909
2. The region $50 \leq Z \leq 82$ ; $50 \leq N \leq 82$ . . . . .	870	Appendix II . . . . .	909
3. The region $28 \leq Z \leq 50$ ; $50 \leq N \leq 82$ . . . . .	875	Appendix III . . . . .	911
4. The region $28 \leq Z \leq 50$ ; $28 \leq N \leq 50$ . . . . .	876		
D. Energy levels of odd-odd nuclei . . . . .	877		
IV. Odd-even mass difference . . . . .	882		
V. Magnetic dipole moments . . . . .	885		
A. Magnetic dipole moments of odd-mass nuclei . . . . .	885		
1. Quasi-particle and collective contributions . . . . .	885		
2. Higher seniority contributions . . . . .	886		
3. Results and discussion . . . . .	890		
B. Magnetic dipole moment of one-phonon states . . . . .	891		
VI. Electric quadrupole moments . . . . .	892		
A. Odd-mass nuclei . . . . .	892		

## I. INTRODUCTION

THE large accumulation of data on the low-energy spectra of many nuclei has made it possible to study systematically and in detail the variation from nucleus to nucleus of various nuclear properties, such as level energies, moments, transition rates, and reaction rates. In many cases it has been possible to identify, in the low-energy spectrum, states which seem to correspond to the motion of a single particle

\*Supported in part by the National Science Foundation, the United States Army Research Office, Durham, and the United States Office of Naval Research.